VILNIUS UNIVERSITY

Mangirdas Malinauskas

FABRICATION OF FUNCTIONAL 3D MICRO/NANOSTRUCTURES BY LASER MULTIPHOTON POLYMERIZATION TECHNIQUE

Doctoral dissertation
Physical sciences, Physics (02P)

Vilnius 2010

The doctoral dissertation was prepared during 2006 – 2010 in Vilnius University. Part of the experiments were done in Hannover Laser Center (*LZH*, Hannover, Germany) and Foundation for Research and Technology Hellas (*FORTH*, Heraklion, Crete, Greece).

Scientific supervisor:

Prof. Dr. Roaldas Gadonas
(*Vilnius University*, Physical sciences, Physics – 02P)

Scientific advisors:

Prof. Dr. Saulius Juodkazis
(*Swinburne University of Technology*, Physical Sciences, Physics – 02P).

Dr. Maria Farsari
(*FORTH institute*, Physical Sciences, Physics – 02P).

Contents

1 INTRODUCTION

List of acronyms, symbols and Greek letters:

2D - Two-Dimensional
3D – Three-Dimensional
AOM - Acousto Optic Modulator
AFM - Atomic Force Microscopy
β - experimentally derived photosensitivity constant
CPhC - Chirped Photonic Crystal
CAD - Computer Aided Design
CCD - Charge-Coupled Device
CMOS - Complementary Metal-Oxide-Semiconductor sensor
d – voxel diameter
DFBL - Distributed FeedBack Laser
DLW - Direct Laser Writing
DM - Dichromatic Mirror
I – light intensity
I_{th} – threshold light intensity needed for irreversible photomodification
I_d – light intensity at which material is optically damaged
IR - InfraRed
FLMP - Femtosecond Laser Multiphoton Polymerization
f – focal length of the lens
FWHM - Full Width at Half Maximum
LCP - Long-Chained-Polymers
LED - Light Emiting Diode
LET - Long Exposure Technique
LOC - Lab On Chip
l – voxel length
M - monomer molecule
M* - radicalized monomer molecule

MOE - Micro Optical Element
MOEMS - Micro Opto Electro Mechanical System
MPA - MultiPhoton Absorption
n – optical refractive index
N – order of nonlinear absorption
NA - Numerical Aperture
NIL - Nano Imprint Lithography
NIR - Near InfraRed
OPA - Optical Parametric Amplifier
ORMOCER - ORganically MOdified CERamics
ORMOSIL - ORganically MOdified SILica
P - polymer molecule
P – average laser power
P_P - peak laser power
PAG - PhotoAcid Generator
PhC - Photonic Crystal
PDMS - PolyDiMethylSiloxane
PEG-DA - Poly(Ethylene Glycol)Dia-Acrylate
PI - Photo-Initiator
R – radius of the sphere
SCP - Short-Chained-Polymers
SEM - Scanning Electrone Microscope
SIL - Solid Immersion Lens
t – the total irradiation (exposure) time
UV - Ultra Violet
v - sample scanning (translation) speed
VIS - VISible
voxel - Volumetric piXel
w_0 – beam diameter (waist) at the focus
z_R –*Rayleigh* length
λ – light wavelength
ν – laser pulse repetition rate
β - material photosensitivity constant
τ – laser pulse duration
TPA - Two-Photon Absorption

INTRODUCTION

Multiphoton absorption induced laser true *3D* fabrication of polymers with submicrometer spatial resolution has been introduced a decade ago [1]. Up to date this kind of *Femtosecond Laser Direct Writing (FLDW)* technique is being already applied widely in the fields of photonics, microoptics, micromechanics, microfluidics and being transferred to production of artificial polymeric scaffolds, metamaterials and plasmonic devices [2, 3, 4, 5]. *Femtosecond Laser Multiphoton Polymerization (FLMP)*, being a branch of rapid prototyping techniques, enables to form *3D* microstructures of complex geometry with 100 nm spatial resolution with unmatched flexibility (structure geometry and/or scale can be changed easily). *FLMP* is based on nonlinear light and matter interaction, when a pulsed light beam having high peak power from the range of *VIS* or *NIR* being tightly focused into the volume of the photosensitive polymer. Due to temporal and spatial overlap several photons are absorbed simultaneously in the beam waist. This is followed by further irreversible photochemical processes which are of threshold behaviour, like minimal concentration of photoexcited highly reactive radical molecules. The thresholding also arises from the postprocessing of light exposed samples and depends on the material chemical properties and the mechanical rigidity of the structure itself. This way, precisely tuning the intensity of light and exposure dose one can reach sub-diffraction (up to $< \lambda/30$) spatial structuring resolution [6, 7, 8, 9]. After the point-by-point exposure the trace of the scanned laser focus becomes a part of the polymer material resistant to organic solvents. Applying proper developing and rinsing conditions, to yield rigid structures, up to 120 nm reproducible spatial resolution can be achieved to form functional *3D* micro/nanoobjects. To date *FLMP* offers possibility to produce objects out of various photosensitive polymer materials such as acrylates, organic-inorganic hybrids and epoxies which are distinguished for assorted optical, mechanical, chemical as well as biological properties offering possibility to tune the material to case specific application. Finally, *FLMP* setup is not complicated to use and does not require clean-room or any additional costly in maintenance facility.

In this thesis, experimental results on *FLMP 3D* micro/nanostructuring of various photopolymers are presented. It starts from the construction and development of the laser fabrication setup. Issues like optimization of the

laser structuring parameters for increasing fabrication resolution and production throughput are presented and discussed. Functional microdevices manufactured out of acrylate, hybrid organic-inorganic and biodegradable photopolymers are demonstrated and their performance is investigated.

During the work several problems were met and had to be solved:

1) Development of novel laboratory setup based on diode pumped solid state femtosecond *Yb:KGW* amplified laser system combined with high translation speed and precision linear motion stages designed for rapid *FLMP* micro/nano-structuring over a large area. Various irradiation wavelenghts (not only *NIR*, but *VIS* and also longer *NIR*) are needed to optimize the nonlinear excitation of the photosensitive material. High sample translation speed (increasing from μm/s to mm/s) corresponding to rapid structure writing is needed in order to make samples over a large areas (from tens of μm to tens of mm).

2) Investigation on improvement of *3D* structuring spatial resolution choosing the appropriate photosensitive materials and optimizing fabrication parameters. Hybrid materials containing metal isopropoxides were found to be best for complex-shaped rigid structure formation at micro/nanoscale with 200 nm reproducible resolution and acrylate based materials can be applied to initiate self-polymerization which can reach $<$ 100 nm spatial resolution. Precise *3D* structuring can be performed in not photosensitized materials (containing no photoinitiator) initiating the photopolymerization reaction via avalanche ionization.

3) Fabrication of microoptical elements and characterization of their optical properties in order to estimate *FLMP* applicability for production of integrated and bi-functional microoptical components. Refractive index matching ultra-low shrinking materials were found to be suitable for manufacturing of custom shaped microoptical elements and bi-functional components ensuring surface roughness to be sufficient ($< \lambda/20$) for optical quality requirements ($< \lambda/10$). It can be applied in molding of flight flow at microscale, for introducing as well as registering light.

4) Study on photostructuring of biocompatible materials in *3D* with < 1 μm resolution required for biomedical applications. Optimization of fabrication over a large area had to be done in order to manufacture microstructured samples suitable for biomedical applications.

OUTLINE

The structure of the whole *PhD* thesis is presented in this way:
In *2nd chapter* the motivation of the work is explained; *3rd chapter* are statements of the novelty and relevance of the obtained results, and the *4th Chapter* is accenting the practical gain; *PhD Thesis* is stated in *5th Chapter*; in *6th Chapter* participation in projects and other scientific activities of the author is listed; *7th Chapter* describes the existing techniques of *3D* micro/nanostructuring; the principles and applied approach of *FLMP* technique are presented in *Chapter 8* and *Chapter 9*; information about photosensitive materials and experimental details are given in *Chapter 10* and *Chapter 11*; original results revealing the mechanisms of *3D* structuring are presented in *Chapter 12*; characterization of microoptical components and their performance are described in *Chapter 13th*; production of *3D* scaffolds and their biocompatibility investigation is provided in *Chapter 14th*; *15th Chapter* is the summary and outlook of the whole work; in *Chapter 16th* input of cooauthors is distinguished; approbation and brief biography of the author are the *Chapters 17th and 18th.*

2 MOTIVATION

Femtosecond laser multiphoton polymerization technique owning enormous potential of possible applications in fabrication *3D* functional micro/nano-devices is still in its early stages of development, especially concerning mass production of devices required by industry. In order to expand the practical applicability to reach the horizons of potential it is necessary to optimize laser source and exposure conditions, sample positioning and/or beam scanning control, photosensitive material's response as well as developing and post-development steps. For this goal it is a requisite to have a synergetic collaboration between interdisciplinary science fields, such as laser optics (including ultrafast laser phenomena), material sciences (material properties at nanoscale) and chemistry (femtochemistry and nano-scaled chemistry). All together this could lead to overcome the challenges and offer direct and single step process to structure micro/nano objects with $<$ 100 nm spatial resolution in all three dimensions [10, 11, 12, 13, 14]. This would open a way not only to greatly minimize the size of nowadays used complex micro-devices, but also would allow creation of manmade materials with properties which are non-existing in the real world naturally, for e.g. create plasmonic metamaterials, that would realize invisibility cloaking [15, 16, 17]. Production of artificial bio-attractive and biodegradable scaffolds would enable to control stem cell proliferation and differentiation sequenced by advances in tissue engineering and regenerative medicine [18, 19, 20]. Additionally, *FLMP* allows formation of complex shaped micro/nano-devices on various surfaces and materials easing the integration of single elements into sophisticated systems like *Lab-On-Chip (LOC)* [21, 22] or *Micro-Opto-Electro-Mechanical-Systems (MOEMS)* [23, 24].

TECHNIQUES

Four years ago, by the time when the *PhD* project began, practically one could get only commercially available photopolymers and structure them by using femtosecond *Ti:Sapphire* lasers due to their abundance based on historical reasons. In parallel, alternative femtosecond laser sources where starting to emerge in modern laser microfabrication and microprocessing labs. For eg., *Yb:KGW* femtosecond laser could offer higher and tunable amplified pulse repetition rate as well different irradiation wavelength. This has intrigued to experimentally test their applicability for *FLMP* structuring, benefits and drawbacks, and on the other hand, to investigate the mechanism of light-matter interaction from different angle going deeper in the details. This pace was followed by supervening synthesis and investigation of new photosensitive materials specially designed for *FLMP 3D* micro/nanostructuring. Since, the application field of *FLMP* was growing and branching dramatically rapidly, possibility to tune-up the material for the specific needs became crucial [25, 26]. This let two approaches to be practically realized aiming to find the optimal material performance: 1) to create novel material with desired properties or 2) to apply the existing and widely used material for *FLMP* structuring. Both contentions had their advantages and disadvantages, and different scientific background of materials sciences/chemistry and laser physics/optics, both being in ultralow spatial (nanoscale) and temporal (femtosecond) dimensions. However, it had to be supported by experimental work to be done in order to acquire data for concluding knowledge.

APPLICATIONS

These above mentioned reasons has initiated the direction of *PhD* project to be focused on novel laser systems and their applicability for *3D* micro/nanostructuring of common and new photopolymer materials. In the beginning of the work this has not been done in details. From the very first demonstration and emergence of *FLMP* as micro/nanostructuring technique it has drawn a great attention for prototyping *Photonic Crystal (PhC)* templates [27, 28]. Recently, concentrated research is being done for its application in plasmonics and metamaterial production experiments [29, 30, 31]. Yet, almost only few papers have been published showing the potential to create sophisticated microoptical devices as well as their integration into complex *3D* optical circuits. *FLMP* fabricated artificial polymer scaffolds were shown to be biocompatible *in vitro*, yet lacking in practical demonstration of their biological functioning as the common overall size of the scaffolds was less than 100 μm resulting to the fact preventing from *in vivo tests*. Then, based on contemporary situation it was essentially meaningful to focus the research for the creation of functional micro/nanodevices mainly on these topical vectors.

3 NOVELTY AND RELEVANCE

Femtosecond laser multiphoton polymerization technique due to its high spatial structuring resolution and possibility to directly produce *3D* micro/nanostructures is attractive for scientific and industrial applications in the fields of photonics, micromechanics, microfluidics and tissue engineering [32, 33, 34, 35]. That is why the first commercially available *FLMP* setups are appearing from several suppliers. However, the novelty of the technique and point-by-point (serial) structuring as well as still lack of complete understanding of limiting factors for high throughput mass production are the issues to be solved in the near future.

For the increase of photostructuring spatial resolution one needs not only to optimize laser source and exposing conditions, but also to improve the material response at micro/nanoscale. Commonly used photopolymers and photoresists created for *UV* and e-beam as well as nanoimprint lithography are not always suitable for *FLMP 3D* structuring in the meaning of efficiency and workability. Few years ago novel type hybrid organic-inorganic metal isopropoxides (alcoxides) containing photosensitive materials were introduced in the *FLMP* application field [36, 37]. They were specially designed for *3D* nanostructuring offering unprecedented structure rigidity and ultralow shrinkage and since being custom made – tuning of the material properties by changing the ratio of ingredients or the components. Yet still many efforts have to be done in order to fully identify their optical, mechanical, chemical and biological properties important for case specific applications. Serial writing offers flexible and easy change of the geometry and/or scale of the prototype model, though is not highly efficient in fabrication of large scale objects sustaining high feature spatial resolution. The problem arises if for eg., an array of microlenses or a relatively

large scaffold template is needed. The solution could be offered in several approaches, interference lithography or multi-beam parallel writing. The first way provides rapid processing of larger areas by producing periodic structures up to millimeters in size keeping hundreds of nanometer precision, yet it is limited to introducing defects [38, 39]. The alternative of multi-beam writing meets the best sides of both directions – possibility to form multitude of elements at once as well as modify their production over the larger areas (volumes) [40, 41]. This question is triggered not only by the industrial demand to increase fabrication throughput, but also by the *"ecological"* fact that only 1% or less of generated femtosecond laser optical power is used for sample exposure.

The novelty and relevance of the presented results in this work can be distinguished into:

1) An automated novel *FLMP* setup based on high and tunable pulse repetition rate diode pumped solid state *Yb:KGW* amplified laser system combined by high translation speed and positioning precision linear motion stages has been designed and assembled. The fabrication system enables rapid production of *3D* microstructures with 200 nm reproducible spatial resolution on various substrates.

2) Self-polymerization (*"repolymerization"*) phenomenon occuring under below threshold laser exposure in various photopolymers was observed and explained for the first time. Conditions of laser beam scanning, critical distance between rigid supports and developing for self-forming ultrafine (< 100 nm) fibers and membranes were defined. The possibility to predict and control the assembling of nanofibers and nanomembranes was shown.

3) The potential to manufacture integrated and bi-functional microoptical components out of hybrid photopolymers was revealed. Their performance was investigated and technique enabling an increase of fabrication throughput (up to 300 times) was offered.

4) For the first time it was experimentally shown that *3D* photostructuring can be achieved reaching near to optical damage threshold light intensities due to avalanche ionization. Deeper understanding of these processes is essential for the optimization laser exposure and the response of the material in order to go sub-100 nm reproducible high quality structuring.

5) Biocompatibility of *FLMP* structurable photopolymers was tested *in vitro* and *in vivo*. Adult myogenic stem cells proliferation tests on polymeric substrates showed that the selected laser structurable materials such as *ORMOCORE b59*, *SZ2080* and *PEG-DA-258* are applicable for biomedical practice. It was supported by the biocompatibility tested for these polymer materials implanted in living organism.

4 PRACTICAL GAIN

1. In cooperation with *Altechna Ltd.* a novel *FLMP* fully automated setup has been designed and constructed based on high pulse repetition rate amplified *Yb:KGW* laser system (*Light Conversion, Ltd., Lithuania*) combined with high translation speed and precision linear motion stages (*Aerotech Inc., UK*) for rapid micro/nanofabrication over a large areas. It enables *3D* structuring of photopolymers over areas as large as cm ensuring 200 nm reproducible spatial resolution.

2. Investigation on *FLMP 3D* micro/nano-structuring of acrylate and hybrid photosensitive materials was done, optimization of fabrication parameters were determined, possible fields for their applications were defined. The highest spatial resolution could be achieved applying custom prepared acrylate photopolymer *AKRE* ($\sim$100 nm resolution was reached). Due to low shrinkage and refractive index matching hybrid photosensitive material *SZ2080 (FORTH, Heraklion, Crete, Greece)* was recognized as being best for production of microoptical and photonic elements. Cell proliferation *in vitro* and *in vivo* tests with animals showed the widely used biocompatible and biodegradable *PEG-DA-258* material to be suitable for *3D* structuring with sub-micrometer spatial resolution.

3. Photosensitive acrylate based material *AKRE19/23/37* was developed. It is suitable for high resolution *3D DLW* structuring and being custom made can be optimized for used laser's irradiation wavelength upon demand. The material cost is significantly lower ($>$ 200 times) comparing to commonly used commercially available photopolymers used for *3D* micro/nanostructuring. It is easy to use and has been shown to be biocompatible.

4. The developed *FLMP* technique was successfully adapted to be used for the production of microoptical elements. It enables flexible and rapid fabrication of custom geometry microlenses and bi-functional (refractive-diffractive) microoptical components. Possibility to manufacture microoptics on fiber tip was demonstrated.

5. In cooperation with *Vilnius Biochemistry Institute* and *Vilnius University Faculty of Medicine Heart Surgery Center* artificial *3D* polymer scaffolds and templates with required pore sizes for stem cell growth were successfully fabricated. *In vivo* and *in vitro* studies have shown the photostructurable materials to be biocompatible. This implies *FLMP* technique to be perspective for applications in tissue engineering.

5 PhD THESIS

I) A novel automated laboratory *3D* micro/nanofabrication system based on high pulse repetition rate femtosecond *Yb:KGW* laser and precise linear *XYZ* translation stages enables rapid and flexible production of functional micro/nanodevices over a large area with reachable 100 nm spatial structuring resolution.

1) M. Malinauskas, V. Purlys, M. Rutkauskas and R. Gadonas, Two-Photon Polymerization for Fabrication of Three-Dimensional Micro- and Nanostructures over a Large Area, Proc. SPIE 7204, 72040C (2009).

2) M. Malinauskas, V. Purlys, M. Rutkauskas, A. Gaidukevičiūtė and R. Gadonas, Femtosecond Visible Light Induced Two-Photon Photopolymerization for *3D* Micro/Nanostructuring in Various Photopolymers and Photoresins, Lithuanian J. Phys. 50(2), (2010).

II) Using *FLMP* technique self-polymerization of suspended ultrafine fibers (diameter < 100 nm) and membranes (thickness < 100 nm) can be initiated in *AKRE37* photopolymer. Their self-formation can be predicted and controlled by generating excess radicals between support structures under the conditions when the distance between rigid fabricated supports is below the critical ($\sim$1 μm for fibers and up to 15 μm for membranes) and the exposure is below the threshold needed for the irreversible material modification.

M. Malinauskas, G. Bičkauskaitė, M. Rutkauskas, V. Purlys, D. Paipulas and R. Gadonas, Self-Polymerization of Nano-Fibers and Nano-Membranes Induced by Two-Photon Absorption, Lithuanian J. Phys. 50(1), 135-140 (2010).

III) *FLMP* technique is suitable for direct and flexible fabrication of microoptical elements of complex geometry integrating several functions in one component which can be manufactured on various substrates. Surface roughness of the components is $< \lambda/20$ what is sufficient for applications in *VIS* range.

1) M. Malinauskas, H. Gilbergs, V. Purlys, A. Žukauskas, M. Rutkauskas and R. Gadonas, Femtosecond Laser-Induced Two-Photon Photopolymerization for Structuring of Micro-Optical and Photonic Devices, Proc. SPIE 7366, 736622 (2009).

2) M. Malinauskas, H. Gilbergs, A. Žukauskas, V. Purlys, D. Paipulas and R. Gadonas, A Femtosecond Laser-Induced Two-Photon Photopolymerization Technique for Structuring Microlenses, J. Opt. 12(3), 035204 (2010).

3) M. Malinauskas, V. Purlys, M. Rutkauskas, A. Gaidukevičiūtė and R. Gadonas, Femtosecond Visible Light Induced Two-Photon Photopolymerization for *3D* Micro/Nanostructuring in Various Photopolymers and Photoresins, Lithuanian J. Phys. 50(2), (2010).

4) A. Žukauskas, M. Malinauskas, L. Kontenis, V. Purlys, D. Paipulas, M. Vengris and R. Gadonas, Doped Polymeric Microstructures for Optically Active Functional Devices, Lithuanian J. Phys. 50(1), 55-61 (2010).

5) M. Malinauskas, H. Gilbergs, A. Žukauskas, K. Belazaras, V. Purlys, M. Rutkauskas, G. Bičkauskaitė, A. Momot, D. Paipulas, R. Gadonas, S. Juodkazis and A. Piskarskas, Femtosecond laser fabrication of hybrid micro-optical elements and their integration on the fiber tip, Proc. SPIE, 7716-9 (2010).

6) E. Brasselet, M. Malinauskas, A. Žukauskas, and S. Juodkazis, Photopolymerized microscopic vortex beam generators: precise delivery of optical orbital angular momentum, Appl. Phys. Lett., accepted (2010)

IV) High spatial resolution in *3D* structuring can be achieved at near optical damage threshold light intensity conditions in the focus of the laser beam initiating avalanche ionization in polymer materials.

M. Malinauskas, A. Žukauskas, G. Bičkauskaitė, R. Gadonas and S. Juodkazis, Mechanisms of Three-Dimensional Structuring of Photo-Polymers by Tightly Focused Femtosecond Laser Pulses, Opt. Express 18(10), 10209-10221 (2010).

V) Artificial *3D* scaffolds and templates with custom pore sizes and variable geometry for stem cell growth can be fabricated out of biocompatible and biodegradable photopolymers. *In vitro* and *in vivo* experiments revealed that the photostructurable materials are as biocompatible as a glass or a surgery suture, respectively.

1) M. Malinauskas, P. Danilevičius, D. Baltriukienė, M. Rutkauskas, A. Žukauskas, Ž. Kairytė, G. Bičkauskaitė, V. Purlys, D. Paipulas, V. Bukelskienė and R. Gadonas. 3D artificial polymeric scaffolds for stem cell growth fabricated by femtosecond laser. Lithuanian J. Phys., 50(1):75-82, (2010).

2) M. Malinauskas, V. Purlys, A. Žukauskas, G. Bičkauskaitė, T. Gertus, P. Danilevičius, D. Paipulas, M. Rutkauskas, H. Gilbergs, D. Baltriukienė, L. Bukelskis, R. Širmenis, V. Bukelskienė, R. Gadonas, V. Sirvydis and A. Piskarskas. Laser Two-Photon Polymerization Micro- and Nanostructuring Over a Large Area on Various Substrates. Proc. SPIE, 7715:-77151F, (2010).

3) M. Malinauskas, V. Purlys, A. Žukauskas, M. Rutkauskas, P. Danilevičius, D. Paipulas, G. Bičkauskaitė, L. Bukelskis, D. Baltriukienė, R. Širmenis, A. Gaidukevičiutė, V. Bukelskienė, R. Gadonas, V. Sirvydis and A. Piskarskas. Large Scale Laser Two-Photon Polymerization Structuring for Fabrication of Artificial Polymeric Scaffolds for Regenerative Medicine. Proc. ICO-Photonics: Emerging Trends & Novel Materials in Photonics 2009, (in press 2010).

6 PARTICIPATION IN PROJECTS, INTERNSHIPS AND SUMMERSCHOOLS

NATIONAL PROJECTS:

(I) Ministry of Economy special program *"Development of industry, export and business"* project *„Submicrometer precision positioning system for femtosecond laser applications"*, 2006.

(II) Lithuanian National Science and Education foundation High technology program *„Laser microfabrication and prototyping with high repetition rate femtosecond pulses" (FEMTOPROCESSING)*, project *No. B09/08*, 2007-2009.

(III) Lithuanian Science Council *"Artificial tissues for regenerative medicine"*, project *No. MIP-10344*, 2010-2011.

INTERNATIONAL PROJECTS:

(I) European Union project *„Quantum Engineering and Space-Time Research (QUEST)"*.

(II) European Union Marie Curie transfer of knowledge project *„Nonlinear Optical Imaging for Biological Applications (NOLIMBA)"*.

(III) European Union 7-th framework program *"LASERLAB EUROPE"* project. *(LASERLAB-EUROPE, No. 228334, OPTOBIO).*

(IV) European Union 7-th framework program *"Ultra-thin Conductive Ceramic Mesh to Monitor Stress and Wear on a Steel Surface (MesMesh)"* project, 2010-2012.

INTERNSHIPS:

2005 04 – 2005 08, 2007 11 – 2008 01 and 2008 10 – 2008 12: internships in *Laser Center Hannover (LZH), Hannover, Germany.*

2009 09 17 - 12 23: internship in *Foundation for Research and Technology Hellas - Institute of Electronic Structure and Laser (FORTH-IESL), Heraklion, Creete, Greece.*

SUMMERSCHOOLS:

2006 07 10 – 22: summer school on *„Optoelectronics, lasers and applications"* in Crete Institute of Technology and Education, Chania, Crete, Greece.

2010 04 23 – 04 25: training on *"Novel Applications of Lasers in Physics, Industry and Medicine", Institute of Solid State Physics, Riga, Latvia.*

AWARDS:

2008 07 13 – 15: Young Scientist Award for presentation in *"5th international conference on Nanosciences and Nanotechnologies", (NN08), Thessaloniki, Greece.*

2010 05 27-28: Young Scientist Award for presentation in *"Conference of Young Scientists on Energy Issues", (CYSENI 2010), Kaunas, Lithuania.*

7 TECHNIQUES FOR 3D MICRO/NANOSTRUCTURING

Interest in down-scaled functional micro/nanodevices is growing steadily as low-cost and high-efficiency devices are being applied wider in everyday life. During last decades, efforts in improving the fabrication methods of such components have advanced dramatically. *UV* lithography [42], electron beam writing [43], X-ray lithography [44] and NanoImprint Lithography (*NIL*) [45] techniques are widely used for nanostructuring, however, these methods are suffering lack of flexibility, cost efficiency and sometimes are limited in true *3D* structuring. Recently, development of novel less expensive technical routes of *3D* fabrication in industrial applications have emerged. It is represented by ink jet and *3D* printing [46, 47], dip coating [48] and selective laser sintering [49] techniques. However, these methods are lacking fabrication resolution and are limited to usable materials. During last decade a non-linear lithography technique employing ultrafast laser has emerged as *FLMP* [1]. Illustrations showing method's feasibility and flexibility for production of *3D* microstructures are shown in the later chapters. A comparison of *FLMP* and alternative technologies for micro/nanostructuring is given in Table. 7.1.

Direct *3D* writing in photopolymers enables rapid, flexible and cost efficient fabrication of microstructures required in fields of photonics [50, 51, 52], microoptics [53, 54], microfluidics [55, 56], biomedical components [57, 58] and tissue engineering [59, 20]. Compared to its anterior alternative, *UV* μ-stereolithography [60, 61], it offers higher spatial resolution and easier fabrication of true *3D* structures [62, 63]. Novel hybrid materials are expected to ensure higher structuring resolution and control, optimized mechanical, optical and electrical or even magnetic properties [64, 37]. Possibility to selectively metalize these nanostructures provides opportunity to make it applicable in plasmonics or metamaterials production [65, 66, 67, 68].

Table 7.1. *FLMP* among alternative micro-/nanofabrication technologies: the typical dimensions of processing areas, the spatial resolution limit, the typical throughput, the typical costs per fabricated part, and the flexibility to fabricate different structures as well as *3D* structuring possibility.

Technology:	Processing area	Resolution	Throughput	Cost per sample	Flexibility	*3D* structuring
Optical lithography	wafer	30 nm	rapid	low	low	no
NIL	wafer	10 nm	rapid	low	low	no
Self-assembly	wafer	100 nm - 1 μm	medium	low	low	low
Ink-jet Printer	cm	50 - 100 μm	medium	low	medium	medium
μ-stereolithography	cm	10 - 100 μm	medium	medium	medium	medium
fs laser ablation	mm/cm	1 - 50 μm	medium	medium	high	no
FLMP	**mm**	**100 nm - 10 μm**	**medium**	**medium**	**high**	**high**
e-/ion-beam lithography	μm	10 nm	low	high	high	medium
AFM printing	μm	10 nm	low	high	medium	no

Using *FLMP* technique, near 100 nm spatial structuring resolution was demonstrated [69, 70, 71] (prototype systems are already commercially available [72, 73, 74, 75]), but the structures were not much bigger than several tens or hundreds of micrometers. It complicates the nano-featured microstructures practical applications or even characterization of their properties. This implies that demand of *3D* micro/nanostructures over a large area is still high [76, 77, 78]. For example, larger *PhCs* or microlens arrays can increase their applicability; artificial scaffolds have to be big enough for the biologist or surgeon for comfortable handling.

8 FEMTOSECOND LASER MULTIPHOTON POLYMERIZATION TECHNIQUE

Nowadays, photopolymerization is an indispensable part of industrial processing for vast variety of everyday used and hi-tech products. Yet, the history of modern applications of photopolymerization on the industrial scale is relatively short compared to metallurgy and wood processing. First commercial applications of this technique in coatings started in early 1960s. Many new material systems, fitting a wide variety of possible industrial applications, were soon developed. Appropriate equipment allowing fast material photo- and thermocuring providing control over the process on the industrial scale was introduced. In 1980s application of this technique expanded till the wide acceptance in the industry as a rapid prototyping technology based photopolymerization. Stereolithography, also known as *3D* printing, a technique allowing to create complex *3D* models from photosensitive materials, soon was followed by μ-stereolithography which in accordance to provided *CAD* design enabled to produce objects at microscale [79]. Polymerization is defined as a process of reacting monomer molecules together in a chemical reaction to form three-dimensional networks or polymer chains. It can be initiated via energy introduced from light or heat. The photopolymerization is defined as the light-induced chemical reaction of monomers or oligomers that results in a solid polymeric network. Modern material systems for photopolymerization contain two main components: a photoinitiator and a monomer (or a mixture of monomers and oligomers). Photoinitiators are the molecules which have low photo dissociation energy

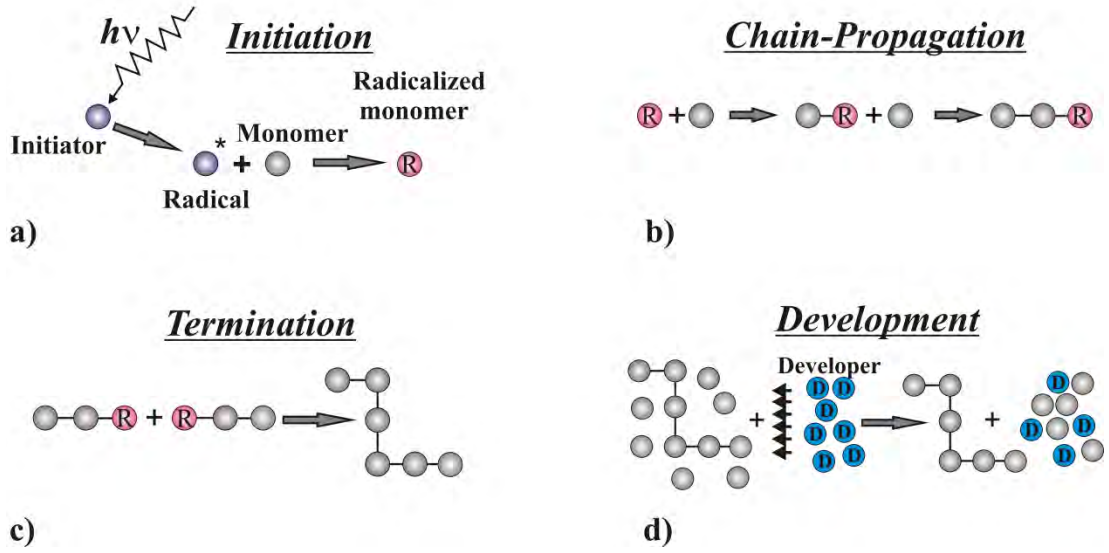

Fig. 8.1. Photochemistry of laser microfabrication Photoinitiator molecule absorbs a photon and turns to a radical (a); then it radicalizes monomer and triggers chain-propagation reaction (b); when two radical-monomers meet the chain propagation is terminated (c); during development process the non-polymerized part of the material is washed out leaving only insoluble polymer chains (d).

and are added to increase the material photosensitivity. Photopolymerization reactions that form a cross-linked network follow the characteristic steps of any chain polymerization mechanism: photoinitiation, propagation and termination (8.1a)-c)). Then the sample is immersed in the developer bath to selectively remove the non-polymerized part of the material (8.1d)).

Photopolymerization is advantageous compared to thermal or mechanical polymerization routes due to the provision of spatial and temporal control of the initiation reaction through control of illumination conditions. Thus point by point structuring enables "*materialization*" of *CAD* model out of the photopolymer as shown in Fig.8.2. It is worth mentioning that most of the photopolymers have just a slight change in refractive index and, thus, enables further structuring focusing the beam through the already produced structure. Additionally, some hybrid or epoxy materials are in gel or solid state while being processed and the photomodified areas are not floating being fixed in space. This lets to flexibly choose the starting and the ending point of the scanning without any restrains which is sometimes convenient for specific geometries.

However, it still has drawbacks such as structure shrinkage and geo-

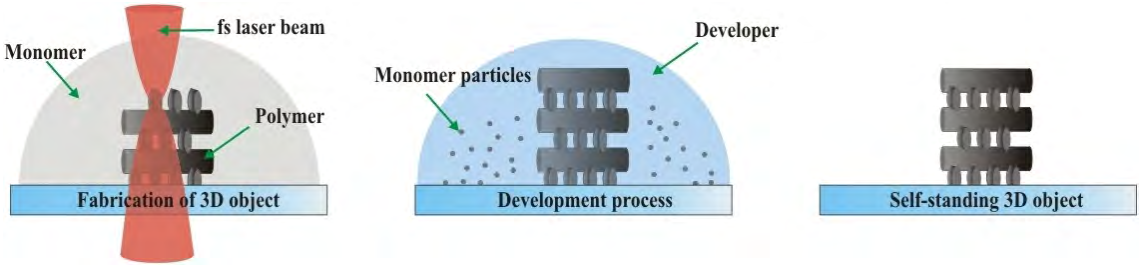

Fig. 8.2. Fabrication steps. The structure is inscribed in a point-by-point manner, as the localized photomodification follows the scanned contour of the focussed beam. It changes the materials solubility, after the developing a free-standing *3D* structures can be obtained.

metrical deformations. Shrinkage is a result of material densification compared to the original material formulation before polymerization. Since the amount of material before and after polymerization does not change, this density change will result in volume reduction corresponding to shrinkage [80]. Geometrical deformations occur when the structure is not rigid enough to withstand the developing and drying process. It is known, that the material rigidity is proportional to the volume of the material. So, at microscale ir would mean that 10 times smaller feature would be 1000 ($\sim 10^3$ lesser in volume) times fragile/soft. This become crucial when getting near to 100 nm spatial resolution in *3D*. One more issue which is important for the structure formation is the bulk material hardness. Usually it is better to apply harder material (with higher *Young's* modulus) in order to achieve lesser distortions, yet if the overall structure size increases, the material densification caused stress can induce mechanical cracks to release the accumulated tension. These questions are explained in a more detailed manner in *Chapter 11*.

Femtosecond Laser Multi-photon Polymerization is a *DLW* technique employing point-by-point photomodifying of the resin in *3D* space. It comes as a novel *μ-stereolithography* technique employing non-linear light-matter interaction (an analogue to laser scanning multiphoton microscopy). Resolution of the structured features is defined by the above threshold intensity distribution in the volume of the tightly focused laser beam waist. Precisely varying light intensity within the so called *"fabrication window"* allows fine tuning the *voxel* size. Fabrication window is defined as the I_d/I_t ratio, which is intensity of material optical damage divided by threshold intensity

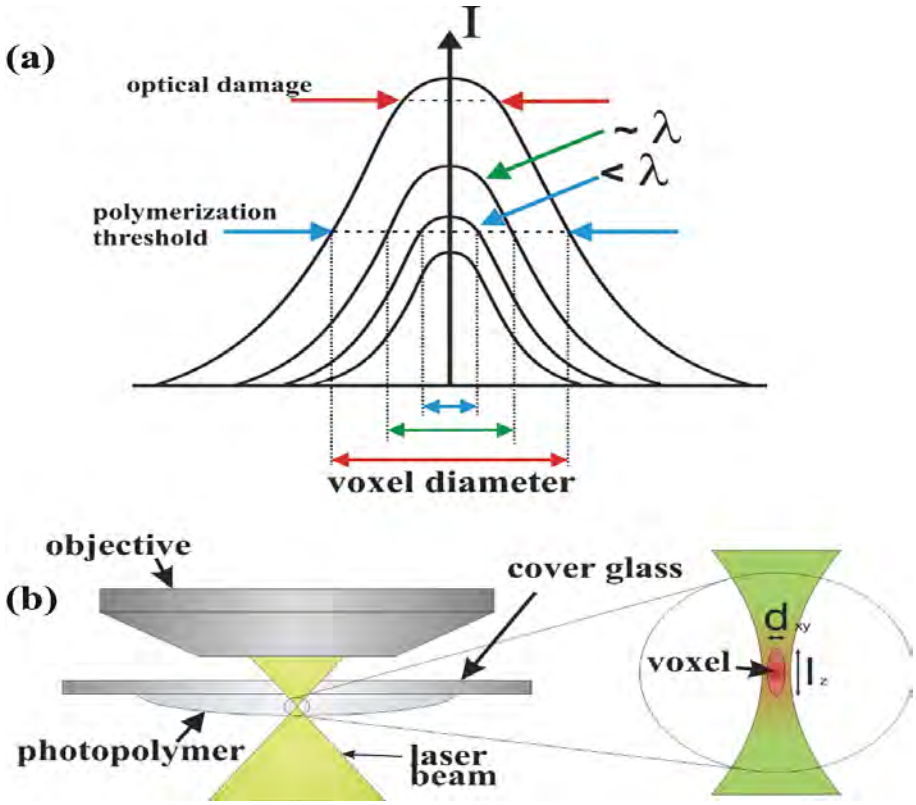

Fig. 8.3. a)*Fabrication window and sub-wavelength resolution.* Fabrication window defined as I_d/I_{th}. By precise adjusting introduced laser intensity I one can tune the voxel dimensions and overcome diffraction limit corresponding to applied laser light wavelength. b) *Voxel size and aspect ratio.* Voxel size follows light intensity distribution and has form of ellipsoid.

required for the polymerization (Fig.8.3a)). Wider fabrication window ensures easier photostructuring and enables to tune the voxel size by changing the laser intensity I (Fig.8.3). By moving the sample relatively to the fixed focus spot one can photomodify the material along the scanning direction. Later, the negative photopolymer (usually a droplet on a substrate) is developed in organic solvent and all the unexposed pre-polymer is washed out revealing a free standing *3D* structure.

The simultaneous excitation mechanism involves a virtual intermediate state which is created by the interaction of first photon and the second photon is absorbed only if it arrives within the virtual state life time of 10^{-15} s [81]. For this it is imperative to have a high intensity source that would ensure that the second photon arrives within the life time of the virtual state. In the case of *TPA*, the electron transition is induced by two photons, each with half the required energy of the gap between the two

energy levels. This condition can be easily fulfilled when ultrashort light pulse lasers (usually ∼100 fs or less) are used. The laser beam is closely focused with a high numerical aperture objective lens into a volume of a photocurable resin creating highest photon densities within the vicinity of the focus. Since two-photon absorption rate has a quadratic dependence on the photon density profile, the integrated photosensitive material response is greatly enhanced at the focal spot. The two-photon absorption cross-section is generally extremely low, so a very high spatial resolution beneath the limit of diffraction of the light used in the *FLMP* process can be realized. On focusing a high intensity laser closely into the volume of a liquid or gel state photoresin transparent to *VIS* or *NIR* light is absorbed by the photoinitiator molecules which generate free radicals (initiation). The radicals react with monomers producing monomer-radicals, so the monomer-radicals expand in a chain reaction (chain-propagation) until two radicals meet (termination). The irreversible photopolymerization reaction efficiency is proportional to multiphoton absorption rate and occurs only in the region where light intensity is above the threshold required for the polymerization $I > I_{th}$.

$$d = w_0\sqrt{2\frac{1}{N}ln\left(\frac{I}{I_{th}}\right)}; \tag{8.1}$$

$$l = 2z_R\sqrt{\left(\frac{I}{I_{th}}\right)^{\frac{1}{N}} - 1}; \tag{8.2}$$

here, d and l is voxel diameter and length, w_0 is beam waist at the focal position, z_R is *Rayleigh range*, N is the order of absorption nonlinearity. A volumetric pixel (*voxel*) is considered to be the smallest repeating element which adds up to make a *3D* structure. On the focal spot initial voxels take the shape of the intensity distribution of the focused laser beam. The voxel growth follows the prolonged exposure in all directions uniformly and becomes especially enlarged along the intensity distribution with an increase in applied laser power. The voxel expansion is radical diffusion-dependent process. The effect of variation of power and exposure time on the growth of voxels to formulate the scaling laws for voxels has been studied in details [82]. Though the final dimensions of photomodified region depend on the

spatial light intensity profile, material response including total exposure dose, photoinitiator concentration and pulse repetition rate has to be taken in account especially at the close-to-threshold conditions:

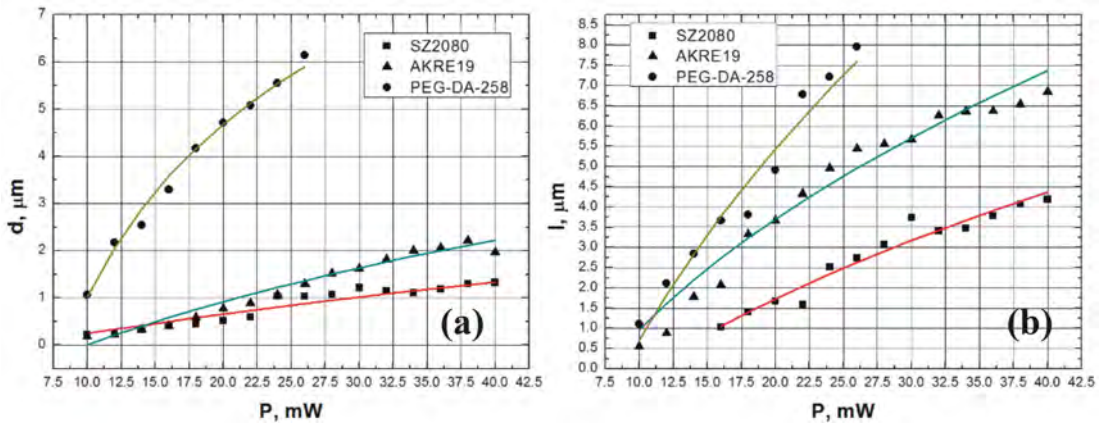

Fig. 8.4. FLMP resolution graphs. Voxel diameter d (a) and length l (b) versus applied laser power P in different used photopolymers.

$$d = \frac{\lambda}{NA}\sqrt{ln\frac{I_0^N t\beta\tau\nu}{I_t}}; \tag{8.3}$$

$$l = \frac{2z_R}{n}\sqrt{exp\left(\frac{1}{2}\left(\frac{dNA}{\lambda}\right)^2\right) - 1}; \tag{8.4}$$

here, τ is exposure time, β is experimentally derived constant (photoinitiator two-photon absorption cross-section , concentration and quantum efficiency), τ and ν are laser pulse duration and repetition rate, n is refractive index of the photosensitive material. Theoretically calculated and experimentally measured resolutions (voxel sizes) are graphed in 8.4. It is evidently seen that achievable structuring resolution (as well as aspect ratio of the voxel) greatly depends on the material properties.

Using this technique outstanding periodic and non-periodic micro/nanostructures can be obtained as shown in Fig.8.5: a) 65 nm width diameter polymeric nano-fiber from *AKRE37* photopolymer. b) Photonic crystal (face cubic centered woodpile structure) having lateral period and line resolution 1.5 μm and 0.45 μm, respectively. c) Four layers of nano-chain-

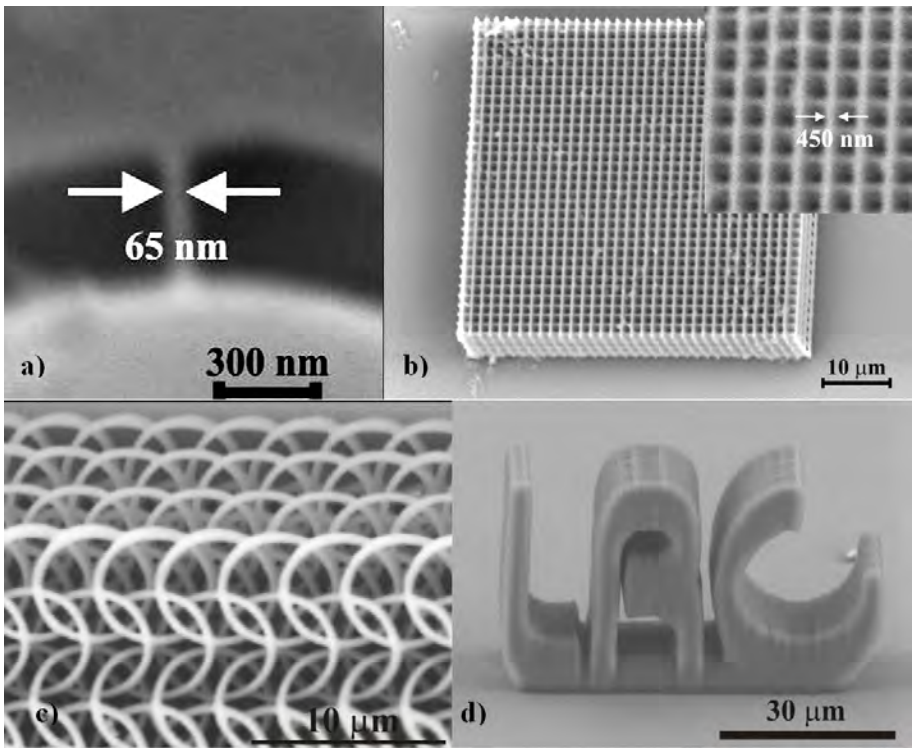

Fig. 8.5. Sample micro/nanostructures fabricated by FLMP method.

mail structure out of intertwined rings, ring radius 2.5 μm, brim thickness 400 nm. d) Free standing micro-letters *LRC* (corresponding to *Laser Research Center*). b, c and d are produced out of *SZ2080* hybrid photopolymer. They can be used in vast variety of scientific and industrial applications where *3D* functional microobjects or templates are required.

The fields of applications has expanded dramatically since the first experimental demonstrations of the principle itself to nowadays *FLMP* micro/nanostructuring. Capability of this technique to create complex *3D* structures with resolution, reproducibility and throughput superior to other approaches has established this young technology as a serious and sometimes unique. The interest in the *FLMP* has been continuously growing from both sides, the fundamental and technological and there still a lot of room for improvement of both.

9 EXPERIMENTAL FABRICATION SYSTEMS

9.1 *Yb:KGW* laser fabrication setup

In our experiments we have used *AltSCA (Altechna Co. Ltd.)* positioning system designed for fast and precise laser microfabrication in *3D* space for scientific and industrial applications. Amplified *Yb:KGW* femtosecond laser system *Pharos (Light Conversion Co. Ltd.)* with tunable repetition rate from 1 to 200 kHz, average power 6 W, 280 fs pulse duration, 1030 and 515 nm (second harmonic) wavelength was used as an irradiation source. The experimental setup used for *FLMP* nanostructuring is shown in Fig.9.1. The expanded femtosecond laser beam is guided through objective, focusing it into the volume of the photoresin. The sample is mounted on large area XYZ positioning stages. By moving the laser focus inside the photoresin one is able to write complex *3D* structures. Since, upon irradiation the resin undergoes transition from liquid to solid (or from gel to solid), wide-field transmission microscopy is used to monitor the process of *FLMP* in real time. The *CMOS* camera *(mvBlueFOX-M102G)* enables online fabrication supervision. The ability to image the sample while performing *FLMP* is an important feature for a successful fabrication process. It is of utmost importance to anchor the microstructures to the substrates if they are to survive the washing step of the unsolidified resin. The pin-point structuring has no restrains since the polymerized material is still highly transparent to *NIR* or *VIS* laser light. The positioning system consists of linear motor driven stages *(Aerotech, Inc.)*: *ALS130-100* for XY, *ALS130-50* for Z. These stages ensure an overall travelling range of 100 mm into XY dimensions and 50 mm in Z dimension as well as support sample translation speed up to 300 mm/s. The system can be used for rapid *FLMP* structuring in various photosensitive materials at large scale with reproducible feature sizes

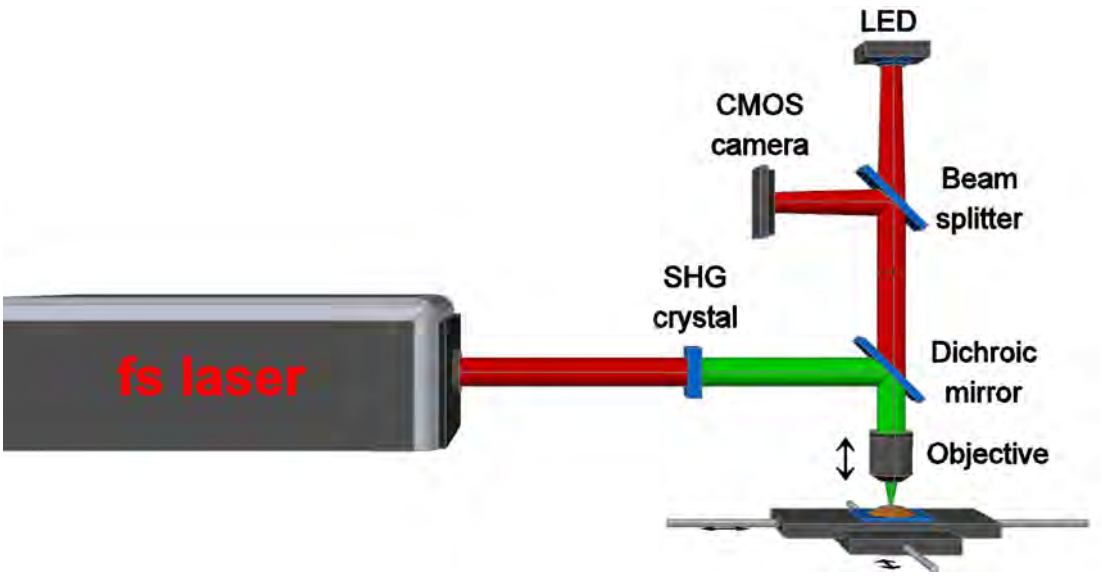

Fig. 9.1. *3D* fabrication setup. fs pulsed *IR* light is frequency doubled propagating through Second Harmonic Generation element (*SHG*, nonlinear crystal). Dichroic mirror is used to guide the laser beam, which is tightly focused by microscope objective into the sample which is translated using XYZ stages. *LED* light illuminates the sample and is collected for real time fabrication imaging on *CMOS* camera.

as small as 200 nm (achievable up to 150 nm or even higher). The ability to scale up and speed up the fabrication is offered by simply changing the laser beam focusing objective. In this work, several microscope objectives were used and corresponding fabrication resolution was measured. Control of all equipment is automated via *3D-Poli* computer software specially designed for *FLMP* applications.

Using this fabrication method 200 nm spatial structuring reprocibility can be be achieved as a free-hanging line *3D* structure (Fig.9.2a)) or a line on a substrate as a *2D* structure (Fig.9.2b)) out of the most materials suitable for *FLMP*.

9.2 *Ti:Sapphire* laser fabrication setup

Alternative to the first system a *Ti:Sapphire* oscillator system *Tsunami, Spectra Physics* providing 800 nm irradiation wavelength 80 fs pulses at 80 MHz repetition rate combined with the positioning system consisting of three micrometer-step motor stages *(Standa Ltd)* stacked on each other and piezo nanopositioning stage *(Nanocube, Physik Instrumente GmbH)* mounted on was used. The step motor stages are used to increase fabrication

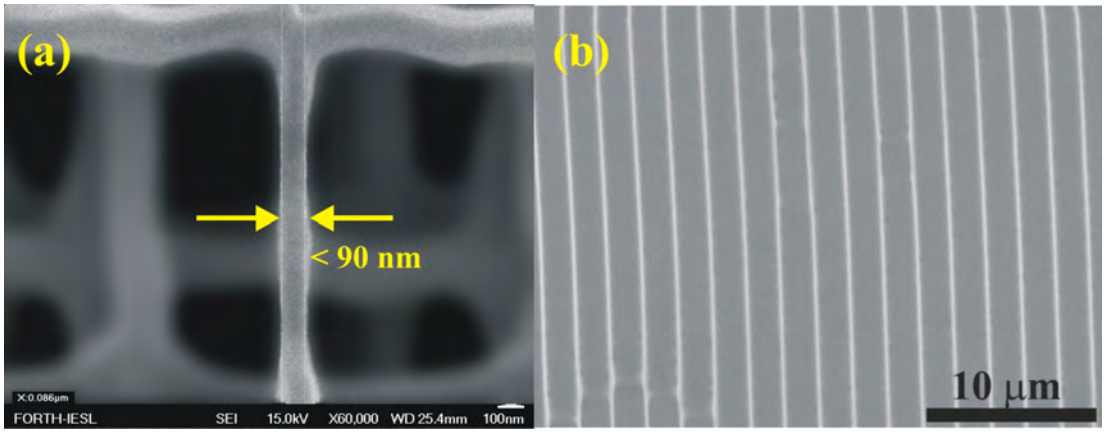

Fig. 9.2. FLMP structuring resolution. A suspended line of sub-90 nm width out of *Ge* containing sol-gel hybrid material (a); 200 nm reproducible lines on a glass substrate out of *SZ2080*, (b).

field were the structures will be localized on the substrate while the piezo stage ensures precise fabrication of the microstructure. The positioning resolution of piezo stage is 1 nm. The exposure time is controlled by a home-made mechanical shutter with a stable response time of up to 5 ms. The main difference from the first system is the irradiation wavelength and pulse repetition rate as well as positioning hardware.

9.3 Other laser fabrication setups

The adequate systems used in the *LZH* and *FORTH* differed mainly for using galvo-scanner for a beam guiding instead of the sample translation. Femtosecond laser pulsed irradiation (60 fs/20 fs, 90 MHz/75 MHz, 400 mW, 780 nm/800 nm, *Fusion, Femtolasers/Chameleon, Coherent, LZH/FORTH*, respectively) was tightly focused into the volume of a photosensitive resin, galvo-scanner (*Hurryscan II, Scanlabs*) enabled fast and precise beam deflection, however, limited processing field (∼40x40 μm^2 in case of 100x objective was used and up to ∼800x800 μm^2 if 20x objective was used). *AOM* or mechanical shutter was used for a beam blocking when needed. Shorter pulses (sub-20 fs) provided higher pulse peak power thus enabled reduction of average applied laser power. This was beneficial for ultra-precise structuring ($<$ 200 nm) and enabled to process wider range of materials.

9.4 Sample characterization

The samples depending on the structure, geometry and substrate were characterized by: transmission and reflection optical microscopies (various microscopes), optical (*PLμ 2300, SENSOFAR*) and *AFM* profilometries (*Scanning Probe AFM Dimension 3100, Digital Instruments*), and *SEM* (various *SEMs*). For high quality *SEM* analysis, the samples were coated with a 10-50 nm thick *Au*, *Ag* or *Cu* layer in order to increase their electro-conductivity.

10 PHOTOSENSITIVE MATERIALS

Photosensitive materials are divided into negative and positive tone. The exposed volume of the negative resists undergoes photomodification and becomes insoluble in developer. Unexposed material is removed during the sample development (Fig. 8.2), thus revealing the *DLW* inscribed object. In the case of positive resists the light induces dissociation (photochemical bond breaking) of the molecules in the irradiated volume. Here exposed material is removed during the development step. Conventionally, for μ-stereolithography (so, also for *FLMP*) negative resists are mostly used. In this work only negative photoresins were tested, though *FLMP* enables positive to be used as well if needed. Samples for the fabrication were prepared by drop-casting or spin-coating the pre-polymer on a substrate (cover glass, metal plate or plastic pad). It is recommended to clean the substrates with acetone and heat prior to covering it with the polymer to avoid organic material traces and water. Adhesion promoter for eg., *MATPMS* (*methacryloxypropyl trimethoxysilane*) can be used to improve the structured polymer adhesion to the substrate. After the exposure the sample is immersed in the bath of adequate developer. Additional rinsing or *UV* fixation can be applied if needed. Solid by it's nature materials mixed with the solvent have to be pre-exposure-baked to evaporate it, some of them need a post-exposure-bake. In this work an acrylate based *AKRE*19/23/37 [83, 84, 85, 86], epoxy based *SU-8 (Gersteltec)* [87, 88, 89], hybrid organic-inorganic *SZ2080* (*FORTH*) [25, 90, 64] and *Ormocore b59* (*Micro Resist Technology GmbH*) [91, 92, 93], and acrylated biodegradable *PEG-DA-258* (*PolyEthylenGlycol Di-Acrylate* of *M.w.* = 258, *Sigma-Aldrich GmbH*) [94, 95, 96] photosensitive materials were used. The prepolymers were photosensitized by adding 0.5-2 wt.% of *thioxanthen-9-one, 2-benzyl-2-(dimethylamino)-4'-morpholinobutyrophe-*

Table 10.1. Photosensitive pre-polymer materials.

Material	Chemical formula	Developer	Developing time	Shrinkage	Reached resolution
AKRE 19/23/37	$C_{18}H_{21}N_3O_9$	ethyl alcohol	20 min	medium	< 100 nm
SU-8	$(CH_3)_2C(C_6H_4OH)_2$	*PGMEA*	30 min	ultra-low	< 100 nm
Ormocore b59	$C_4H_{12}Si_2O_2$	*MIBK*: isopropanol (1:1)	30 min	medium	∼200 nm
SZ2080	$C_4H_{12}SiZrO_2$	*MIBK*: isopropanol (1:1)	30 min	ultra-low	∼120 nm
PEG-DA-258	$C_8H_{10}O_4$	water	1 min	high	∼300 nm

none or 4,4'-bis(dimethylamino)benzophenone (*Michler's ketone*) photoinitiators (*Sigma-Aldrich GmbH*). *Ormocore b59* and *SU-8* were used as received from the manufacturer. To increase the functionality of the materials, they can be chemically bonded or doped with inorganic or organic ingredients upon demand [97, 98]. *PolyDiMethylSiloxane (PDMS, Sylgard 184, Dow Corning)* [99] was used as an elastomer material for replication. Chemical formulas and developers for the used materials are listed in Table 10.1.

All the materials are highly transparent for *VIS* and *NIR* light, so *3D* photostructuring in thick layers (high structures) can be realized. Also, it makes the microstructures to be applicable in the field of optics.

10.1 Acrylate based materials

Acrylates were the first materials which were tested for *FLMP* structuring. Up to date the highest resolution reaching tens of nanometers is achieved in them [9, 100, 70]. They high photosensitivity makes them easy structurable. They are could be widely applicable due to the low price. The majority of acrylate resins are in liquid form before processing. However, the pure acrylate and mixtures of acrylates are relatively high shrinking materials, thus

demanding a *CAD* model precompensation [101]. The home made acrylate material *AKRE* used in this work composed of commercially available ingredients. *Tris (2-hydroxy ethyl) isocyanurate triacrylate* (*SR368, Sartomer Company, Inc.*) is a polymer that is attractive for its properties like strength without brittleness, low skin irritation, and good chemical adhesion [86]. It was easily blended with desired radical photoinitiator needed to tune the material to the laser irradiation wavelength. Thus the name of the material *AKRE19*, *AKRE23* and *AKRE37* corresponds to the added initiator *thioxanthen-9-one, 2-benzyl-2-(dimethylamino)-4'-morpholinobutyrophenone and 4,4'-bis(dimethylamino)benzophenone*, respectively.

10.2 Epoxy based materials

A prominent example of epoxy organic photoresist applied for *FLMP* fabrication is *SU-8* developed by *IBM* [102]. The *SU-8* is supplied as a viscous liquid consisting of an epoxy resin, a solvent (*gammabutyrolactone* or *cyclopentanone* depending on manufacturer's formulation) and a photoacid generator (*triarylsulfonium hexafluoroantimonate salt*). It is photocrosslinked by cationic route as photo-acid is generated in the irradiated volume. *SU-8* (*Gersteltec Sarl*) is widely used in conventional *UV* lithography. During pre-exposure-bake the solvent is evaporated and the material becomes solid. Here it is important to achieve a uniformly dry layer, since inhomogeneities will lead to undesirable variations of photopolymerization threshold. Prebaking conditions have to be adjusted in accordance to the layer thickness. Cross-linking occurs during the post-exposure-bake step, when a temperature is raised to 100^0C. A great advantage of *SU-8* material for *FLMP* processing is no noticeable shrinkage. Also *SU-8* material is processed in a solid form, and the produced pattern is immobilized throughout fabrication step. Therefore highly complex interconnected/interlocking structures can be produced easily. This is particularly advantageous for fabrication of moving micromechanical components. A certain disadvantage is that *SU-8* requires a multistep preparation and processing. By *FLMP* technique suspended rods with lateral size down to 30 nm have been produced [6] and periodic structures with 150 nm [103] have been successfully fabricated out of *SU-8* epoxy material.

10.3 Hybrid organic-inorganic materials

The hybrid materials can be classified in *ORMOCERs* (ORganically MOdified CERamics) and *ORMOSILs* (ORganically MOdified SILicas). Both of them have inorganic part containing *Si*, yet *ORMOSILS* also have metal-isopropoxide ingredient. In both materials, methacrylate functional groups are responsible for cross-linking of monomers. During photopolymerization they are cross-linked and form a dense *3D* network, the final product by its properties is similar to glass. The physical and chemical properties of the final material can be tailored by choosing appropriate precursors and synthesis conditions. The mechanical rigidity and thermal stability can be increased by increasing the inorganic content in the hybrid network. Furthermore, sol-gel materials provide the possibility of the incorporation of various functional groups by using a guest–host approach.

ORMOCER class materials are known as biocompatible photopolymers and were introduced for optical applications. *ORMOCERs* contain a highly cross-linkable organic network as well as inorganic components resulting in high optical quality and mechanical as well as thermal stability. The polymerization process is initiated by the reaction of the radical photoinitiator (*Irgacure^{TM} 369, Ciba*) [104]. Recently, it has been studied intensively for *FLMP* nanostructuring by *Hannover Group* [14, 52, 93]. The concept of hybrid materials is that they combine properties of organic polymers such as toughness, easy functionality, and processing at low temperatures with those of glass-like materials such as hardness, chemical and thermal stability, and optical transparency. The refractive index of *ORMOCER* materials may be adjusted in the 1.47-1.56 range [91]. Due to their superior optical properties and ease of processibility *ORMOCERs* are now widely applied for optical interconnects and multi-chip module assembly. They are conventionally patterned by *UV* lithography or nanoimprinting. Applying *FLMP* technique < 200 nm structuring spatial resolution has been reached [14, 105]

In general *ORMOSILs* can contain *Zr, Ti, Al, Ge, V* or other metalic ingredients. *Zr* containing *ORMOSIL SZ2080* has been specially designed for *FLMP 3D* micro/nanostructuring and synthesized by *Heraklion Group*. Most importantly the properties of the synthesized materials can be modified in accordance to the structuring technique's demands or for the final application. By adjusting the synthesis conditions materials exhibiting

ultra-low shrinkage and negligible geometrical distortions occuring during the development were realised [106, 25, 37]. Additional dopants such as non-linear chromophores, quantum dots or organic dyes can be introduced easily [26, 107, 97], thus increasing their functionality. Being by design optimized for high resolution quality structuring these materials are photostructurable up to 120 nm resolution. These properties make such materials especially attractive in the fields of photonics and metamaterial production. As it is presented in *Chapter 14*, the biocompatibility *in vitro* and *in vivo* of *SZ2080* has been shown to be comparable (not worse) than that of surgical suture [108].

10.4 Biodegradable materials

A variety of biocompatible as well as biodegradable materials can be cured by *UV* light or laser [109], thus *3D* microstructured by *FLMP* [20]. An example of biodegradable organic photopolymers are *Poly(Ethylene Glycol)'s* (*PEGs*). *PEGs* have been proven to be non-toxic and they are widely used as dispersants in commercial products, such as tooth paste, soft drinks, shampoos and creams [110, 111, 112]. *PEG* molecules are usually functionalized with acrylic groups in order to produce a photosensitive resin, processible via free-radical polymerization, what enables photopolymerization structuring. *PEG-DA* (Di-Acrylated *PEG*) is well known material in biomedicine [113, 114, 115]. *PEG-DA* molecular mass usually is in the range of 200 to 20 000. Recently, in *Hannover* [94, 116] and *Vilnius* [95] these materials have been explored for *FLMP* micro/nanofabrication. *PEG-DA's* with molecular mass of ∼200-700 were found to be suitable for *3D* photofabrication. The degradation rate of the materials in a living organism depends on the molecular weight, mass of the material and surface area (filling ratio and geometry). As most of the photopolymers *PEGs* can be additionally functionalized with various biomolecules and proteins in order to selectively influence specific biological processes. Flexible material content and geometry tuning at microscale enables one to create the *3D* scaffolds with desired features to control cell growth and proliferation. This is in the scope of interest for the cell growth experiments and tissue engineering. Since, being biodegradable, *PEG-DA's* can be used for drug release and micro/nanostructurization can be a way to control the sustain.

Up to date sub-micrometer resolution has been achieved in *3D* structuring of *PEG-DAs* [80, 117].

11 EXPERIMENTAL

11.1 Limitations and optimization of *FLMP* fabrication

It is obvious that for the nanostructuring precise sample positioning is indispensible. When a *CMOS* or *CCD* camera is applied for online monitoring of the fabrication process it is not complicated to find the correct focal position along depth coordinate z. Yet this is hardly can be kept constant moving the sample laterally. While scanning along X or Y axis the deviation of Z positioning will be inevitable. This means that the structure might be partly *"buried"* in to the cover glass (substrate), not touching the substrate or even be out of the photopolymer. The situation is illustrated in Fig. 11.1a). The real sample structure suffering from this type of fabrication distortion when the substrate surface was not parallel is shown in Fig. 11.1b). The importance of this problem grows as structure size (actually, area not volume) increases. To solve this problem we have used z pre-compensation integrated in our *"3D Poli"* microfabrication software. It is based on passive autofocus realized by first determining coordinates at three points on substrate surface and then getting the equation of substrate surface plane. The determination of each focal position corresponding to the substrate surface is realized monitoring online fabrication of the micro/nanostructures with *CMOS* camera. Precompensation of z coordinate during direct laser writing ensures the focus position with 1 - 2 μm precision if sample is not bended. That is enough for the most of the cases.

Despite extensive development of photopolymers suitable for the fabrication of *3D* micro/nanostructures, it is still challenging to produce a larger structure without any kind of geometrical distortions due to the material densification while photocuring and postprocessing. It has been shown that shrinkage plays an important role in the fabrication of tiny structures with

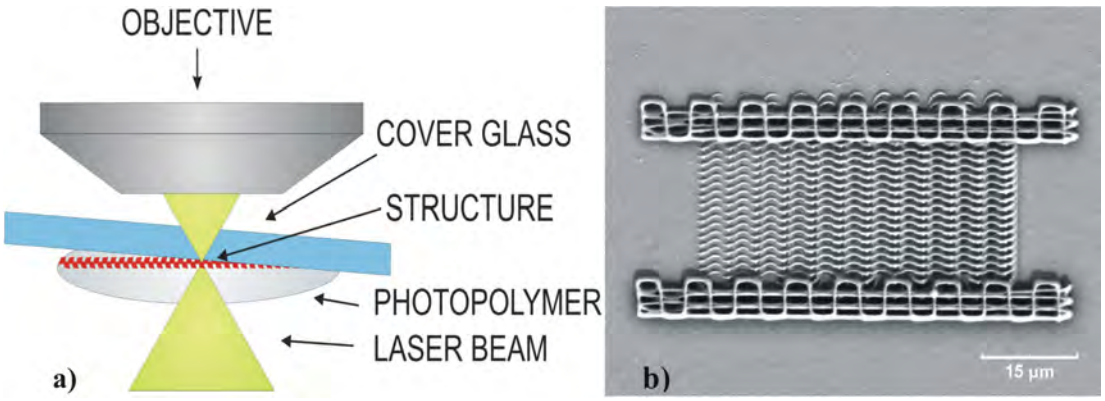

Fig. 11.1. Sample non-flatness problem. Common sample positioning and routine problem of substrate being not perpendicular to laser beam. While moving along X or Y axis it causes deviations in Z coordinate and part of the structure can be not touching the substrate or buried in the substrate.

features of high resolution [70, 62]. However, shrinkage itself also introduces additional challenges in the free-form fabrication of complex structures. This is the side effect of working in the sub-diffraction spatial resolution regime: when the polymerized volume is minimized, the monomer-to-polymer conversion rate is also reduced. It decreases the rigidness of the structures. Additionally, the finer are the structural elements, the more sensitive they are to capillary forces and it is a very challenging task to remove the unexposed resin without distorting the fabricated structures [118, 119]. Schematic sequence of these problems is shown in Fig. 11.2.

One more aspect which should be mentioned when discussing structuring over the large areas is material cost. It is worth to mention that most of the commercially available materials usually cost up to few Euros a gram

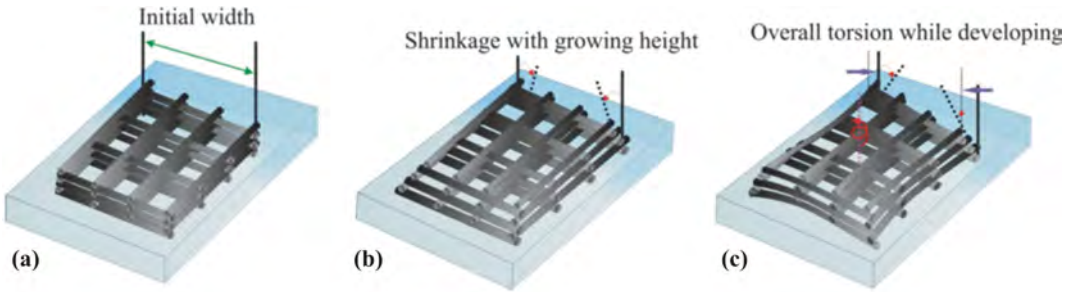

Fig. 11.2. Structure distortion occuring during fabrication: the initial width (a) is reduced because of material volume shrinkage (b) and deformation due to drying developer introduced capillary forces (c).

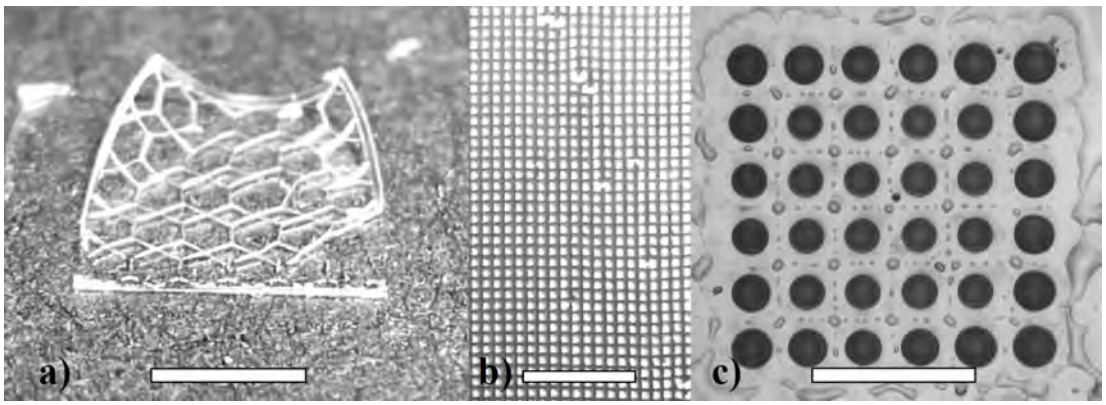

Fig. 11.3. Illustrations of polymer structure deformation. Shrinkage and breakage of millimeter scale structures. Scale bars represent 2 mm for a), 0.5 mm for b) and c), respectively. a) 4x4 mm hexagonic structure out of *Ormocore b59* is distorted due to shrinkage. b) Breakage of large scale micro-grid produced out of *AKRE19* photopolymer. Due to tension forces breakage appears to release tension. c) Structure of *Ormocore b59* keeps the initial form due to separation of structural elements.

or more. It is negligible if only a droplet per sample is used. However, fabricating larger structures the importance of material cost will be increased significantly. As a cost-effective solution we have proposed to use a negative photosensitive material *AKRE19/23/37* which is much cheaper (∼200 times) comparing to commercially available photopolymers. As it has been shown earlier by our group, it is suitable for fabricating *3D* structures with high resolution [120, 85]. The photoinitiator can be added corresponding to laser's irradiation wavelength, so it can be *"tuned"* to fit the applied laser. The photopolymer is a highly viscous liquid which makes it suitable for *FLMP* applications. However, when fabricating micro/nanofeatured structures over a large area shrinkage seems to remain a serious problem. Since polymerization is the process of material densification, the shrinkage is inevitable. The solution to use *"non-shrinking"* materials seems to be case sensitive depending on the structure geometry. Fig. 11.3 shows three millimeter size structures of different geometries representing three different cases of distortions created by tension forces.

Table 11.1 shows the voxel lateral size limit dependence on focusing objective. Voxel diameter was fine-tuned by adjusting applied average laser power (corresponding to light intensity at the vicinity of the focus at the same focusing conditions), minimal and maximal diameters were estimated from *SEM* micrographs. It is seen that voxel size varies few times depending

on applied laser power and it can be modified significantly by changing the objective. Such resolution tuning can fit different demands for versatile applications.

Table 11.1. Obtained structuring lateral resolution using different focusing objectives (M - magnification of the used microscope objective, AR - aspect ratio of lateral and axial *voxel* dimensions). Applied laser irradiation wavelenght was 515 nm. Values are just orientational as the specific value depends on material, photoinitiator and sample translation velocity.

M	NA	x, μm	AR
100x	1.4	0.2 - 0.5	1:3
40x	0.65	0.4 - 1	1:5
20x	0.5	0.7 - 2	1:7
10x	0.25	2.5 - 15	15

To calculate time needed for fabrication of a specific structure one can use a simple estimation:

$$t = \frac{xyzF}{Rv}$$

where t is fabrication time, x, y, and z are width, length, and height of the structure, R is structuring resolution depending on the NA of the used objective and applied laser power P, v is sample scanning speed, and F is fill factor (the ratio of polymerized versus non-polymerized volume of the whole structure). It is seen that the increase of structure volume dramatically increases the fabrication time as well as fill factor F does. Through changing to appropriate optics and applying high sample scanning velocity it is possible to produce a relatively large in filled volume structure in less time. For example, fabrication of woodpile structure with lateral and axial period of 8 and 2 μm, respectively, having overall structure size of 800×800×40 μm^3 and roughly 0.5 filling ratio, scanning the sample at 1000 μm/s speed would take just 25 min using a $NA = 0.25$ objective. Using $NA = 1.25$ it would take up to 7 h to fabricate an identical structure. However, if huge volumes are needed to be polymerized and high feature resolution is required, a sophisticated strategy to overcome the drawback of time consuming fab-

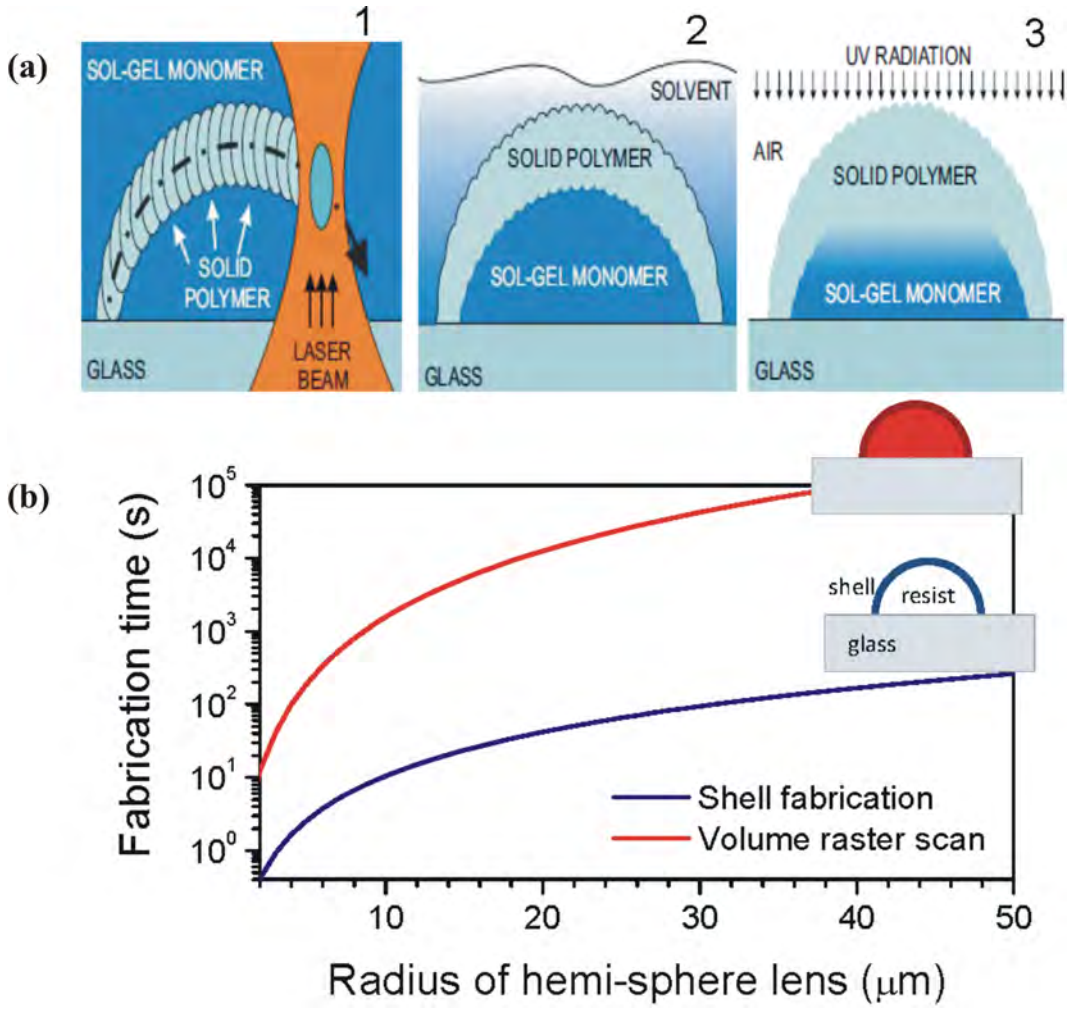

Fig. 11.4. Schematic illustrations of fabrication outer shell of a spherical lens. a) The used fast fabrication sequence: *(1)* contour scanning for a shell-hardening, *(2)* development, and *(3) UV* exposure for the final volumetric polymerization. b) Comparison of time required to fabricate a hemi-spherical lenses of different radii, r, by the proposed shell exposure vs. a full-volume raster scan.

rication can be invoked. For instance, if a cantilever with a sharp tip is needed, the huge in volume body of the cantilever can be fabricated using a low *NA* objective and then the sharp tip can be fabricated with a high *NA* objective. This combination enables fabrication of relatively large (mm in overall scale) volumetric structures with submicrometer feature resolution.

Choosing correct fabrication strategy is crucial for saving time usage of costly *FLMP* machinery. Our group has developed an efficient way to manufacture volumetric microoptical elements. In order to speed up the fabrication process, only the outer shells were made using *DLW*, and the interior was polymerized using a post-fabrication *UV* treatment. The di-

ameter d and height l of single photopolymerized voxels was controlled by modifying the laser power, scanning speed, and focusing optics [121, 85]. This allowed the fabrication of enclosure shells mechanically strong enough and the formation of unexposed regions inside the optical elements for further processing steps (Fig. 11.4a). The procedure of shell fabrication, development, and post-treatment with UV light enabled the fabrication time reduction by approximately $\sim 200 - 400$ times. This approach has been already demonstrated for producing sample *3D* microstructures of complex geometry and components for microfluidics [122, 56]. The time required to fabricate a compact, hemi-spherical lens of radius R, by volumetric raster scanning with pitch d, (the same pitch in lateral and axial directions is considered) at scan speed, v, is: $t_v = \frac{V}{d^2 v}$ where the volume of hemi-sphere $V = \frac{1}{2} \times 4\pi R^3$; the pitch is at least two times smaller than the diameter of the voxel actual fabrication. One the contrary, for only the shell fabrication the required time is $t_s = \frac{S}{dv}$ with the surface of hemi-sphere $S = \frac{1}{2} \times \frac{4}{3}\pi R^2$. Hence, the factor of the efficiency increase is $f_c \equiv \frac{t_v}{t_s} = 3\frac{R}{d}$. As the radius of a lens increases, or the voxel size decreases (hence, the pitch, d, too), the fabrication time becomes impractical for the volumetric raster fabrication. In the case of the microoptical elements discussed in this study, an improvement of approximately $(1-3) \times 10^2$ times is achieved using the shell-fabrication approach (Fig. 11.4b). The actual exposure time required for the fabrication of a $R = 50$ μm radius lens of focal length ~ 100 μm at volume filling by a raster scan with 200 nm overlap between voxels is 14.7 h, reducing to approximately 2.6 min by employing the proposed shell-exposure (Fig. 11.4a). The step between exposure spots was varying $d = 25 - 200$ nm and scan speed was kept in the $v = 50 - 200$ μm/s. The time requirements are similar if any other bulky (volumetric) structures (for eg. nanochannels in microfluidics or microporous scaffolds in tissue engineering) are desired to be produced.

11.2 Supplementary nanoimprint lithography technique

For fabrication of series of identical *2.5D* micro/nanostructured samples (for eg. scaffolds for cell growth experiments or *2D* optics, photonics, plas-

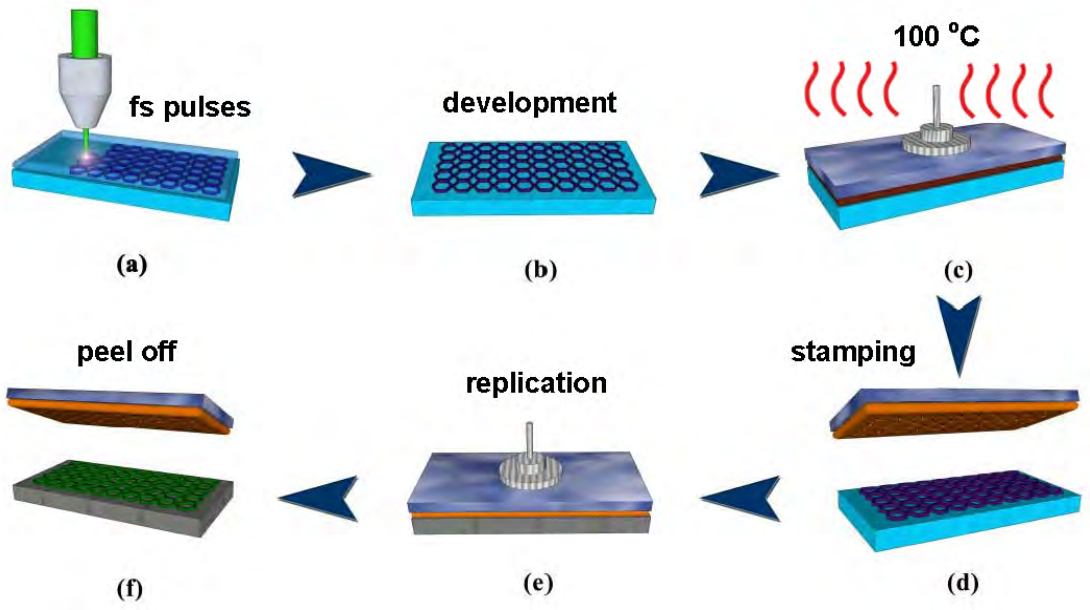

Fig. 11.5. A desired *2.5D* structure is fabricated by a serial *FLMP* writting in a well structurable photopolymer (for eg.: *SZ2080*) and developed, a) and b). A layer of *PDMS* elastomer is placed on original structure and cured via thermopolymerization reaction c). Transparent *PDMS* mold is placed on fresh photopolymer and it is cross-linked by exposing with *UV*, d) and e). Finally, the mask is removed and replica remains on a new substrate, f).

monics, metamaterials) there is a way to speed up the production process dramatically. In such case, time consuming and expensive fabrication via *FLMP* direct writing is needed only once to initially produce a *master* template. Later a standard NanoImprint Lithography (*NIL*) replication method employing thermopolymer *PDMS* can be used [123, 124, 125]. This micro/nanomolding can be applied for rapid production of series identical samples with resolution up to tens of nm. The replication steps are shown in Fig. 11.2. A transparent *PDMS* elastomer mold is produced on original structure and is later used for stamping structures via *UV* polymerization. The stamping process can be repeated up to 10^3 times without noticeable quality degradation [126]. The elasticity of the stamp can be tuned by changing the ratio of thermoinitiator or curing temperature and time. Lower concentrations of the thermoinitiator as well as lower applied curing temperatures (corresponding to longer duration needed for the cross-linking to occur) makes the mask softer, thus easier to peel off from the replicated structure, yet slightly lower spatial resolution. It is noteworthy, that in principle *PDMS* can be structured via *DLW* as well, thus enabling

direct fabrication of replica masks [127]. It is also known that *PDMS* is a biocompatible material [128] and extensively studied for applications in microoptics [129] and microfluidics [130]. More important such transferring of *"inverted"* structure empowers one to apply the materials (not transparent, containing electric or magnetic nanoparticles) and substrates (opaque, not possible to be illuminated through) which may be not possible to use for direct and quality *FLMP* structuring.

12 FEMTOSECOND LASER WRITING INDUCED MECHANISMS AT NANOSCALE

12.1 *3D* nanopolymerization via photochemical, thermochemical and avalanche ionization

This section is based on the data presented in the reference [131]. Though in all of the thesis it was taken a common opinion that during *FLMP* process *TPA* is a dominant and the only process, here a contradicting results are presented and argumented opinion showing complexity of the *3D* structuring at nanoscale is described. The most widely used materials in *3D* laser photopolymerization are acrylate and epoxy based resins and resists developed decades ago before the era of tabletop femtosecond lasers for *UV* μ-stereolithography. Traditional photopolymers are photosensitized for wavelength of eximer laser at 308 nm or i-line of *Hg*-light source at 365 nm. Photosensitization and initiation of a nonlinear photopolymerization is different by its nature from that developed for the one-photon processes in the case when ultrashort laser pulses ($<$ 1 ps) at longer wavelengths are employed. Excitation of electronic subsystem occurs faster than an uptake of energy into ionic subsystem proceeding via electron-ion equilibration, recombination, thermal diffusion in the case. Since thermal processes are known to be efficient in chemical modifications of materials, by tuning a photon energy with a controlled thermal activation the materials' processing

is acquiring new functionalities when fs-laser pulses with tens-of-megahertz repetition rate are used [1, 28, 14, 132, 133, 7, 83]. Better understanding of the photo-physical and chemical mechanisms of polymerization is required [134, 135, 136] via direct measurements of photopolymerization nonlinearity [10, 137]. Such studies would allow to optimize response of materials and tailor their composition for the higher resolution or sensitivity in *3D* structuring applications.

Plenty of successful two-photon initiated microfabrication works has been done applying a variety of femtosecond irradiation sources while processing different photosensitive materials - acrylates, epoxies and organic-inorganic hybrid materials. Initially and up to date most of them has been done using *Ti:Sapphire* oscillators generating 780-800 nm irradiation wavelength and operating at 75-80 MHz pulse repetition rate [1, 28, 92, 132, 133, 138, 83]. Alternatively, *Ti:Sapphire* amplified systems have been applied successfully having 1 kHz pulse repetition rate [139, 51, 140]. Both light sources were emitting 100 - 200 fs duration pulses. Despite that, novel *Yb:KGW* lasing media based systems were expected to ensure even better results in resolution meaning due to shorter irradiation wavelength (1030 nm frequency doubled gives 515 nm) providing slightly longer pulses 300 - 400 fs and varying pulse repetition rate from 200 kHz to 26 MHz [141, 142, 85]. Though this has enabled processing wider range of photosensitive materials it did not ensure higher resolution than obtained applying 780-800 nm exposure. Precise wavelength tuning to target the two-photon absorption peak could be helpful to increase the efficiency and thus result to increase in structuring resolution [70], yet contradicting results were demonstrated that rather miss-matching excitation and absorption spectra can be used for steady microfabrication [10]. Additionally, 400 nm exposure has been shown to be efficient for two-photon induced *3D* structuring [27, 143]. Furthermore, 300 fs 1030 nm irradiation has been demonstrated be suitable as a three-photon absorption induced *3D* microstructuring in the commonly used materials like *ORMOCER* and *SU-8* [144, 145]. Finally, two-photon initiated polymerization fabrication using *Nd:YAG* frequency doubled 532 nm wavelength and 500 ps pulse duration laser operating at 5 kHz has been reported [146, 147]. This diversity of applied pulsed light sources evokes a question whether always two-photon absorption plays a dominant role in initiating the ultra-localized modification of the material?

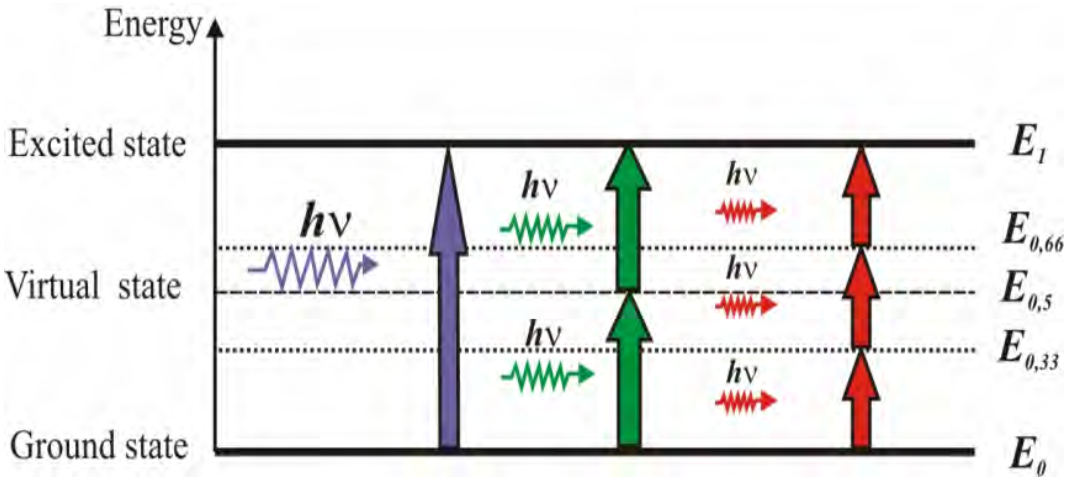

Fig. 12.1. Schematic diagram of excitation by one photon and several photons simultaneously. Like in non-linear microscopy, a photosensitizer molecule can be excited by few photons if the sum of their energy is matching the one needed for linear absorption.

It is noteworthy to mention that in this manner variety of acrylate, epoxy and hybrid materials can be processed in near-100 nm resolution. Detailed theoretical models on sub-100 nm feature fabrication estimates has been already reported [134, 135].

By this experimental work and it's interpretation it is demonstrated how a choice of photoinitiator and its concentration defines and in some cases limits the achievable *3D* resolution in direct laser writing by femtosecond laser pulses, as well as it has not such a direct dependency as only sum of the energies from several photons to fit the energy required for linear absorption Fig.12.1. It is shown that avalanche ionization plays an important part in photopolymerization at tight focusing conditions even though a seeding stage of bond breaking and radical generation occurs via a nonlinear two-photon absorption (*TPA*). Resolution of *3D* structuring at different formulations of photopolymers followed prediction of two-photon nonlinearities [148], i.e., when *TPA* becomes stronger resolution worsens due to an enhanced polymerization rate. However, in the *TPA* photo-sensitized resists there is a wider processing window where high-quality and fidelity *3D* structures can be prototyped. In practical use of photopolymerization the quality of *3D* structure, its resolution, mechanical and optical properties are the most important. By setting different pulse energies and scanning speeds the required window of photo-polymer processing is empirically found. Even the one-photon absorption can be used to obtain *3D* micro-

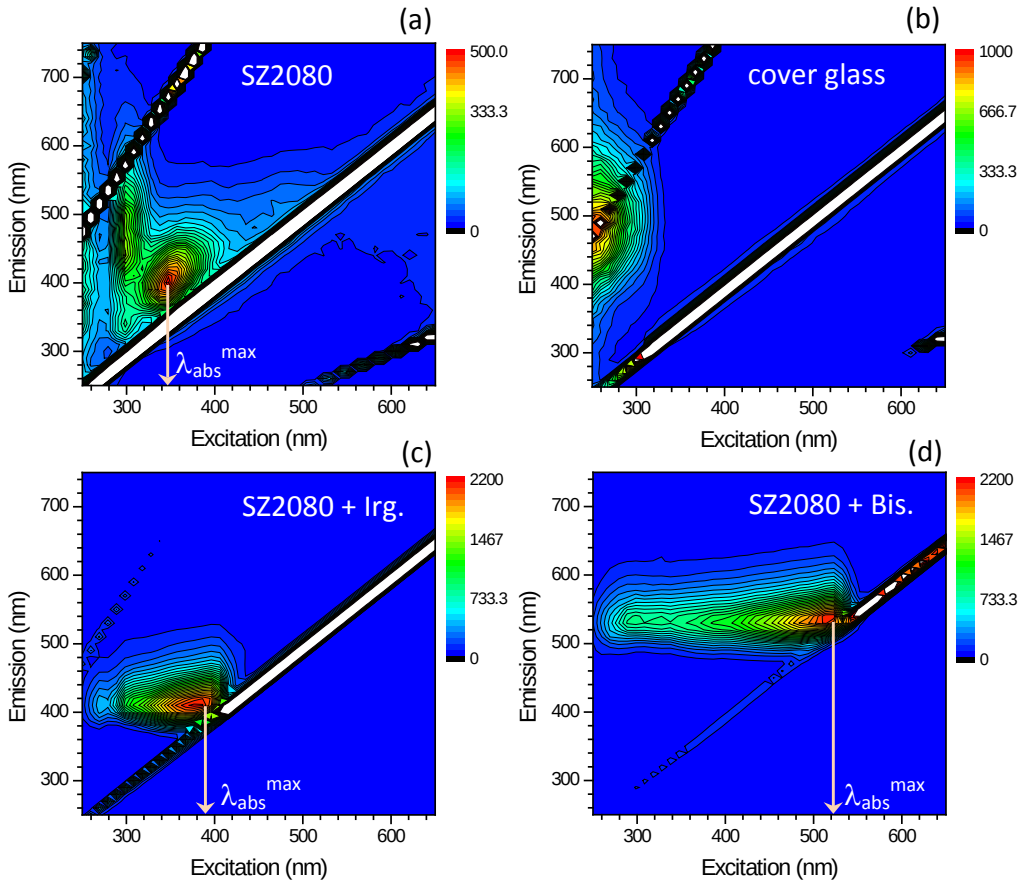

Fig. 12.2. (The photoluminescence excitation (*PLE*) spectra of the pure resist *SZ2080* (a), uncoated cover glass, resist with 2wt% of *Irgacure 369 (Irg.)* and *4,4'-bis(diethylaminobenzo phenone) (Bis.)* in (c) and (d), respectively. The wavelength of *PLE* maximum, λ_{abs}^{max}, corresponds to the most efficient energy delivery in *3D* structuring of chosen resists.

structures when tight focusing is used [149, 150]. This explains why so different resists and resins optimized for the one-photon absorption at the *UV* wavelengths still can be employed for *3D* laser structuring at 800 and 1030 nm wavelengths using fs-laser sources. At those wavelengths *TPA* is usually negligible (Fig. 12.3).

The most probable optically nonlinear effects occurring at the lowest irradiance/intensity are the *TPA* and refraction change via *Kerr* effect. The direct measurements of these nonlinear parameters are carried out by a *Z-scan* method [151] using ultra-short laser pulses, eg., the best fit of an open aperture *Z-scan* data for the *Gaussian* spatial distribution of a laser pulse provides a measure of the *TPA* cross section. Other methods such as transmission measurements and photoluminescence are usually overestimating the actual *TPA* cross section [152, 153]. The intensity dependent

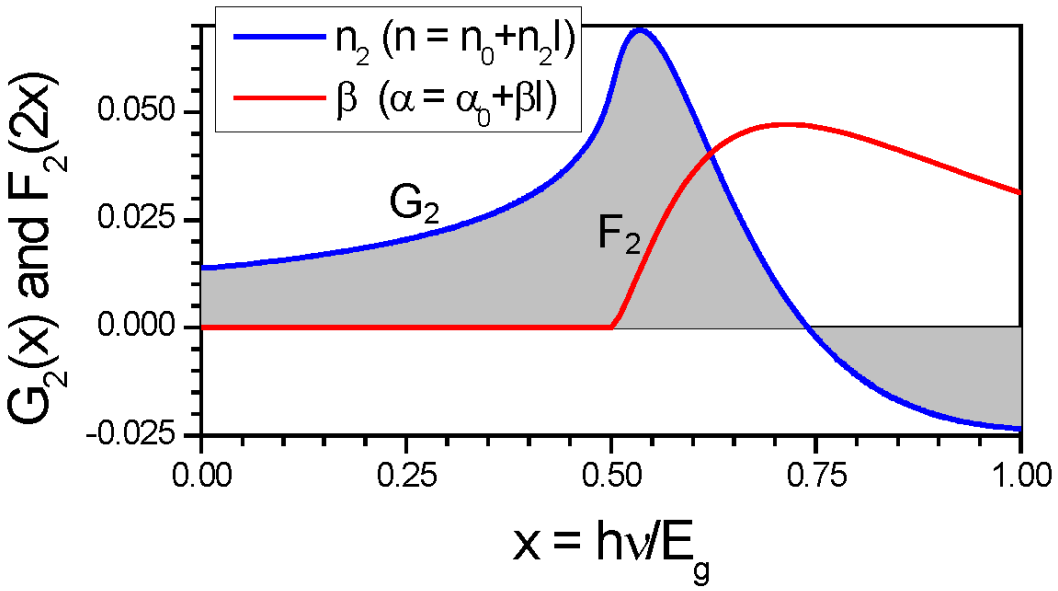

Fig. 12.3. Functional dependencies of the *TPA* coefficient, β, and nonlinear refractive index, n_2 on the normalized photon energy determined by the polynomial functions G_2 and F_2.

TPA coefficient, β, and nonlinear refractive index, n_2, has been measured for many crystalline and amorphous materials [148, 154]. The same characteristic dependencies are also valid for molecular solutions of a highly efficient *TPA* absorber *MBAPB* [155] which is similar to photoinitiators used in resists [156, 38]. Optical nonlinearities of dyes and photoinitiators measured by fs *Z-scan* corroborated the expected spectral dependencies established in the case of inorganic solid state materials [152].

The nonlinear refractive coefficient, n_2 ($n = n_0 + n_2 I$) is given by [154, 148]:

$$n_2[cm^2/W] = K\frac{\hbar c\sqrt{E_p}}{2n_0^2 E_g^4}G_2(\hbar\omega/E_g) \tag{12.1}$$

where $E_p = 21$ eV, is an empirical constant, and G_2 is the universal function plotted in Fig. 12.2. The nonlinear *TPA* absorption coefficient, $\beta(\alpha = \alpha_0 + \beta I)$ is given by [154, 148]:

$$\beta[cm/W] = K\frac{\sqrt{E_p}}{n_0^2 E_g^3}F_2(2\hbar\omega/E_g) \tag{12.2}$$

where F_2 is the universal function plotted in Fig. 12.2. The G and F functions are defined by the following polynomial expressions: $G_2(x) = (2+6x-3x^2-x^3-3x^4/4-3x^5/4+2(1-2x)^{3/2}\Theta(1-2x))/(64x^4)$, here the Heaviside

function $\Theta(y) = 0$ for $y < 0$ and $\Theta(y) = 1$ for $y \geq 0$; $F_2(2x) = (2x-1)^{3/2}/(2x)^5$ for $2x > 1$. Figure 12.2 shows the functional dependencies for β and and n_2. The abscise value $x = 1$ corresponds to the one-photon (or fundamental) absorption when photon energy is equal to the bandgap E_g. For our analysis, we use the corresponding λ_{abs}^{max} (Fig. 12.2) as the wavelength of the most efficient *3D* structuring, i.e., it is well absorbed and the autofluorescence *PL* is efficiently emitted. This wavelength defines the central wavelength of overlap between the absorption and emission spectra. For justification of such wavelength choice for $x = 1$ condition, we tested following procedure for the *MBAPB* [38]. The $\lambda_{abs}^{max} = 470$ nm is considered as the bandgap wavelength ($x = 1$) while the strongest *TPA* has a plateau region at 680-710 nm close to the expected location of the most efficient *TPA* [154, 148] (see, Fig. 12.3) at the 671 nm ($x = 0.7$). Hence, such choice of λ_{abs}^{max} for the photo-sensitizer is following expected spectral dependency of two-photon nonlinearities. It may appear counter intuitive that at the half of bandgap energy $x = 0.5$ the *TPA* is not taking place (Fig. 12.3) [148]. Moreover, photons of half of bandgap energy experience the largest n_2; or self-focusing. However, this is consistent with the white light continuum generation which is related to the nonlinear refraction and is efficient when the photon energy of driving radiation is smaller than half of the bandgap.

In terms of *3D* laser structuring the spectral dependence of the G and F functions would hint that a choice of irradiation wavelength for the most efficient photo-initiation of absorption is to be carefully chosen. The most optimal case for two-photon structuring is at a photon energy of $0.7E_g$ when β is the largest and n_2 is small. One can also recognize an expected tendency that closer to the fundamental absorption ($x = 1$) the n_2 values become negative as it would be expected due to free carrier absorption. Free carriers cause defocusing and alters light beam delivery to the focus. When linear absorption is present along with the nonlinear one, the refractive index changes per free electron, the dispersion volume, should be taken into account as well as the free carrier absorption. The procedures are well established by approaches in semiconductor physics. In solid state nomenclature, when band-to-band transitions are taking place simultaneously with the virtual ones (at $\hbar\omega < E_g$ as discussed above) the overall

refractive index change can be described by [148]:

$$\Delta n = n_2 I + n_{e-h} N_c, \tag{12.3}$$

where N_c is the electron density in conduction band and n_{e-h} is the "dispersion volume" [157] [cm^3] or the change of the refractive index per one electron-hole pair, which can be estimated as:

$$n_{e-h} = \frac{-e^2}{2 n_0 m^* \varepsilon_0 \omega^2}, \tag{12.4}$$

here $m^* and\ e$ are the effective electron mass and charge, respectively, and n_0 is the unperturbed refractive index.

The rates of multiphoton absorption and avalanche multiplication of electrons are estimated for the optical breakdown conditions in photoresists. The number density of electrons n_e created to the end of the pulse by the avalanche and multi-photon processes can be obtained from a rate equation [158]:

$$\frac{dn_e}{dt} = n_e w_{imp} + n_a w_{mpi}, \tag{12.5}$$

where n_a denotes the molecular density, i.e., available electron donors after photo-cleavage of bonds. If the laser intensity is constant during the laser pulse (corresponding to a flat-top intensity distribution) and when recombination during the pulse is negligible. Then the solution of Eq. (12.5) with the initial condition $n_e(t = 0) = n_{e0}$ and w_{imp} and w_{mpi} is straightforward [158]:

$$n_e\left(I, \lambda, t\right) = \left\{ n_{e0} + \frac{n_a w_{mpi}}{w_{imp}} \left[1 - \exp\left(-w_{imp} t\right)\right] \right\} \exp\left(w_{imp} t\right). \tag{12.6}$$

It is commonly accepted that breakdown of a dielectric occurs when the plasma frequency of excited electrons equals to the frequency of the laser light [159]. The critical electron density, the breakdown threshold, for 800 nm wavelength ($\omega = 2.35 \times 10^{15}$ s^{-1}) is $n_c = \frac{m_e \omega}{4\pi e^2} = 1.735 \times 10^{21}$ cm^{-3}. Free electrons will oscillate in the electromagnetic field of the laser pulse. These electron can gain net energy by multiple electron-lattice/atom collisions and eventually be accelerated to reach the energy in excess of the ionization potential J_i. Energetic electrons create an avalanche which has

the ionization rate estimated as follows [160]:

$$w_{imp} \approx \frac{\varepsilon_{osc}}{J_i} \frac{2\omega^2 \nu_{e-ph}}{\left(\nu_{e-ph}^2 + \omega^2\right)}. \tag{12.7}$$

Here ν_{e-ph}, and ω are electron-phonon momentum exchange rate and laser frequency, respectively. Electron-phonon momentum exchange rate, the rate of collisions at the breakdown can be estimated as $\nu_{e-ph} = 6 \times 10^{14}$ 1/s. The oscillation energy of electron in a scaling form reads [160]:

$$\varepsilon_{osc}[\text{eV}] = 9.3 \left(\frac{I}{10^{14}\ [\text{W/cm}^2]} \right) \lambda_{\mu m}^2, \tag{12.8}$$

which for 1 TW/cm^2 irradiance at 800 nm wavelength, yields $\varepsilon_{osc} = 30$ meV and is twice larger for a circularly polarized light.

The multiphoton ionization rate, a probability of ionization per atom per second, can be calculated according to [160]:

$$w_{mpi} \approx \omega\, n_{ph}^{3/2} \left(\frac{\varepsilon_{osc}}{2J_i} \right)^{n_{ph}}, \tag{12.9}$$

where n_{ph} is the integer part of $(J_i/\hbar\omega + 1)$ and defines the number of photons required for ionization [161]. The electron production rates via nonlinear *TPA* and avalanche are estimated for the experimental conditions. This analysis is only valid for order of magnitude estimates, however, it is insightful to determine the dominating mechanism of ionization, bond breaking, radical generation, and, hence, cross-linking.

The threshold in *3D* laser structuring appears as a result of cross-linking as it defines solubility of the resist during development and elastic properties of final the structure [162]. When a photopolymerized structure is allowed to shrink freely in space during drying, the final size depends on the pulse energy exponentially [163]. Cross linking is temperature dependent following the *Arrhenius* mechanism and the thermal effects are important. In the case of tight focusing, the strong light intensity gradients create strongly localized thermal field. Hence, a *3D* structuring of resins and resists is possible even at the wavelengths close to the direct absorption band as was demonstrated by 355 nm 20 ps pulses in the acrylic resins [150].

Photopolymerization of *3D* structures at the (pre-)breakdown conditions was carried out in sol-gel resist by tightly focused femtosecond laser

pulses. The mechanisms relevant to the optically nonlinear and thermal pathways of photopolymerization have been discussed as well as the method for the best wavelength selection for *3D* structuring. When fs-pulses at high irradiance are used, the avalanche ionization plays an important role in chemical bond breaking and promotes cross-linking. By better understanding of the photophysical and photochemical processes we can expect to create new resist and resin materials where true nanostructuring with resolution with sub-100 nm in all *3D* can be achieved. The same resins can be *3D* structured by 150 fs pulses of 400 nm central wavelength by *TPA* as was demonstrated by measuring the power dependence of polymerization [143]. Though *TPA* of those resins is not optimal at 400 nm where the resonant *TPA* and linear absorption are already present, a *3D* structuring is possible.

The best resolution was achieved in non-photo-sensitized resist and worsened for more longer wavelength sensitive (larger λ_{abs}^{max}, see, Fig. 12.2) and larger concentrations of sensitizers. The widest pulse energy window for high fidelity microstructuring of resist was in the case of resist with Irg. photoinitiator. The other contribution which might affect the photopolymerization is the thermal emission of hot electron plasma at the focus. The black-body emission estimations showed that free electrons which have high temperature $T = 1000$ K at the pre-breakdown conditions can be efficient emitters at the $2 - 3$ μm where many organic compounds have a strong absorption. The black body emission according to the Wien's law has the maximum at $\lambda_{Em}^{max} = \gamma/T$, with $\gamma = 2.9 \times 10^{-3}$K. This mechanism can also contribute to the final efficiency of photo-polymerization as has been demonstrated by a scaling behavior [164].

Especially when chemically amplified resists such as the popular negative tone *SU-8* are used. In this case one polymerization event is releasing photo-acid which promotes polymerization in a chain reaction manner. Considering possible eight cross-linking sites per monomer, propagation of polymerization is nonlinear but would appear with a reduced slope if polymerized feature size is plotted against the incident laser irradiance (slope 2 would be expected for a typical *TPA* process when one cross-linking occurs for two absorbed photons).

The ways to improve resolution of *3D* laser structuring of materials is discussed in terms of optical and material aspects. It is shown that opti-

mization of *TPA* of photoinitiator in the irradiation region of low nonlinear refractive index changes is critical for the achievement of nanostructuring when $\sim$ 100 nm resolution in all three dimensions is to be achieved. The critical electron density at 800 nm is 1.735×10^{21} cm^{-3}. Thus one can conclude that the above simple model predicts the breakdown threshold to be around 1.5×10^{12} W/cm^2 in semi-quantitative agreement with reported earlier experiments in glass [165].

In practical use of photopolymerization the quality of *3D* structure, its resolution, mechanical and optical properties are the most important. By setting different pulse energies and scanning speeds the required window of photopolymer processing is empirically found. Even the one photon absorption can be used to obtain *3D* microstructures when tight focusing is used [149, 150]. This explains why so different resists and resins optimized for the one photon absorption at the *UV* wavelengths still can be employed for *3D* laser structuring at 800 and 1030 nm wavelengths using fs-laser sources. At those wavelengths *TPA* is usually negligible (Fig. 12.3). Figure 12.2 shows the *PLE* spectra of *SZ2080* with different photosensitizers used in this study. In contrast to the *SU-8*, where the auto- fluorescence is recognizable at wavelengths $\lambda_{abs}^{max} < 320$ nm [166]. In *SZ2080*, the *PLE* peak is observed at $\lambda_{abs}^{max} \sim 340$ nm in a pure resist and at 390 and 520 nm in case of resist with *Irg.* and *Bis.* sensitizers, respectively (Fig. 12.2). For two-photon structuring at 800 nm wavelength the optimized resist is expected to have the λ_{abs}^{max} peak corresponding to the absorption wavelength of $1.24/(0.7 \times 3.1[\text{eV}]) = 571$ nm (Fig. 12.3).

At the 1030 nm wavelength, the ionization rates slightly changes but the conditions $w_{imp} \gg w_{mpi}$ is even stronger fulfilled since the quiver energy of light-driven electrons scales as $\varepsilon_{osc} \propto \lambda^2$ (Eq. 12.8). In actual polymerization at 1030 nm/300 fs, the *SZ2080* with *Bis.* showed much larger feature sizes of fabricated logpile structures as compared with the ones recorded in *SZ2080* with *Irg.* below breakdown threshold (Fig. 12.4) for the very same irradiation conditions. In order to be able to recover *3D* logpile structures in the case of all three different resists the concentration of photosensitizes was reduced to 1wt.%. In such case, the structures recorded in resists with photosensitizer were at the breakdown threshold similar to Fig. 12.4(c). As resist gets more optimized for laser structuring by *TPA* (closer to $x = 0.7$), the feature sizes become larger. This is consistent with the analysis pre-

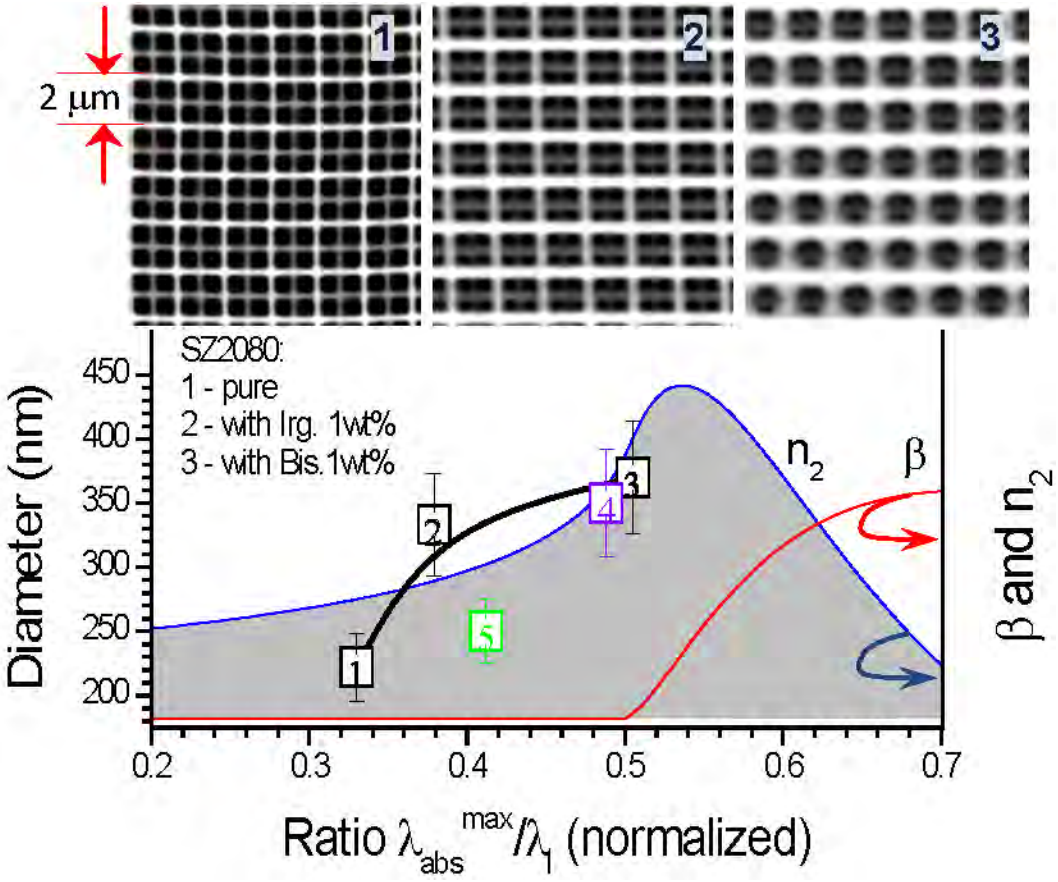

Fig. 12.4. The smallest width of a photopolymerized log vs the ratio $\lambda_{abs}^{max}/\lambda_l$, where the λ_{abs}^{max} is the absorption maximum of the *PLE* (see, Fig. 12.2) and λ_l nm is the laser wavelength: 1030 nm *(1-3)* and 800 nm *(4,5)*. Right axis shows functional behavior of *TPA*, β, and refraction, n_2, (see, Fig. 12.3). Inset *SEM* images *(1-3)* show structures made at the same focusing conditions corresponding to: 13 TW/cm^2 at focus $I_0 = \frac{2(E_p/t_p)}{\pi w^2}$ for pulse duration of 300 fs, wavelength 1030 nm, pulse energy $E_p = 14.5$ nJ) in pure *SZ2080 (1)* and doped with 1 wt.% of Irg.*(2)* and Bis. *(3)*. The markers *(4,5)* corresponds to *SZ2080* with 2 wt.% of Irg. and *SU-8*, respectively, structured with 800 nm, 150 fs pulses focused by $NA = 1.42$ objective lens.

sented above: as seeding electrons are produced more efficiently and at the considerably higher avalanche rates as compared to multi-photon, the ionization is stronger facilitating polymerization via bond cleavage and thermal effects. The smallest achievable width of *3D* logpile structures are plotted in such a way (Fig. 13.4) that resists with different sensitization (λ_{abs}^{max}) structured at different wavelength λ_l can be compared with expectations for the two-photon absorption and refraction (the right axis). A recognizable trend is that as λ_{abs}^{max} increases or/and λ_l decreases the smallest feature size increases even when *TPA* $\beta \to 0$ at $x \leq 0.5$. The smallest feature sizes can be obtained in non-sensitized resist.

Table 12.1. Qualitative comparison of different laser structuring regimes for 1030 nm/300 fs pulses in *SZ2080* at different photosensitization; focusing $NA = 1.4$ and scanning speed 100 μm/s.

Condition at focus:	SZ2080	SZ2080 + Irg.1wt%	SZ2080 + Bis.1wt%
Polymerization threshold, nJ (TW/cm^2)	14 (12.5)	5 (4.5)	4 (3.6)
Quality structuring (middle of the range), nJ (TW/cm^2)	16 (14.4)	7 (6.3)	5 (4.5)
Explosion threshold, nJ (TW/cm^2)	17 (15.2)	12 (10.8)	12 (10.8)
Uncontrolled burning, nJ (TW/cm^2)	18 (16.1)	18 (16.1)	17 (15.2)

A qualitative comparison of fs-laser structuring regimes at 1030 nm and 300 fs is summarized in Table 12.1 for *3D* logpile structures in terms of pulse energy at focus (as usually measured in experiments) and in terms of irradiance for tight focusing with a $NA = 1.4$ objective lens. A narrow window of photostructuring exist in undoped resist however the smallest feature sizes can be obtained, while laser structuring of more *TPA* sensitive material ($x \to 0.5$) results in larger feature sizes which are more sensitive to laser power fluctuations. Other important parameters for the *3D* laser structuring are the laser repetition rate and overlap between laser pulses. The cooling time of the focal region can be estimated as the $t_c = d^2/D$, where d is diameter at focus approximately equal to the wavelength of irradiation at a tight focusing considered here; $D \simeq 10^{-3}$ cm^2/s is a typical thermal diffusion constant in polymers [167]. This yields in cooling time of $\sim 10\mu$s which is much longer than 12 ns between adjacent pulses in the case of 80 MHz repetition rate of fs-oscillators. Hence, the *3D* laser structuring by oscillator irradiation is very different in terms of mechanisms from that by amplified fs-lasers at kHz repetition rates when the focal spot has time to cool down [168]. Here, we discuss a low repetition rate fabrication, which is the simplest case.

It is noteworthy, that heat generated by exothermal photopolymerization reaction is yet another factor enhancing polymerization. Since thermal polymerization of many photopolymers occurs at approximately 150°C, thermal accumulation can be used for a controlled heating of the focal vol-

ume providing a required control over *3D* structuring [164]. Since polymerization and cross-linking depends exponentially on temperature this can provide an efficient method for *3D* laser structuring of photopolymers.

For the considered here case of the pre-breakdown and breakdown polymerization, the mechanism of electron generation, i.e., chemical bond breaking changes the effective photo-initiation pathways and the bond cleavage required for generation of radicals and cations can proceed directly via ionization of the host (in addition to the standard pathway via photoinitiator absorption and chemical bond opening). It has been established that unless pulse duration is less than approximately 10 fs, the avalanche (an impact ionization) is an efficient process fueled by multiphoton ionization [159]. It is also noteworthy that a standard role of photoinitiator (or a pair of photosensitizer with initiator) in providing free radicals (or cations) becomes different for a high-irradiance fs-pulse exposure. Once photoinitiator absorbed a photon and an electron in an excited state can undergo avalanche in a quasi-continuum of excited states and promote bond breaking, hence, polymerization. In a strongly ionized photopolymer the avalanche is expected to be a prevalent mechanism in chemical bond cleavage as demonstrated by this order of magnitude estimation here. The avalanche usually proceeds with heating of the focal region since the kinetic energy of electron should exceed that of the bandgap by up to 50% in the case of fs-laser pulses in order to comply with energy and momentum conservation of the avalanche process [161].

12.2 Self-formation of nanofibers and nanomembranes

FLMP is a technique enabling formation of *3D* nanostructures in photosensitive resins with sub-wavelength resolution and unmatched flexibility. However, controllable fabrication of sub-100 nm features by this technique is still a challenge. Self-polymerization, also known as non-local polymerization, is considered to be promising in this ultra-high resolution structure formation. Recent observation of fragile self-polymerized fibers with tens of nanometers diameter (nano-fibers) encourages the use of self-polymerization to produce nanometer scale structures of different profile than fibers and define the con-

ditions for controllable fabrication. "X"- shaped polymerized supports are used as rigid structures to produce suspended self-polymerized features of different nature (shape and dimensionality) in-between the walls of "X". By laser writing a network of lines parallel to the substrate and perpendicular to the long symmetry axis of "X" under different conditions, self-formation of periodic nanofibers (diameter < 100 nm) and nano-membranes is induced in acrylate photopolymer *AKRE37*. Depending on introduced exposure dose spatial density, threshold behaviour of no-structure, nano-fiber, nano-membrane and laser written lines is deduced. Preliminary model including laser intensity, concentration of radicals, collapse force and distance between supports as variables having threshold effect on final self-polymerized structure's geometry is proposed to explain non-local self-polymerization.

Focused femtosecond beam introduces energy in a highly localized volume of a bulk photoresist via multiphoton absorption at the focal point. Pre-polymer containing special photoreactive molecules (photoinitiators) are excited at the beam waist. Generated radicals initiate local irreversible cross-linking reaction resulting in formation of tiny rigid polymerized elements - voxels [169]. These photomodified volumes can be produced in a serial manner by light exposure of the photoresist and joined together in a way to form any desirable *3D* structure. After processing by laser beam, unexposed material is washed out during development process so that free-standing *3D* structures anchored to the substrate sustain. Non-linear character of the two-photon absorption and chemical threshold of required radical concentration (C_{th}) for irreversible cross-linking result the photomodified volume to be highly localized and the minimum size of a voxel to be far below the size of beam waist limited by diffraction [170]. Thus, moving of the beam focus position in *3D* enables *DLW* of arbitrary polymer structures with sub-wavelength resolution [171]. This *DLW* technique often referred as *FLMP* has emerged as a tool for the rapid, cheap, and flexible fabrication of *3D* nanostructures for photonics, microoptics, nanofluidics and nanomechanics. Though the lateral size of the smallest features of *3D* structure fabricated by *FLMP* can be as small as 100 nm, further decrease in size is of great importance and possibilities to produce sub-100 nanometer structures still represent an appealing challenge.

Recently, self-polymerization of fragile fiber-like structures with sub-100 nm diameter suspended in-between rigid supports has been reported when

distance between the supports is below critical, $D_{th} \sim 1$ μm [172, 173]. Critical distance refers to a maximum spacing between the supports sufficient for self-polymerized features yet to form and sustain rinsing. Self-polymerization occurs when laser generated radical concentration becomes close to threshold ($C \sim C_{th}$) and is enough to self-assemble a feature which sustains rinsing in an organic solvent. *LET* has been proposed by *S.-H. Park* et al [172] to induce and control self-polymerization of nano-fibers at the interior region of rigid microstructures. Weakly polymerized regions consisting of *SCP* were assumed to form around densely polymerized line patterns formed of *LCP* varying lateral size of the voxels via *LET*. When both sides of the line patterns were close enough that the weakly polymerized regions overlapped ($D < D_{th}$), numerous ultrafine nano-fibers of less than 30 nm in diameter appeared throughout the overlapped region. *D. Tan* et al [173] have demonstrated that nano-fibers can be produced in controllable manner by increasing the incident laser power and accelerating scan speed in order to shorten the exposure time. Both groups named the D_{th} to be the most important factor for self-formation of nano-fibers though their proposed exposure conditions are rather opposing. In our work we present results of experimental study on self-polymerization of nano-fibers as well as *2D* case of self-polymerized structures - suspended nano-membranes. This phenomenon is investigated in custom made acrylate photopolymer *AKRE37*.

AKRE37 was made by blending commercially available *tris(2-hydroxy ethyl)isocyanurate-triacrylate* (*Sartomer Company, Inc.*) monomer with radical photoinitiator *4,4'-bis(dimethylamino)benzophenone (Sigma-Aldrich Co.)*. Ethyl alcohol was used as a developer. Self-polymerization has been studied by observing the formation of self-induced structures between the rigid support objects fabricated using *FLMP* system (*Ti:Sapphire* in *LRC*). "X"-shaped polymerized supports were fabricated anchored to the glass substrate in the drop-casted photoresist. The walls of the structure were fabricated using 24 mW average laser power P and scanning speed v was kept 200 μm/s. The length of the supports was 100 μm, they were intersecting at the angle of 20° to have a gradient change of D and the height of the walls was set 16 μm. Self-polymerization has been stimulated by unidirectionally laser writing the network of parallel lines oriented perpendicular to the long symmetry axis of "X" support. Network of lines was written

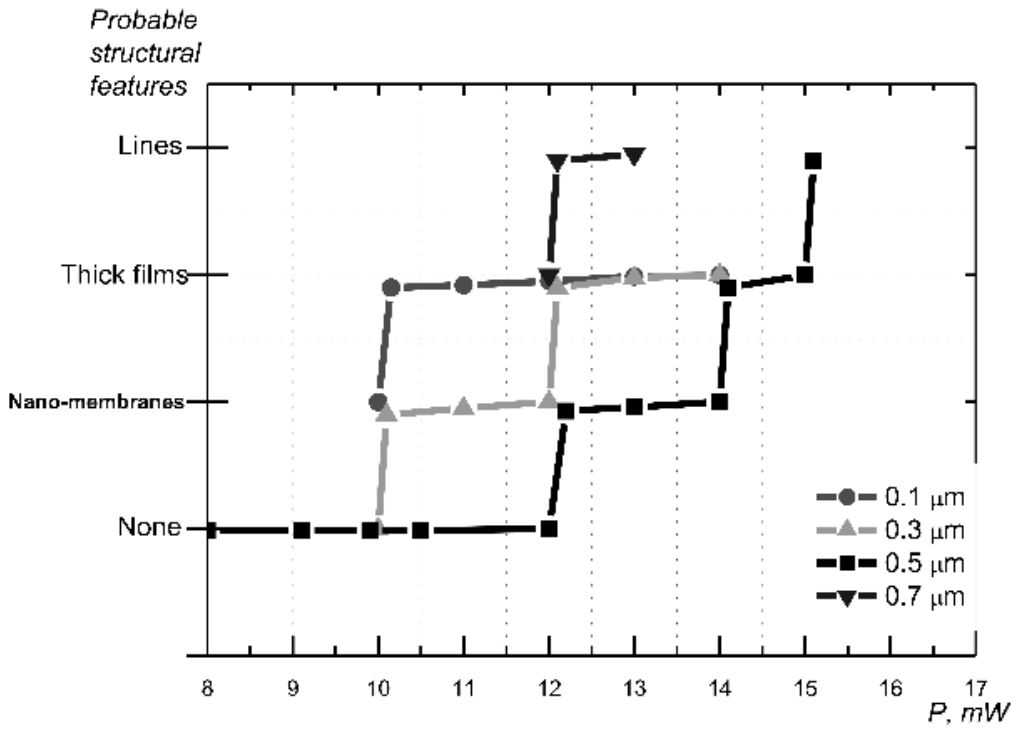

Fig. 12.5. Threshold behaviour for the self-polymerization of structures by varying average laser power P and lines network period L.

at 15 μm height keeping fixed v of 200 μm/s, but changing P and period between written lines L. With an intention to investigate the conditions for self-polymerized structures to form in different exposure approach, v was kept at the level intermediate in the range of that used by *S.-H. Park's* and *D. Tan's* groups to fabricate nanofibers [172, 173]. After rinsing in ethyl alcohol for 20 minutes at 60°C the resulting structures were dried out.

To evaluate the laser writing parameters for the network of lines resulting in self-polymerization of nano-fibers and nano-membranes at least five samples were fabricated and examined at every set of writing parameters (P and L) in order to test the repeatability. The lines with period of 0.1, 0.3, 0.5 and 0.7 μm were written between the walls of the support for several different values of average power P which was varied in the interval from 9 to 15 mW (step of 1 mW). After analyzing the features which were formed between the supporting walls, we identified three types of structures. The first type was self-polymerized films (uniform thin membranes suspended at 15 μm height and covering part of spacing between the supporting walls

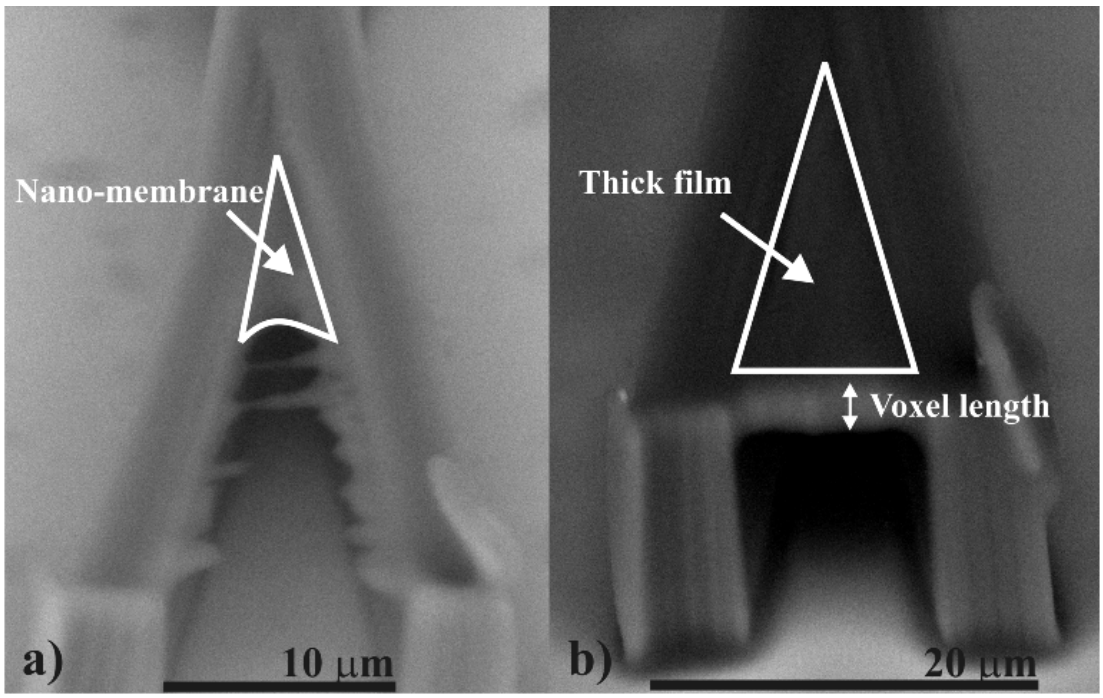

Fig. 12.6. Two types of formed structures: a) self-polymerized membrane (P of 12 mW, L of 0.6 μm); b) thick film (P of 10 mW, L of 0.3 μm). Noticeable difference in films thickness is observed, though due to limited resolution of our *SEM* thickness was not measured exactly.

where lines were written). The membrane edges were curved with the radius of curvature slightly different at opposite sides of the support. Radius of curvature of the membrane edge was found to depend on the radical diffusion direction along the symmetry axis of the support (perpendicular to the laser written lines). Although the *SEM* images did not allow accurate measurement of the membrane thickness, it has been estimated to be far below the longitudinal size of the rigid voxels as was deduced from the *SEM* images of the samples taken at 45° angle. Another two types of structures were thick films, forming when fabricated at certain P and L lines overlap (angular *SEM* image shows thickness of the film to be equal to the longitudinal size of the voxel) (Fig. 12.6), and separate lines, forming when L is increased. Except of these main types of the structures, cracked films, periodic self-polymerized fibers and other intermediate structures were also observed in some cases but fabrication conditions resulting in appearance of these structures were not investigated in detail. Probability for each of the three main structural features to form has been roughly estimated by analyzing the *SEM* images of samples which were fabricated using the same

P and L. If four out of five samples fabricated under the same conditions where of the same type (the same kind of the structures formed), the probability for that type structure to form was assumed to be one. Figure 12.5 reflects the threshold character of self-polymerization in terms of diverse structure formation. It shows that none of the structures appear between rigid supports up to P of 10 mW. Though the threshold power P_{th} for rigid structures to form in *AKRE37* was estimated to be about 12 mW, self-formed membranes were observed both below and above this P_{th} depending on the density of laser written lines. These self-formed membranes extend over considerable area so that the distance covered between the supports is much bigger (up to 8 times) compared to critical distance for nano-fibers ($\sim$1 μm) [172, 173]. At higher P the formation of thick instead of thin films suspended between the walls was observed. Switching to this type structures also showed threshold character for every L of the network. At the $P > P_{th}$, thick film type structures switched to solid lines formation as expected in *FLMP* fabrication. P of 10 mW was found to be enough for self-polymerized membranes to form in-between the walls when scanned lines were packed densely enough. When writing lines with L of 0.5 μm and P of 12 mW, sometimes intermediate structures were formed, including separate lines and small islets of thin film in-between the polymerized and self-polymerized lines. Individual high resolution lines were formed when L was of 0.5 μm and P of 15 mW. Periodic nano-fibers of about 50 - 100 nm in diameter self-composed in-between the polymerized lines (Fig. 12.7) were also evident. Those fibers were formed periodically within $\sim$350 nm in the gap of 400 nm of previously photopolymerized lines corresponding to be the support structures, which tend to interact among each other resulting in diminished distanced in-between.

Our results show that nano-fibers could self-form when laser writing at $P \sim P_{th}$ and at v of intermediate value compared to those in [172, 173] and generating radicals with density which is not sufficient to form robust structural features. Moreover, to our best knowledge self-polymerization of nano-membranes has not been reported previously. The films in-between the walls of "X" form as the *SCP* may be entangled into the surface layers of the laser written network of lines due to the chain elongation during the diffusion dominated processes of chain reaction or polymerization termination [174]. Due to capillary forces self-formed films are concave and

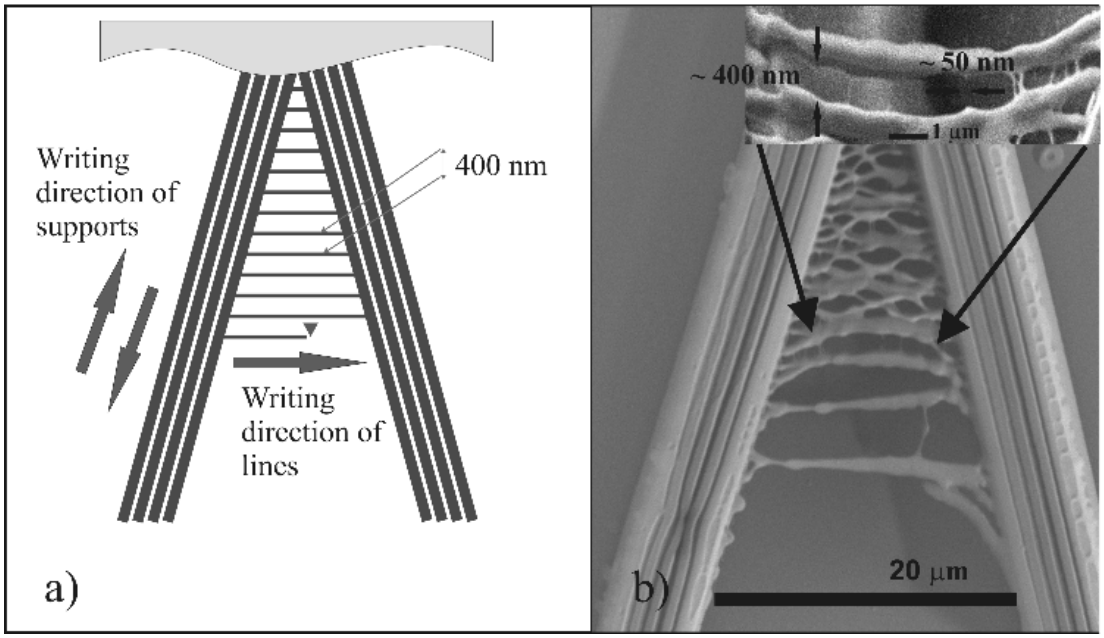

Fig. 12.7. a) Image showing the formation of particular "X" structure and lines network; b) *SEM* image of self-polymerized structures in-between the laser polymerized lines (P of 14 mW, period of 0.7 μm): thin fibers compose within periodic distance in the gap of 0.5 μm.

curved at the edges. During the rinsing the solvent evaporates faster from the membrane surface than from under it and the capillary forces bend the film downward. The edges of the membrane curve because evaporation of the solvent makes the polymer deform. Noticeable difference in radius of curvature of membrane edges dependent on the direction of the lines network formation might be explained by the preferential direction of *SCP* diffusion towards the existing structures (in this case, the "X" walls) [175]. In one case, the creation of high radical and *SCP* concentration starts away ($D > D_{th}$) from already polymerized "X" walls and is extended towards the intersection point ("X" center) of the walls. That means that chains tend to propagate the same direction as the concentration of radicals and *SCP*, and do not terminate until *LCP* meet which is more likely to happen in the area where irradiation started or near the "X" walls. If the chain is terminated before one of its ends is attached to the "X" wall, the whole chain is washed out during development process. The probability of this to happen reduces as the irradiated area gets closer to the center of "X". In other case, radicals and *SCP* are started to generate already close to the center of "X" and tend to connect into chains and attach to the "X" walls first, because the distance

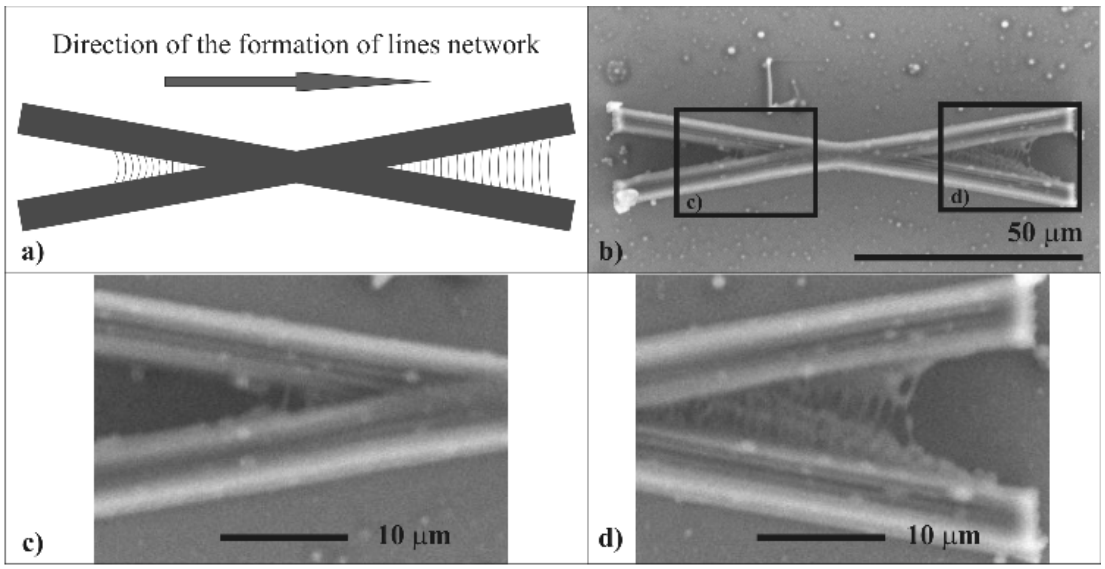

Fig. 12.8. Images showing the expected profile of lines formation in-between the supports: (a) the model; (b) the actual *SEM* image of the sample; (c) and (d) magnified images of structure ends reflecting different quantity of formed lines dependent on the direction of network formation.

for those *SCP* to diffuse towards already polymerized supports is already minimal and only increases as the network of exposed lines is extended away from the center. Therefore, the curvature radius of the membrane edge, formed when radicals were started to generate away from the supports, is smaller than the one of the membrane edge, formed when radicals were started to generate at the center of "X". Due to the same reasons the number of lines polymerized in-between the supporting walls discussed in the first case is much smaller than in the other (Fig. 12.8). Obtained results show that the distance between the supporting structures definitely influences the formation of self-polymerized membranes. That is why D_{th} plays crucial role determining self-formation of nanofibers and nanomembranes. Though our results on studying self-polymerization of nano-membranes are well consistent with earlier data referring to critically important role of the D_{th}, we suggest that the practical success of controllable fabrication of nano-features is actually greatly influenced by the collapse force threshold (F_{th}), emerging during developer evaporation process, which is the feature of both the material and the structure [176]. To fully describe the critical factors influencing the final self-formed feature, four conditions has to be fulfilled: 1) average laser power $P \sim P_{th}$ in order to initiate two-photon

absorption; 2) concentration of radicals $C \sim C_{th}$ to initiate polymerization chain-reaction; 3) material rigidity $F < F_{th}$ not to sustain structure having geometry of laser scanned trace; 4) distance between supports $D < D_{th}$ in order for the *SCP* to be entangled in higher polymerized regions of supports instead of being washed out. It is worth to mention that all these parameters are very crucial for self-polymerized features, making them extremely case sensitive.

The current study shows that, when laser writing the line network between solid polymerized supporting structures under appropriate conditions, suspended nanofibers and nanomembranes can be formed in repetitive manner. Compared to the previously reported works, our experimental results confirm the most important parameter to be critical distance between the supports. Nevertheless, it contradicts to the assumption that the *LET* [8] or high laser power and sample translation velocity are required to induce self-polymerization [9]. Additionally, we found threshold behaviour of no-structure, nanofiber, nanomembrane, laser written line formation depending on average laser power P and distance between written lines L. A simple model is proposed predicting required average laser power, concentration of radicals, material rigidity and distance between supports for self-polymerization to be induced. These conditions are defined in relation with the threshold parameters respectively $P \sim P_{th}$, $C \sim C_{th}$, $F < F_{th}$ and $D < D_{th}$) and must be satisfied in order to achieve repeatable self-polymerization of nano-features. Precise control of this femtosecond laser induced self-polymerization could open a way for fabrication of nanomembranes which could be widely applied in nanomechanics, nanofluidics, nanophotonics and plasmonic metamaterials.

13 FABRICATION AND CHARACTERIZATION OF MICROOPTICAL COMPONENTS

13.1 Integrated microoptical components

This section is based on experimental results presented in references [177] and [178]. The femtosecond laser-induced multiphoton polymerization of a *Zr-Si* based sol-gel photopolymer was employed for the fabrication of a series of microoptical elements with single and combined optical functions: convex and *Fresnel* lenses, gratings, solid immersion lenses on a glass slide and on the tip of an optical fibre. The microlenses were produced as polymer caps of varying radii from 10 to 90 μm. The matching of refractive indices between the polymer and substrate was exploited for the creation of composite glass-resist structures which functioned as single lenses. Using this principle, solid immersion lenses were fabricated and their performance demonstrated. The magnification of the composite solid immersion lenses corresponded to the calculated values. The surface roughness of the lenses was below ∼30 nm, acceptable for optical applications in the visible range. In addition, the integration of microoptical elements onto tip of optical fibre was demonstrated. To increase the efficiency of the *3D* laser polymerization, the lenses were formed by only scanning the outer shell and polymerizing the interior by exposure to *UV* light.

Microfabrication by multiphoton polymerization *(MPP)* is a relatively new, direct laser-write technique which allows the flexible *3D* structuring of photopolymers at the micro/nanoscale [1]. To date, it has been employed

in the fabrication of photonic [179, 35, 180, 132, 51, 52, 50], micro-optical [53, 181, 182, 54, 92, 183], and microfluidic [184, 163] micro/nanodevices. As new photopolymers, specifically designed for *MPP*, emerge, detailed investigation on damage threshold, resolution improvement, and search for methods to increase fabrication throughput evokes further efforts in controllable and reproducible manufacturing of optical components. New designs of complex miniaturized and integrated optical, opto-fluidic devices and sensors are required.

For the fabrication of high quality MicroOptical Elements *(MOE)*, the photopolymer properties play an important role. The low post-fabrication shrinkage of hybrid resists is desirable for the fabrication of microoptical devices and photonic crystals over larger areas with cross sections above 100 μm, as shrinkage is a primary cause of deformation and detachment at the periphery of polymerized structures with larger cross-sections. This is because the strain, $\varepsilon = \frac{\Delta l}{l}$, for a small lateral shrinkage length Δl over length l would cause the force defined by *Hooke's law* $F = \varepsilon Y$ and predicts a strong deformation of material with a lower Young modulus, Y, on the polymer-substrate boundary. As the material employed here, the silicon-zirconium containing hybrid *SZ2080* material suffer less from shrinkage compared to commonly used acrylate based or other sol-gel organic-inorganic materials [25, 185, 101, 186], the microstructures fabricated using it are prone to a lesser extent to such failure. Also, its glassy nature makes it compatible with glass substrates for microfluidic applications, where hydrophilic surfaces are required. It is of outmost importance to anchor the fabricated microstructures onto the substrate, to withstand the development of the unsolidified resin [118]. When required by design, the polymerized regions can be re-exposed since the polymerized material is still highly transparent to *IR* light.

An 100 nm spatial overlap of neighboring pulses corresponds to a scanning speed of 100 μm/s. The spherical aberration due to refractive index mismatch between the immersion oil ($n = 1.515$) and the glass substrate is negligible and spherical aberration-free structuring conditions exist for focusing depths up to $\sim$30 μm [187].

The focal lengths of the fabricated lenses were varied from several tens to hundreds of micrometers. For measuring such small focal distances a microscope setup mounted on a micrometer step-motor with step size of

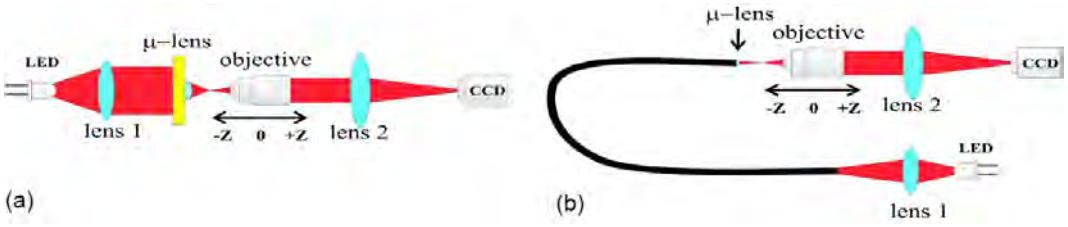

Fig. 13.1. Optical characterization of micro-optical element (a μ-lens) formed on a cover glass (a) and optical fiber tip (b).

2.5 μm (*Standa)* was used, as shown in Fig. 13.1a). As the stage moved, the focal plane of the microscope objective crossed through the focus of the fabricated microlenses, which was illuminated by collimated light from a *LED*. An image of the light distribution was captured using a *CCD* camera. The images were analyzed by fitting a *Gaussian* function to the acquired light distribution and the focal length of the lens was calculated. The same approach was used for the fibre-integrated microlenses (Fig. 13.1b). Spherical lenses with different radii of curvature and therefore different focal lengths were fabricated. The glass surface was considered as the reference for the focal distance measurement using the experiment described above and using the thickness of the lens as an offset (fabrication parameter). For validation, spherical lenses were fabricated and their focal length, which should be twice the radius of curvature, was measured.

Faster processing makes cost-effective the fabrication of multiple optical elements and arrays such as those used in micro-imaging and in light collection for solar cells. As recently demonstrated [131], shorter wavelengths of fs-laser irradiation increase the polymerization rate, hence, smaller overlap between adjacent pulses and smaller laser power can be used making laser polymerization more practical. Here, an array of aspheric microlenses was fabricated in *SZ2080* with frequency-doubled 515 nm/300 fs pulses at a fast 200 μm/s scanning speed using an immersion oil objective lens of numerical aperture $NA = 1.25$. Their diameter was $d = 50$ μm and maximum height $h = 11.7$ μm. The radial distribution of the height of a positive aspherical lens is given by a condition:

$$h(r) = \frac{1}{n^2}\left(F - n\sqrt{R^2 + F^2} + \sqrt{(n\sqrt{R^2 + F^2} - F^2)^2 - (1 - n^2)(r^2 - R^2)}\right) \tag{13.1}$$

where n is the refractive index of lens, F is the focal length, and R is the radius. This condition was derived for geometrical optics rays parallel to optical axis and converging to a single focal point, thus reducing spherical aberrations. The fabricated lens was tested by setup shown in Fig. 13.1 using a $NA = 0.9$ objective lens. The experimental value of the focal length $F_{exp} = 48$ μm was close to the designed focal length $F = 50$ μm. An error might be reduced by taking into account the height of the voxel.

In order to minimize the structural distortions of the photopolymerized *MOEs* and to make the fabrication sequence fast and practical, the area photopolymerized by direct writing should be minimized. The function of a volumetric microlens [54] can be also carried out by a Fresnel microlens (Fig. 13.2c)) which occupies a smaller volume and, hence, has advantages for integration into micro-electro-mechanical systems *(MEMS)*, their optical counterparts *(MOEMS)*, or microfluidic chips. The used shell-formation approach without lengthy raster-scanning of the entire volume (Fig. 11.4a) serves this purpose. The entire laser exposure process is reduced by a factor of $f_c \simeq 335$ for the case described previously in *Chapter 11.1.* The used shell-forming fabrication is a favorable approach for *Fresnel* lenses which require high precision in surface definition.

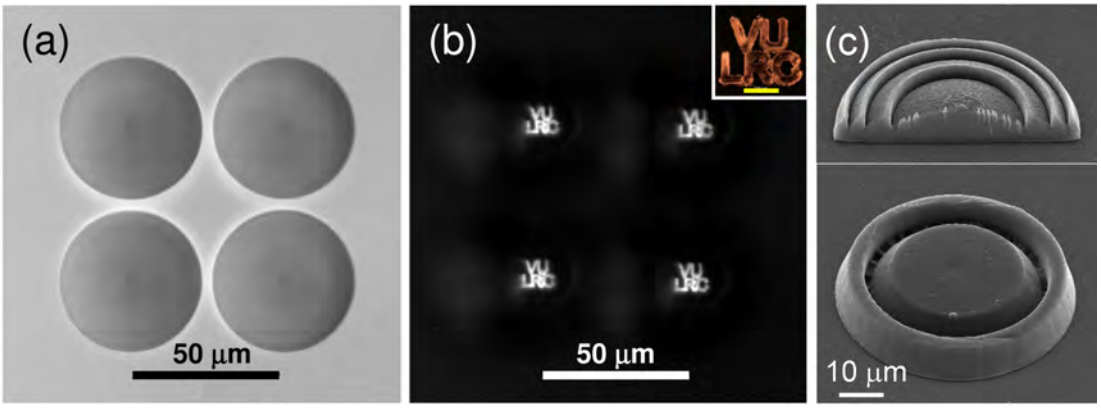

Fig. 13.2. μ-lenses and their performance. (a) an optical image of polymerized aspherical lenses; see text for details. (b) Image of the laser ablated logo pattern taken by the lenses shown in (a). The inset shows the image of pattern maks *VU LRC* ablated in copper film; scale bar 500 μm. (c) *SEM* images of test samples: a *Fresnel* half-lens and structure for a surface roughness determination on a cover glass formed by the fast polymerization sequence

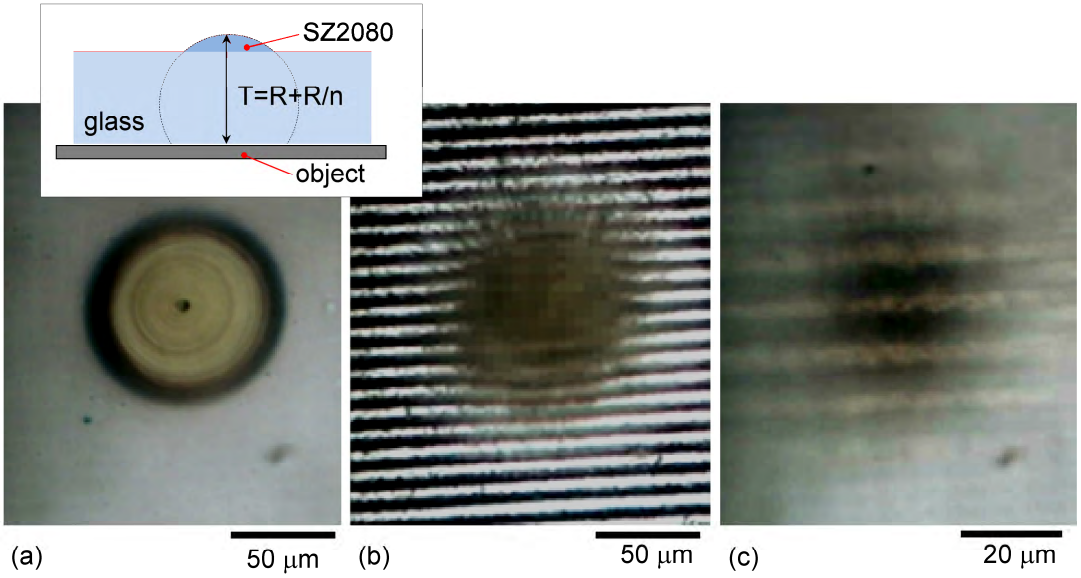

Fig. 13.3. (color online) (a) Top-optical view of the polymerized Weierstrass-sphere solid immersion lens (SIL). The inset shows the design where truncation, T, is defined by the radius, R, and refractive index, n, as $T = R + R/n$. (b) Top-view of the micrometer grid (the imaging object shown in inset of (a)). (c) The image of the scale through polymerized SIL. All images were taken with the same objective lens *(Olympus plan FL N 10× 0.25).*

Results showed that formed microlenses have near spherical surface, which closely corresponds with a spherical computer model, used for polymerization. Average deviations from the spherical shape were less than 0.5 μm which is $< 2.5\%$ of absolute value (Fig. 13.4a). It is important to note that voxel size and shape was taken into consideration while constructing the computer model used for polymerization. This allowed forming more precise shape of a microlens.

SILs are spherical plano-convex lenses that can be used to increase the numerical aperture, as well as the magnification of a microscope objective [188]. *SILs* are an interesting possibility for microscopic and spectroscopic applications, especially when liquid immersion techniques with water or oil cannot be used, eg., at temperatures below freezing. Another advantage is that a wide range of materials can be used to tailor the optical and mechanical properties of the immersion medium to the application as needed.

SILs increase the numerical aperture of an imaging system in two different ways. Firstly, the NA depends linearly on the refractive index n_{SIL}. *SILs* that have a half-sphere geometry rely on this effect, and refraction

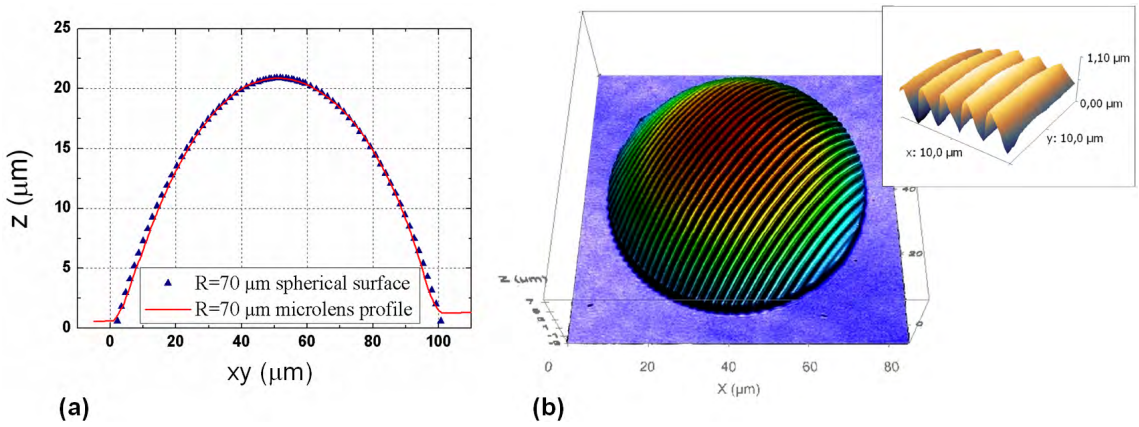

Fig. 13.4. (a) *µ-lens shaper and bi-functional microoptical component.* Comparison of $R = 70$ μm cut off sphere and fabricated microlens. Average deviations from the spherical shape were less then 0.5 μm. (b) Hybrid micro-lens with a phase grating. The curvature radius of the lens is $R = 67$ μm, grating period $d = 2.4$ μm. The crosection and topography images taken by profilometer (*Pl µ* 2300, Sensofar). Inset shows a profile measured by *AFM (Scanning probe, AFM dimension 3100, Digital Instruments).*

on the surface is kept minimal as the incident angle on the lens is nearly 90° degrees. The optical path length inside the medium is also constant, so chromatic aberrations are minimal. Secondly, by using the refraction on the surface of the *SIL* an opening angle can be increased. Typically a Weierstrass-sphere geometry (a sphere of radius R with refractive index n_{SIL} truncated to a thickness T of $T = R + R/n_{SIL}$) is used as it does not introduce additional spherical aberrations into the optical system [189]. Because this geometry uses both effects the increase of the numerical aperture is greater than the one of the half-sphere *SIL* and $NA \propto n_{SIL}^2$.

The second effect that solid immersion lenses have on optical imaging is the increase in magnification, which depends on the refractive index n_{SIL} of the lens, its radius of curvature R and its centre thickness T:

$$M' = M \times \frac{n_{SIL}}{\frac{T-R}{R}(1 - n_{SIL}) + 1}. \tag{13.2}$$

For a hemispherical *SIL* when $T = R$, the numerical aperture as well as the magnification increases by a factor of n_{SIL}, the refractive index of the lens material. For a *Weierstrass-sphere SIL* the increment factor equals n_{SIL}^2 as follows from eqn. 13.2.

Figure 13.3 shows the design and performance of the polymerized *Weierstrass-sphere* type *SIL*. This was made by only polymerizing the top part

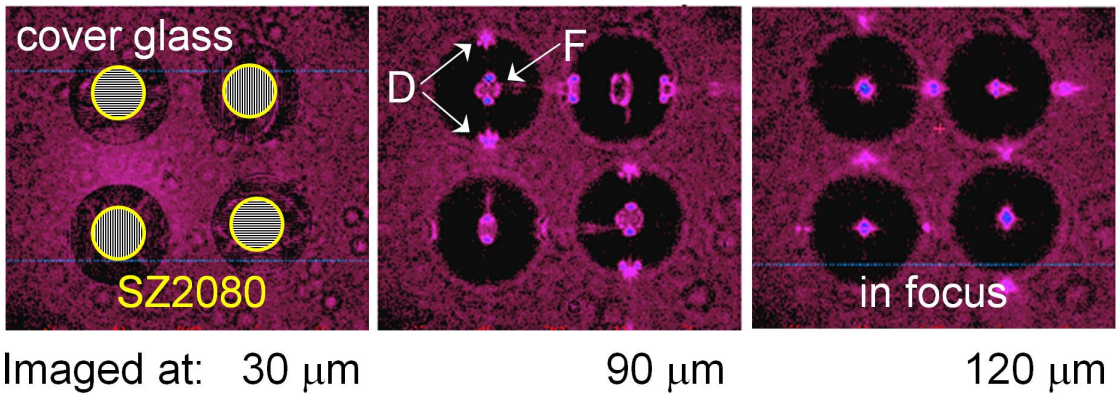

Fig. 13.5. Imaging of the light passed through an array of 2×2 of hybrid microlens-phase grating components at different distances from the cover glass surface as indicated. The orientation of gratings is shown schematically on the left-side image. The curvature radius is 67 μm; diameter 90 μm. Focus position at $\sim$ 120 μm distance from the surface of cover glass. The marks D and F denote diffracted and focused beams, respectively. See, supplementary online movie showing focusing and diffraction of this hybrid lens.

of the lens (see, inset in Fig. 13.3a). The combination of the cap and glass-substrate functions as a *SIL* due to the good matching of the refractive indexes between the *SZ2080* polymer (1.504) and cover glass ($n = 1.52$). The curvature radius of the Weierstrass-sphere *SILs* is 92 μm, the thickness of the glass substrate is 144 ± 1 μm. The manufactured polymer cap has a centre height of about 12 μm and a diameter of 93 μm. The focal length of the microlens was measured to be 175 ± 3 μm. The *SIL* was used to image a line grating (10 μm linewidth) with an ordinary microscope as shown in Fig. 13.3c. The magnification of *SIL* is calculated to be $M = 2.4 \pm 0.1$ which is near to the expected value of $M = n_{SIL}^2 \simeq 2.3$. As arbitrary freeform surfaces can be created it is possible to use complex optical surfaces that are more complex than plain, spherical ones. Aspheric *SILs* could be designed to suppress aberrations and to improve imaging quality. It is also possible to manufacture solid immersion lenses directly onto the sample. It is noteworthy, photo-polymerized photonic crystal templates or microlenses can be used for imaging inside liquid, since the phase delay of light introduced by the *3D* polymeric structure alters the phase of the passing light. As a result an imaging of the out-of-focus plane is possible by a *3D PhC* template [177].

Refractive microlenses are widely used in optical communications, digital displays, optical data storage, beam formation and bio-imaging as well

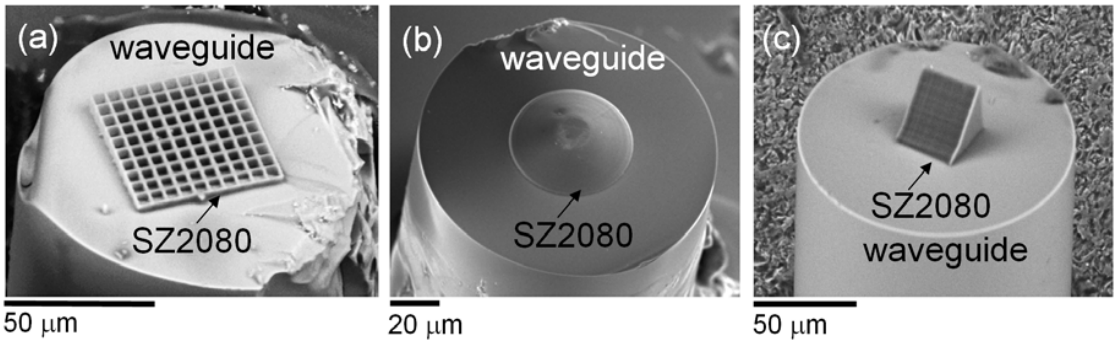

Fig. 13.6. SEM images of a tilted micrograting (a), a microlens (b) and a microprism (c) photo-polymerized on a optical fiber tip.

as biomedical applications. The diffractive optical components offer complimentary beam shaping versatility. There are many different methods to fabricate refractive and diffractive microoptics [190, 191], however, the issue of manufacturing hybrid components in a single step procedure is still outstanding. Direct write polymerization offers unmatched flexibility in the production of bi-functional refractive-diffractive micro-optical devices. For example, microlenses with a phase grating on them can be manufactured in a single step, (Fig. 13.4) as well as microlens arrays, where each lens has on it a differently oriented grating (Fig. 13.5).

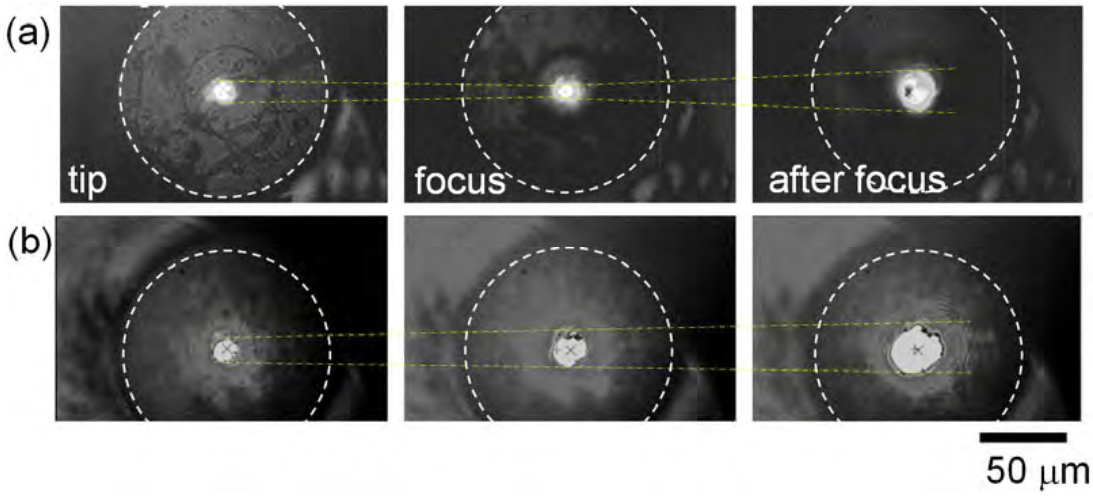

Fig. 13.7. Focusing of light emitted from the fiber with the tip-lens (a) and without (b). The dashed-circle marks the circumference of the fiber tip; lines are eye guides for the focusing and diffraction. The focus of imaging plane is at the fiber tip $z = 0$ μm (left), at the focus $z \simeq 33$ μm, and $z = 100$ μm from the tip of fiber (right side images).

Figure 13.5 shows a light beam propagating through a hybrid micro-optical element, as it is focused by the spherical profile shape and diffracted due to the periodic lines on the surface. Zero to fourth order diffraction maxima were observed. In optical elements arrays diffraction gratings of neighboring lenses can be formed at a varying angle, allowing different light flow control variants to be achieved. There has been already shown that fibre-top micro-optics can increase their coupling or splicing efficiencies [192]. However, their manufacturing is not an easy task, starting from the precise positioning of the fiber. Figure 13.6 shows a tilted *2D* grating, a lens and a prism hybrid structure fabricated on the tip of an optical fibre by direct laser writing. The lens is functional as qualitatively illustrated in Fig. 13.7. The average surface roughness across the polymerized surface was typically $\sim 30 \pm 3$ nm (Fig. 13.8), which is already in the range of a tenth of an optical wavelength in the visible spectral range. The roughness of ∼5 nm is due to grains formed during the fabrication and development process. Such roughness is acceptable for optical devices such as microlenses.

In order to demonstrate versatility and applicability of the laser polymerization technique single optical elements of complex surfaces such as aspherical, Fresnel, and solid immersion lenses were fabricated by raster scanning only outer shell. In addition, *MOE* with combined optical functions and hybrid refractive-diffractive optical elements integrated with optical fibres are presented. The formation of single and hybrid refractive-diffractive elements by fs-laser polymerization was demonstrated using a fast and practical shell-formation and *UV* homogenization procedure. Such processing sequence speeds up the laser exposure by a factor of $\sim 10^2$. The refractive

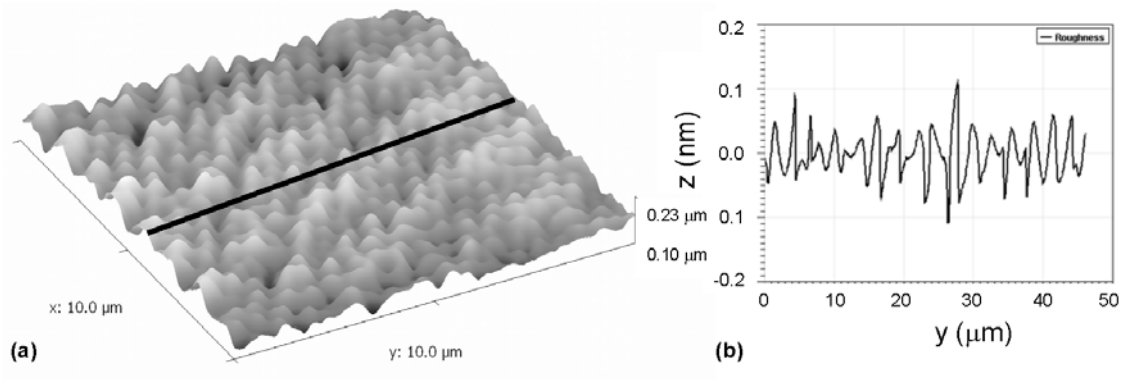

Fig. 13.8. Surface roughness of a fs-laser polymerized *SZ2080*. (a) shows typical *AFM* measured profile and (b) line-marked cross section.

index matching between cover glass and *SZ2080* was exploited for the fabrication of functional *SIL* lens by cap-polymerization. Imaging magnification increase by ~ 2.4 times, as expected for a fully formed *SIL*, was experimentally demonstrated. Arrays of such *SIL* lenses can be formed on cover glass or outside walls of micro-fluidic chambers and used for laser trapping. The integration of a diffractive grating and lens on the tip of optical fibre was demonstrated. The fabrication of single micro-optical elements, and the possibility to make optical elements with combined functions and their integration into fibre optical elements adds new functionalities in the fields of optomechanics, optofluidics, and sensors.

13.2 Elements of photonics

Rapid progress in photonics has been achieved because of continuous advances in nanotechnologies, materials science, microoptics, theoretical physics and development of microfabrication techniques. Polymers have emerged as an important class of materials for applications in photonics. In particular, interaction of light with materials possessing a periodic modulation in their structure has led to a range of interesting and sometimes even unique effects, which have shown promising applications in the production of *Bragg* mirrors, optical switches, spectral and spatial filters [193, 194], superprisms [195], waveguides, and optical resonators [196]. In this section, sample polymeric nanostructures doped with fluorescent dyes are presented as models for opticaly active components.

Though the main attractive features of the *FLMP* are explored in details in the reference papers [197, 63], possibility to fabricate doped polymer structures by *DLW* is still important issue to be examined. For the fabrication of functional devices, doping of polymers with various active dopant molecules or nanoparticles could be essential in order to ensure required function relevant to application. Organic dye molecules could be an example of dopants providing fluorescence and lasing ability of the fabricated microstructures. Wide range of dye molecules with different properties is available in the optical region from *UV* to *NIR* wavelengths [198]. When introduced into polymer structures, these dopants could serve as fluorescence markers in order to examine the interior of *3D* devices using modern laser scanning fluorescence microscopy methods enabling optical section-

Table 13.1. Properties of fluorescent dyes in ethanol (*quantum yield in methanol).

Fluorescent dye	Absorption peak, nm	Emission peak, nm	Quantum yield
R6G	530	556	0.95
Fluorescein	512	530	0.75
DCM LC6500	472	644	0.44
Coumarin 152	397	510	0.19

ing. Internal diagnosis of fabricated structures is of great importance for the development of *FLMP* technology towards high accuracy true *3D* fabrication [199]. In biomedical applications, fluorescing scaffolds for cell culture growth would enable better imaging of proliferating cell cultures [200, 201]. Finally, tunable light sources integrated in *LOC* microsystems are attractive for novel sensor concepts. One of such photonic device for compact integrated light sources is *DFBL* [202], which cavity is based on light-confinement in a *Bragg's* grating. Such microlasers are particularly suitable as *LOC* components because of possibility to integrate them with other functional polymer components. Moreover, in order for the lasers to be used in sensor systems a large *Free Spectral Range (FSR)* of the cavity is required, which often implies having subwavelength features [203]. In this paper, we present recent results on fabrication of organic dye doped polymer microstructures by using direct writing technique based on *FLMP*.

The used *FLMP* setup was *Ti:Sapphire LRC*. In these experiments negative tone sol-gel *SZ2080* material was used photosensitized with *4,4'-Bis(dimethylamino)benzophenone* as the photoiniator. Organic dyes used as dopants were *R6G* (*Molecular Probes Inc*), fluorescein (*Acros Organics b.v.b.a.*), *DCM LC6500* (*Lambda Physik AG*) and *coumarin 152* (*Sigma-Aldrich GmbH*), (see Table 13.1 for data and Fig. 13.9 for graphed spectrum). For doping of the photoresist, dyes were dissolved in isopropanol (*Riedel-de Haen AG*), and then the solution of a dye was mixed with *SZ2080*. The dopant concentration has been varied from 0.01 wt.% up to 0.05 wt.%. The highest concentration used was limited by the dye solubility. If the dyes were not completely dissolved, microexplosions occurred and bubbles appeared in photoresist during fabrication. *R6G* and *fluorescein* have been selected for fabrication experiments using two different dopants due to the high fluorescence quantum yield and the difference in

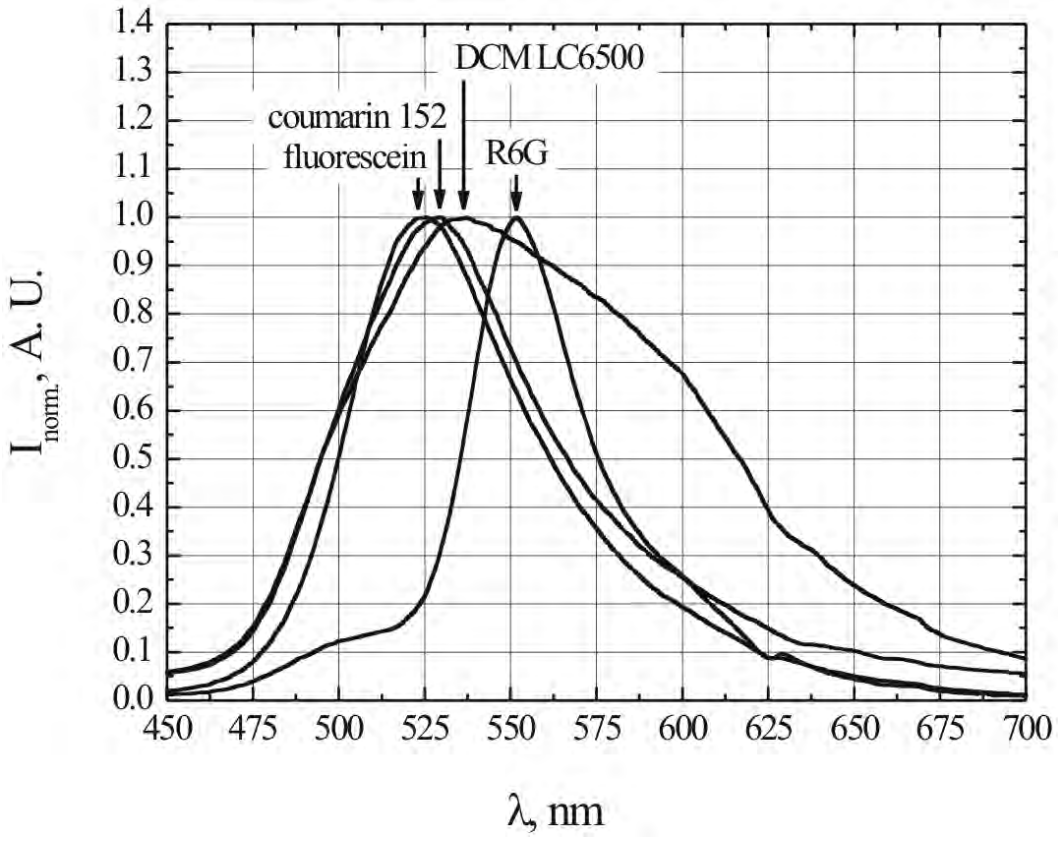

Fig. 13.9. Normalized emission spectra of *SZ2080* doped with fluorescent dyes registered at excitation wavelenght of 409 nm.

the emission spectra.

SEM image of *3D* pyramid fabricated out of *SZ2080* doped with *R6G* up to 0.05 wt.% is shown in Fig. 13.10a). The pyramid is fabricated as hollow woodpile-like structure in which every layer starting from the base consists of two sets of four densely packed parallel rods at opposite sides of the square layer of the pyramid. In every adjacent layer, sets of rods are shifted to the center of the pyramid and rotated by 90 degrees relative to the previous below laying layer. Thus, the resulting structure is hollow square pyramid, which height and base length is 30 μm and 65 μm respectively. As seen from *SEM* image, quality of the fabricated structure is quite good and no negative influence of dopant entrapped in the polymer has been detected. Under illumination by blue-green light the feature fabricated shows bright fluorescence with spectral features characteristic to the dopant *R6G*. It allows usage of the confocal fluorescence microscopy methods in order to examine the interior of the pyramid by optical sectioning. Fluorescence imaging was carried out by using conventional custom made

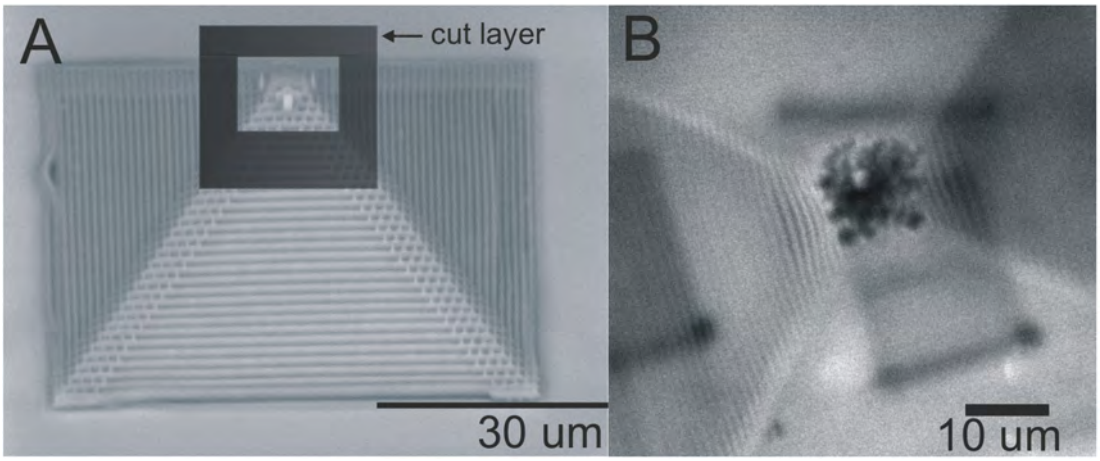

Fig. 13.10. SEM (a) and fluorescence (b) microscope images of *3D* hollow pyramid fabricated out of *SZ2080* doped with *R6G*.

confocal microscope. Femtosecond excitation pulses at 409 nm wavelength were focused by 50x ($NA = 0.8$) objective lens inside the pyramid. Emitted fluorescence was collected by the same lens and detected through dichroic mirror and confocal aperture of 60 μm diameter. Fig. 13.10b) presents the result of fluorescence imaging of the interior of doped hollow pyramid. Optical sectioning was carried out layer-by-layer from the base of the pyramid. The confocal section of the pyramid few woodpile layers below apex, shows clearly resolvable rods forming opposite faces of the pyramid at the particular height. Though *SEM* imaging provides information on rather regular structure of the outside of the pyramid, fluorescence microscopy reveal, that internal surfaces of the pyramid faces are covered with irregular structures probably formed during development procedure and drying of the rinsing solvent (Fig. 13.10b)). Thus, our results demonstrate not only possibility but also the importance of examining the interior of the *3D* structures fabricated by *FLMP* technique. We demonstrate that doping of the materials used for fabrication by *FLMP* with fluorescence marker molecules does not decrease the quality of the fabricated structures. However, it enables study of the interior of *3D* structures by scanning microscopy techniques with optical sectioning capabilities such as confocal or nonlinear fluorescence microscopy.

The possibility to fabricate structures consisting of two or more materials having different mechanical and/or optical properties on the same substrate could offer the way to create *"smart"* microstructures. These struc-

tures act as a pre-designed micromechanism which is affected to changes in environmental conditions (eg. actuator) [204]. To test this idea, we fabricated two component grating out of *SZ2080* doped with *R6G* and *fluorescein* up to 0.05 wt.%. The grating was fabricated in successive manner using standard sample preparation, fabrication and development procedures for every doped component. Firstly, horizontal lines were fabricated out of *SZ2080* doped with *R6G* and then unexposed photopolymer was washed away. Secondly, fluorescein doped *SZ2080* was drop-casted on free-standing horizontal lines and vertical lines were formed. The period of the grating is 5 μm. Fluorescence imaging (wavelength 800 nm, objective 8x ($NA = 0.5$)) results are presented in Fig. 13.11 As emission spectra of *R6G* and *fluorescein* are partially overlapping (Fig. 13.9), better spectral separation of different components of the grating was achieved by narrow bandpass filters (520 nm and 500 nm, spectral bandwidth 10 nm *FWHM*) in front of the detector. Though separation of the grating components was not complete due to spectral overlap and fluorescein emission, horizontal grating lines are well resolved in raw fluorescence image detected through 520 nm bandpass filter (Fig. 13.11a)). The only fluorescein-doped vertical lines of the grating are present in the image taken through 500 nm filter (Fig. 13.11b)). However, concentration distributions of dopants calculated from raw images (Fig. 13.11c) and d)) reveal the presence of fluorescein in *R6G*-doped horizontal line component of the grating as well as accumulation of *R6G* at the edges of vertical lines doped with fluorescein. It is probably that this has happened due to extraction of dopants into rinsing solvent during second development procedure. Drying of the solvent results in accumulation of dopants at the edges where lines are attached to the glass substrate.

Structures fabricated by *FLMP* out of biocompatible polymers are supposed to serve as scaffolds for stem cell growth in regenerative medicine [95]. Marking scaffold with fluorescent dyes helps to trace cell proliferation in it as the structure is highly fluorescent upon investigation [63]. Fig. 13.12a) represents one of possible doped scaffold models for cell growth fabricated over relatively large area (1 x 1 mm^3). The dimension of one honeycomb line is 20 μm. Recently tested fluorescing scaffolds in preliminary cell growth enables more detail observation of growth process using fluorescence microscopy methods.

Finally, one of the ultimate goals of doping polymer nanostructures with

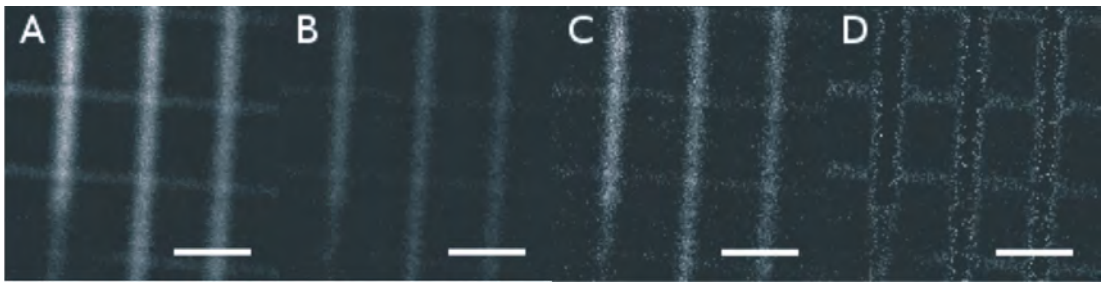

Fig. 13.11. Scanning fluorescence microscopy images of two component grating fabricated out of *SZ2080* doped with *fluorescein* (vertical lines) and *R6G* (horizontal lines). a) and b) are row images taken through 520 nm and 500 nm bandpass filters, respectively. c) and d) are calculated concentration distributions of *fluorescein* and *R6G*, respectively. Scale bars are 5 μm.

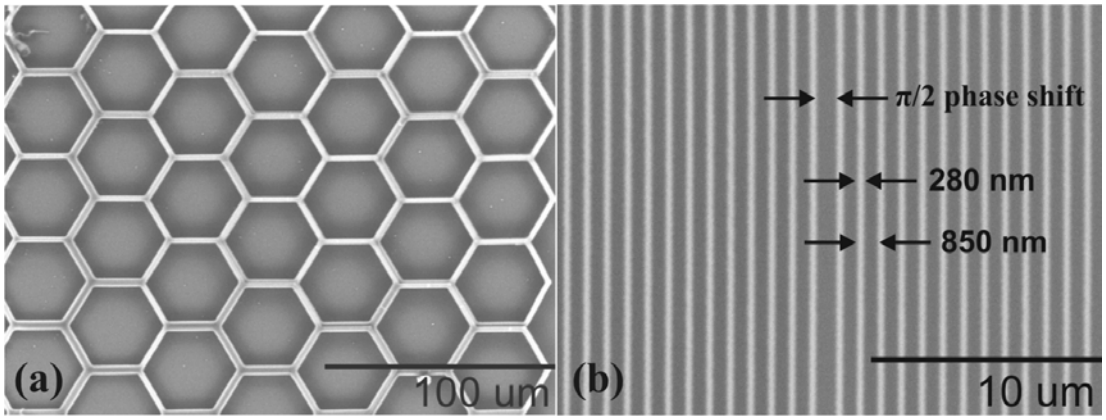

Fig. 13.12. SEM images of: a) scaffold fabricated out of *SZ2080* doped with fluorescein. b) distributed feedback dye laser resonator model fabricated out of *SZ2080* doped with *R6G*.

highly fluorescent molecules is to open the way for constructing optically active devices such as microlasers which would exploit the new possibilities of nanostructuring technologies of the lasing materials. One of the challenges is to produce microlasers such as *DFBL* [205]. An example of *DFBL* resonator model fabricated out of *SZ2080* doped with *R6G* with linewidth of 280 nm and period of 850 nm is shown in Fig. 13.12b). Such lasing microstructures are supposed to be beneficial of compact size, low power consumption and easy integration into more complex *LOC's* fabricated by using the same technological approach. The optical resonator is based on *Bragg's* grating structure with introduced phase shift of a $\lambda/2$ in the middle of resonator in order to obtain a single resonance for each *Bragg's* reflection. The grating parameters were calculated to satisfy the *Bragg's* condition:

$$m\lambda_m = 2\Lambda_{op} \tag{13.3}$$

where m = 1, 2, 3... is the reflection order, λ_m is the wavelength and Λ_{op} is the optical path length of one grating period [205]. Estimated optical path and linewidth for the third order reflection is 846 nm and 282 nm respectively. In order to test lasing ability of the *DFBL* model, the fabricated structure was side-pumped by frequency doubled radiation of Q-switched *Nd:LSB* microchip laser (531 nm, 0.5 ns pulse duration at 5 kHz repetition rate, *Standa Ltd*). Fluorescence of the structure was analyzed with high resolution spectrometer (*HR2000, Ocean Optics Inc.*) expecting the spectral narrowing of the fluorescence at the higher optical pump intensity than threshold required to initiate lasing. However, we noticed bleaching of fluorescent dye when the resonator was pumped at the higher intensities required for the spontaneous emission generation. This implies, that limited photostability of dopant molecules is one of the main obstacles to get lasing of polymer microstructures. Possible solution for this problem could be encapsulation of fluorescent dye's molecules into dendritic macromolecules (dendrimers) [198] making organic dyes less affected by reactive species such as radicals and singlet oxygen.

Here it was shown that doping of *SZ2080* with fluorescent dyes (*R6G, fluorescein, DCM LC6500* and *coumarin 152*) up to 0.05 wt.% does not significantly reduce photostructuring capabilities of *FLMP* technology. Doped *3D* micro/nanostructures were fabricated out of *SZ2080*. We demonstrate that doping with fluorescent dyes enables diagnosis of internal structure of fabricated *3D* features by the means of fluorescence microscopy techniques. Doped artificial scaffolds for cell growth were fabricated facilitating observation of cell proliferation. Finally, *DFBL* laser model was successfully fabricated from *SZ2080* doped with *R6G*. Low photostability of the dye in polymer matrix still remains the main problem to be solved in order to get functioning microdevice.

14 *3D* SCAFFOLDS FOR STEM CELL GROWTH

Due to diseases or traumas the demand of tissues and organs which could be implanted into patient is high [206]. However, in order to engineer artificial tissue out of autologous cells, specific extracellular material of complex *3D* architecture is needed. In nature, cells in living organism are surrounded by extracellular matrix which plays an important role in cell functioning, proliferation, differentiation, adsorption and others. Extracellular matrix forms natural scaffolds for every tissue. At this point, studies are focused on producing artificial scaffolds out of biocompatible materials. Such scaffolds could act as a skeleton for controllable stem cells growth and formation of artificial tissues [207]. *FLMP* technology satisfies the requirements based for *3D* fabrication of scaffolds and range of photostructurable polymer materials are known to be biocompatible [208]. Furthermore, proliferation and differentiation of stem cells can be controlled by changing chemical and mechanical properties of the used materials [209]. Nevertheless, much efforts are still needed to improve the fabrication technology itself, increase efficiency as well as study cell growth and behaviour. Using new approaches, such as embryonic stem cells as cell source and novel design of *3D* scaffolds, tissue engineering brings a promising future to patients requiring tissue repair and organ replacement [210].

Nowadays, complex form polymeric matrices are designed for primary stem cell growth. It can serve as an artificial scaffold for growing tissue in practice of regenerative medicine, which has its special requirements. There is a need for controlled porosity because every tipe of tissue has its individual best pore sizes to grow [210]. For eg., the pore size of 5 μm was shown to be sufficient for neovascularization [211]. For chondrocyte culture, more chondrocytes appeared as spherical chondrocytic morphology and were closely packed in scaffold with 20 μm pore size compared 80 μm

pore size. At bigger pore size, chondrocytes preferred to spread over the wall of the pores as elongated morphology and cell-cell interaction was limited [212]. For fibroblast ingrowth, the optimal pore size was found to be 20 μm [213]. Relatively large pore size such as 500 μm was also successfully used for fibrovascular tissue ingrowth [214]. For adult mammalian skin, 20-125 μm were found to be the optimal pore size range [215]. The pore size range of 135-635 μm was applied to engineer adipose tissue [216]. The effect of pore size on bone ingrowth provided by various scaffolds in bone engineering covers 10-800 μm. Pore sizes of 200-400 μm were suggested to be the optimum and pore sizes of 80-100 μm were considered to be the minimum for bone ingrowth due to osteoconduction [217]. However, the optimal pore size of the scaffolds depended on the mechanism of tissue regeneration, but with *FLMP* porosity can be strictly controlled in a flexible manner. The biodegradation or biostability of the scaffold is essential to match the rate of neotissue formation [218]. *FLMP* can be applied for *3D* out of biodegradable and with biostable materials depending on targeted application. Laser fabricated created scaffolds can have required mechanical integrity and maintain the predesigned tissue structure, also they have been proved to be non-cytotoxic and positively interact with cells, not interfere cell migration, growth, adhesion and differentiation [219].

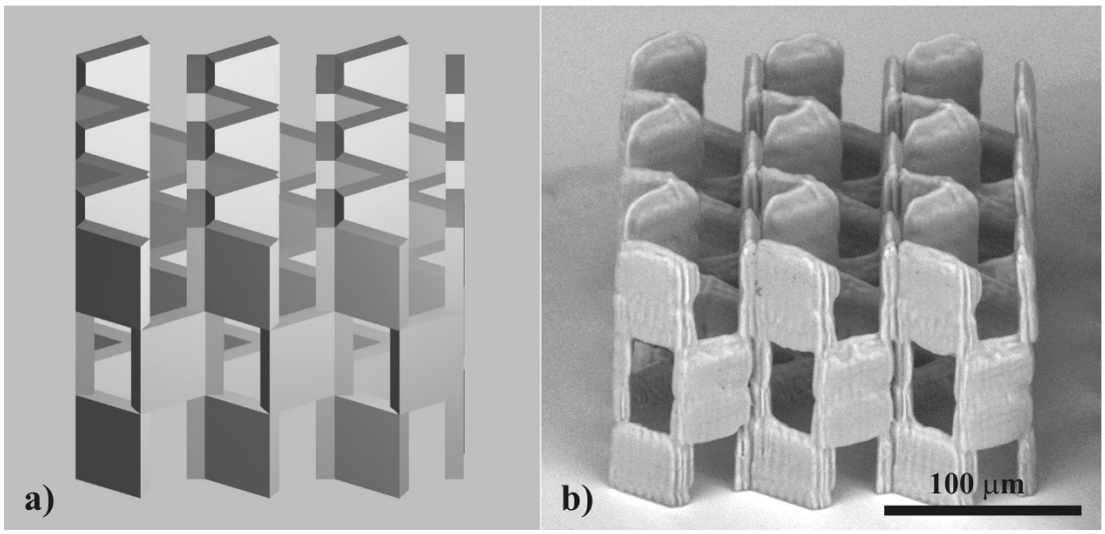

Fig. 14.1. CAD model of microporous *3D* honeycomb structure (a) and a scaffold fabricated out of *SZ2080* biocompatible polymer (b).

As the *FLMP* baser fabrication technology is not restricted to geometry in *3D* and able to process a vast variety of materials it offers a promising perspective for production of specific scaffolds for tissue engineering. Example of a rigid true *3D* scaffold structure fabricated directly from *CAD* model is shown in Fig.14a) and b). Such structures could be promising artificial scaffolds for cell proliferation in *3D* exhibiting high mechanical strength as are made of *3D* honey-comb structures with intentionally introduced gaps. The pore size of the scaffold has to be around twice as big as the size of the single cell, and for mammals it would correspond to be tens of micrometers [220]. Precise control of pore sizes, their homogeneity and interconnection is believed to be beneficial for cell proliferation [221]. Also, scaffold stiffness and biodegradability will depend on inner architecture, filling factor ($V_{material}/V_{scaffold}$) and surface area of the structure [222]. For modern implants and cell-based artificial tissues, it is important to engineer structures with characteristics that closely emulate nature. The advances in various fields of science enable and enforce the scientists to search for novel biocompatible biomaterials with distinct properties and innovative design which are necessary for engineering contemporary composite tissue with a purposeful orientation towards anatomic structures. The *FLMP* technique seems to be suitable for production of *3D* microstructured polymer scaffolds with rigid internal architecture. Flexibility of the geometry change enables to rapid manufacturing of novel design templates and test their biomedical properties experimentally before such constructs will be applied in practice.

In this work the *in vitro* and *in vivo* biocompatibility investigations of non-structured, *2D* and *3D* structured photopolymers were performed in *Vivarium* of *Institute of Biochemistry, Vilnius* by biologists and surgeons using rats and rabbits and their stem cells as test animals.

14.1 Material biocompatability *in vitro*

Artificial microstructured scaffolds covering up to cm area were produced out of *SZ2080*, *Ormocore b59*, *AKRE* and *PEG-DA-258* materials shown in Fig. 14.2a) and b). They were used for cell biocompatibility tests *in vitro*. Additionally, spin-coated films were used to test the biocompatibility of non-structured photopolymers. In both cases the cell growth and proliferation results were comparable to the surfaces of glass or polystyrene plates used

as the control substrates.

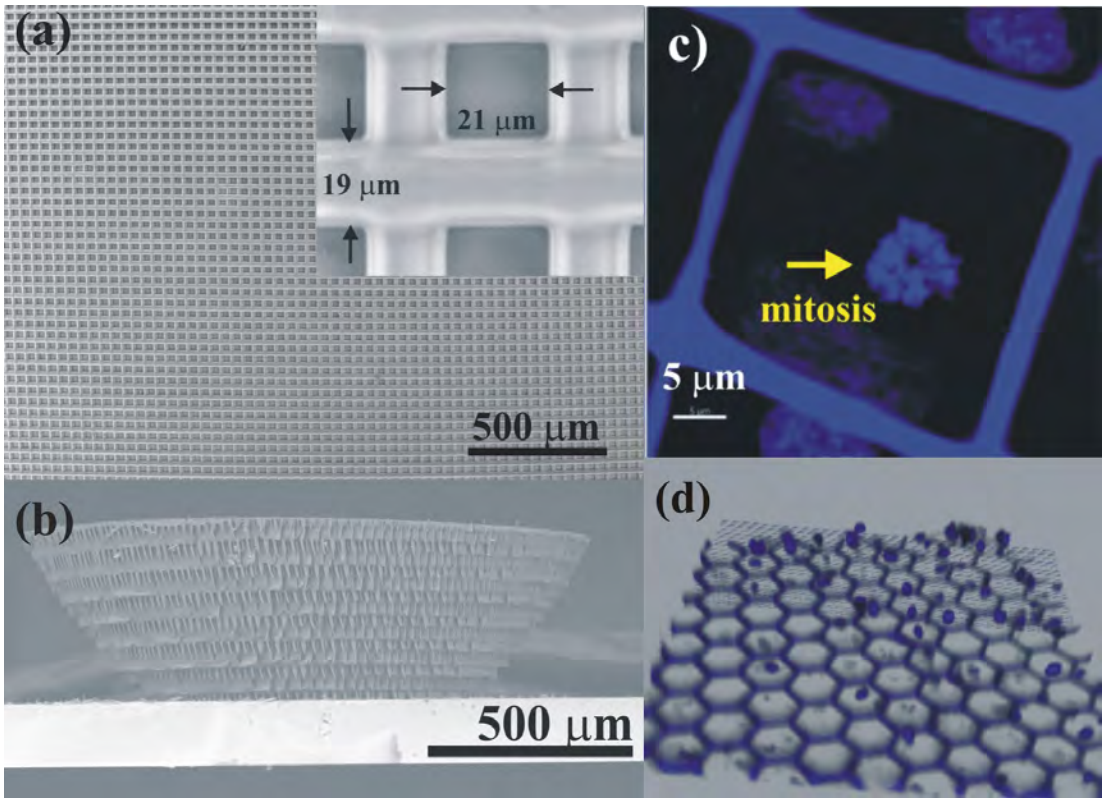

Fig. 14.2. SEM micrographs of artificial *2D* and *3D* polymeric scaffolds fabricated out of *SZ2080* material, (a) and (b). Fluorescence and confocal microscopy images showing blue stained cells attached on a polymeric honey-comb grid, (c) and (d). In c) it noticeable a cell mitosis meaning the cell is ready to multiply and in (d) it is seen that the cells are climbing to up on the *2.5D* honey-comb scaffold.

Adult stem cells derived from rabbit or rat muscle were used for cell-based artificial tissue engineering on the *FLMP* laser fabricated scaffolds. Myogenic stem cells were isolated from skeletal muscle tissue and grown in *Iscove's* modified *Dulbecco* minimum essential medium (*Sigma-Aldrich GmbH*) supplemented with 10% fetal calf serum (*Sigma-Aldrich GmbH*) in multiple polystyrene tissue culture plates (*Orange Scientific, Switzerland*) [223, 224]. After, primary adult myogenic stem cell line was used for the constructing of cell-based artificial tissue on the *FLMP* engineered scaffolds. Prior to cell inoculation to well containing the scaffold, they were stained with 10 μg/ml *diamidino-2-phenylindole (DAPI). DAPI* is the classic blue fluorescent probe for viable cells that fluoresce brightly when it is bound

to *DNA*. Cells were inoculated at a density of 60000 cells per ml, after 72 h cultivation the proliferation of stem cells on the scaffolds was assessed microscopically.

FLMP technique enables creation of flexible scaffolds (having mechanically free movable parts). For eg. a chain-mail structure consisting of separated intertwined rings can be manufactured, as shown in Fig. 14.3. This kind of structure is known to be flexible and light yet strong armor from the Medieval times. The secret strength of the structure is caused for the reason that the applied pressure is distributed to every ring homogeniously making the local tension spread in wider area. Besides to flexibility and strength this kind of geometry allows to mechanically tune the porosity by simply stretching the structure.

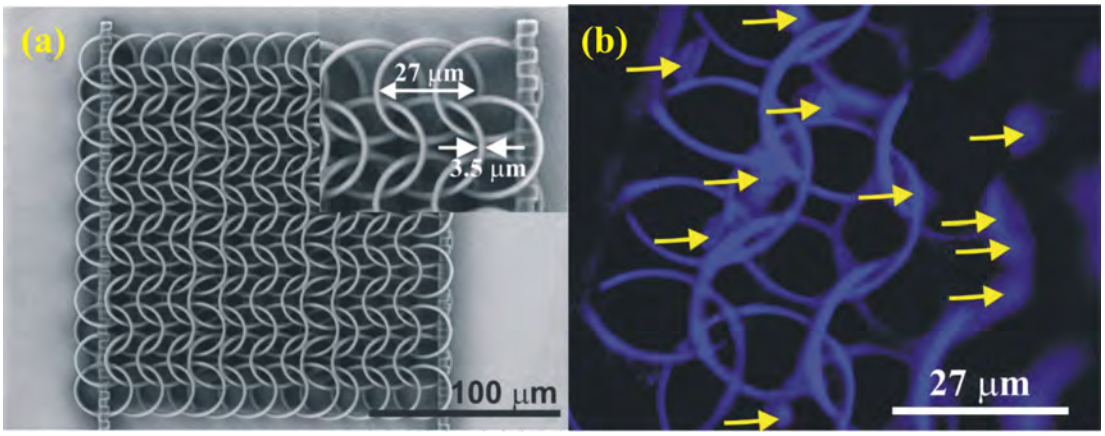

Fig. 14.3. Chain-mail structure consisting of free-hanging intertwined rings as a flexible scaffold (a) and arrows indicating cells growing on it (b). *SEM* and fluorescence microscopy pictures, respectively.

14.2 Material biocompatability in *in vivo*

In animal study, we evaluated biocompatibility of different polymeric samples manufactured as shapeless granules. For the comparison of the tissue response to test-materials, as control, reaction to surgical clips and surgical suture was evaluated also. All test and control samples were inserted intramuscularly into rat‘s organism. During three weeks postoperative period

the animals were observed carefully. It was confirmed that there were no complications of wound healing, the animals were curious and had healthy appetite. The white blood cell count and neutrophil count were identified in normal ranges in all the experimental groups, except for *AKRE* group, during three weeks. Implantation of *Ormocore b59*, *PEG-DA-258* and *SZ2080* did not provoke any clear inflammatory or allergic white blood cell reaction. However, leukocytosis, neutrophilic reaction and increase of monocyte count were noticed in *AKRE* group. The monocyte count was slowly increasing in this group during three weeks, thus showing the formation of chronic inflammatory response. Implantation of surgical clips did not provoke any clear acute inflammatory reaction when evaluating white blood cell fractions. Nevertheless, monocyte count was slowly increasing during the period of three weeks, suggesting easy chronic inflammatory reaction due to implantation of this common surgical device. No eosinofilic reaction was noticed in any of the experimental groups. After three weeks healing the test sample-surrounding tissues were harvested and analyzed histologically. The microscopic slides were stained with *H&E* and immune cell infiltration was evaluated. Lymphocytic infiltration was sparse in almost all the slides except *AKRE* - bearing surrounding tissues. Nevertheless, it is noteworthy that almost the same image was observed in the tissues surrounding surgical clip and surgical suture. It is known that surgical suture as well as traditional surgical metal devices show good biocompatibility and are biologically inert. Taking into account the fact that surgical clips and surgical suture are known as biocompatible implants widely used in surgical practice, we can be not so critical about the biocompatibility of tested polymers including *AKRE*. Comparing tests *in vitro* and *in vivo* we conclude that *AKRE* is less biocompatible polymer than *Ormocore b59*, *SZ2080* and *PEG-DA-258*.

Within the limitations of this study, the following conclusion can be drawn: adult myogenic stem cells proliferation tests on polymeric substrates show that the selected laser *3D* microstructurable materials such as *Ormocore b59*, *SZ2080* and *PEG-DA-258* are applicable for biomedical practice. It is supported by the *in vivo* biocompatibility tested for these polymer materials implanted in living organism. The obtained results are encouraging for the future work.

However, further efforts, like investigation of cell adhesion intensity *in vitro* and biodegradability of scaffolds *in vivo* as well as design of scaffolds with suitable mechanical properties have to be done before the regenerative medicine accepts it into everyday practice. Our approach to engineering of artificial autologous tissues based on stem cell cultures populating custom designed *3D* polymeric scaffolds seems to offer good future prospects. The direct laser writing techniques for fabrication of custom polymer scaffolds for tissue engineering seems to offer both unmatched flexibility needed for laboratory research and sufficient fabrication throughput for practical application. Testing of artificial tissues in the experimental models of laboratory animals is in progress.

15 CONCLUSIONS AND OUTLOOK

15.1 Conclusions

Thanks to the efforts of synergetic work of our group and other collaborative research groups, we have expanded the capabilities of *FLMP* fabrication technique pushing it forwards to the state being applicable for industrial demands. While such issues as improvement of fabrication spatial resolution and incorporation of new materials continue to attract considerable attention, this technology is already at a mature enough stage that the focus is evolving towards applications. Our constructed laser *3D* fabrication system can serve as a laboratory prototype of machinery for rapid and routine *3D* micro/nanostructuring over large areas (volumes) as well as custom small scale production. This has already drawn a great interest for microoptical, photonic, biological, microfluidic and optofluidic applications. The latter growing interest forces further improving of *FLMP* technology. Successive introduction of novel ultrafast laser excitation sources, study on photopolymerization mechanisms and material response at nanoscale revealed important issues in the *3D* nanostructuring to be addressed for the future scientific and technological applications. Avalanche ionization and self-polymerization are of critical importance in order to manufacture high spatial resolution and not distorted functional micro/nanodevices. Lastly, though addressed in this study, possibility to photostructure various materials on different substrates, capability to integrate simple elements into integrated microsystems, as well as incorporation of several functions in a single component, are still of a great importance.

15.2 Outlook

Despite recent advances in the field of direct laser micro/nanofabrication, it is still a great challenge for material scientists to offer suitable materials for true *3D* photostructuring. Though there is a way to introduce shape precompensation in order to minimize structural distortions [225, 186], yet it seems more like the optimization of the materials could be ultimate solution [36, 131]. As in has been presented in this thesis, *FLMP* technique based on femtosecond laser offers opportunity to fabricate *3D* functional micro/nanodevices for various specific applications. Further improvements of this technique could be realized applying Optical Parametric Amplifiers (*OPAs*) and adjusting laser wavelength to the materials two-photon or more photons absorption. It would enable easy laser-to-material tuning which would optimize the multi-photon polymerization efficiency, thus providing higher resolution. Furthermore integration of STimulated Emission Depletion (*STED*) method to *FLMP* can offer unmatched axial resolution which would mean the dimensions of *voxel* to be far less 100 nm and would open a way to nano-realm using *VIS/NIR* light [226]. An excess of available power in amplified laser systems could be utilized by applying Multi Lens Array (*MLA*) [40]. Alternatively advances in beam shaping could also be applied here, like *Bessel* beam, Diffractive Optical Element (*DOE*) or holographic mask could be used to modify light intensity distribution for exposure. This would enable *DLW* nanostructuring in *3D* with increased throughput up to few hundred times. Perhaps, Shaded Ring Filters (*SRF*) will be widely applied to decrease the aspect ratio of the *voxel*. *FLMP* produced structures will be more often used as a templates for further steps as selective metallization, infiltration and double material inversion techniques are being developed rapidly. Besides to that, it will make an advance in new extensively explored fields of nanophotonics and plasmonic metamaterials. Additionally, it will enable fabrication of true *3D* electric circuits, thus transferring planar microchips to the third dimension. One of the coryphaei in the *FLMP* field *M. Hermatschweiler* has recently commented *"The field of* 3D *nanostructures is bigger than we could ever have imagined. And it is impossible to give precise figures about growth when a new technology creates and stimulates the market"* [227].

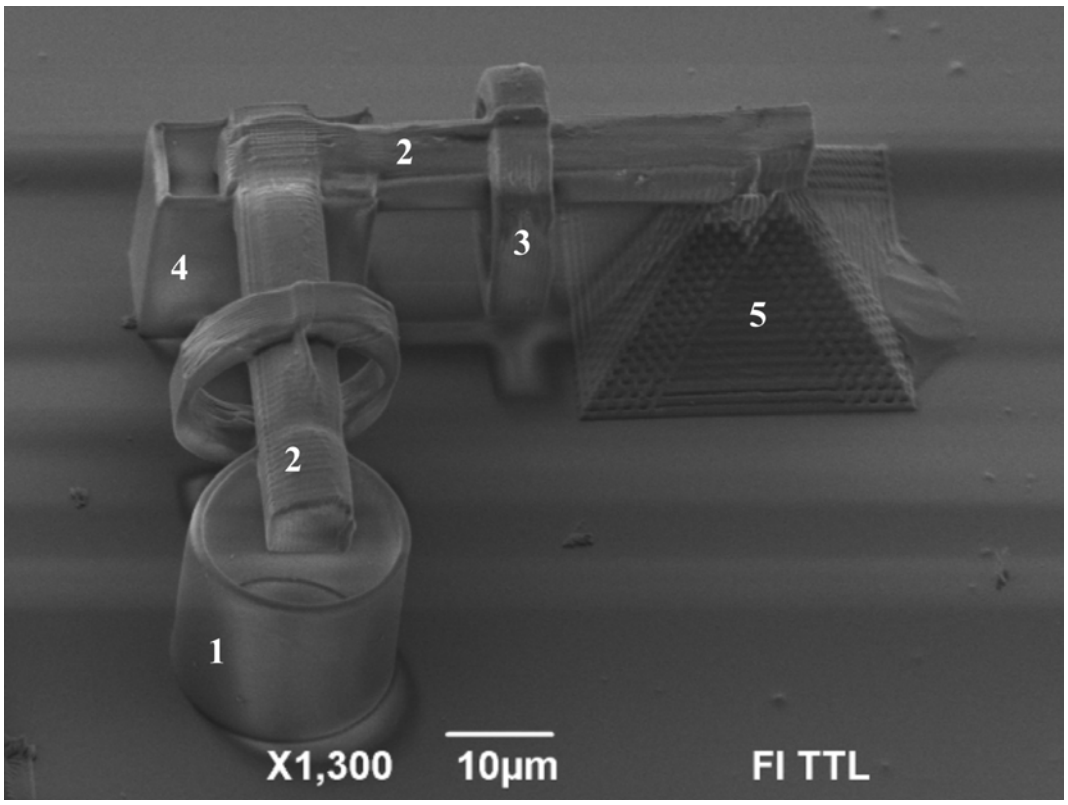

Fig. 15.1. FLMP fabricated Nanocity. It shows a ready state to fabricate fully integrated optical-photonic-mechanical-biological functional micro/nano-device.

A materialized fragment of a future vision of the author about the mature application of the technology is illustrated in Fig. 15.2. Components of *Nanocity* symbolize different functions, which are integrated in the complex microdevice. The whole structure is as small that it could be placed on the cut of human hair. Here incorporated elements are: *1* is a round well, *2* are rods serving as a support structures, *3* is a free hanging ring, *4* is a rectangular well, *5* is woodpile pyramid. It is an example of multifunctional micro/nanodevices which can be fabricated via single step *FLMP* approach. A fully integrated component includes optical, photonic, mechanical, microfluidic and biological performances for sophisticated *LOC*, *μ-TAS* or *MOEMS* in a not so far future.

16 INPUT OF COAUTHORS, ACKNOWLEDGEMENTS

16.1 Input of coauthors

M. Malinauskas takes grant for establishment of *FLMP* technology in *VU LRC*, definition of self-polymerization problem and investigation of it, application of *FLMP* for microoptical components and artificial scaffold production, publication of obtained results.

Author is infinitely grateful to the colleagues for their input:

Laser Research Center (VU LRC), Department of Quantum Electronics, Physics Faculty, Vilnius University:
Prof. R. Gadonas (discussion and guidance of experimental directions, projecting progress and coordination of Nanophotonics Laboratory, interpretation and publishing of obtained results), Prof. A. Piskarskas (strategic management), Prof. V. Sirutkaitis (support in expansion of *Laser Nanopolymerization lab*), V. Purlys (design and construction of *FLMP* setups and their automation via *"3D Poli"* software, preparation and tests of photonic and micro-optic samples, integration of nanoimprint technique into *Nanophotonics* laboratory), A. Žukauskas (fabrication and characterization of multitude samples on integrated microoptics, doped polymers and other topics, publishing of the results), H. Gilbergs (modeling, fabrication and characterization of microoptical components). P. Danilevičius (production of *3D* scaffolds), K. Belazaras (modeling, fabrication and characterization of bi-functional microoptics), G. Bičkauskaitė (investigation of self-polymerization, design of pictures and publication), M. Rutkauskas (fabrication of *PhCs* and *3D* scaffolds), D. Paipulas (planning of experiments and interpretation of results, manufacturing of metal masks, expertee in *TeX*

related questions), A. Čiburys (first steps in lab, consulting and advices), Dr. M. Peckus (characterization of *PhCs*), Dr. R. Piskarskas (introducing to *AO*), Dr. J. Pocius (ultrastable laser), R. Antipenkov (synchronization) and K. Stankevičiūtė (proofreading).

Vivarium, Institute of Biochemistry, Vilnius University:
Dr. V. Bukelskienė and Dr. D. Baltriukienė (cell growth in vitro on artificial scaffolds, planning of future directions and publication of obtained results).

Heart Surgery Center, Santariškės Clinics, Vilnius University:
Dr. R. Širmenis and A. Kraniauskas (in vivo experiments with rabbits and rats).

Applied Research Laboratory, Physics Institute, Vilnius:
Dr. G. Račiukaitis (for continuous interest and support in our works!), P. Gečys (high quality *SEM* micrographs), E. Stankevičius (collaboration transferring direct *FLMP* to the interferential one).

Semiconductor Physics Institute, Vilnius:
Dr. A. Maneikis (making *AFM* profiles).

Department of Nanotechnology, Laser Center Hannover (LZH), Hannover, Germany:
Dr. A. Ovsianikov (introducing to *FLMP* technique!!), Dr. C. Reinhardt (fabrication of plasmonic and microoptical components and discussions regarding it), Dr. S. Passinger (for showing the practical approach to *FLMP*), Dr. A. Kuznetsov (discussions regarding self-polymerization (non-local polymerization) and femtosecond laser processing), X. Shizhou (experiments on self-polymerization), Prof. B.N. Chichkov (possibility to work with world pioneers in *FLMP*).

Swinburne University of Technology, Melbourne, Australia:
prof. S. Juodkazis (ideas, thoughts, experiments, discussions, interpretations of the results for publication - many mails with ending *S.*).

Institute of Electronic Structure and Laser (IESL), Foundation for Research and Technology Hellas Institute of Electronic Structure and Laser (FORTH), Heraklion, Crete, Greece:
Dr. M. Farsari (guiding for experimental work and its publication, provision with novel photosensitive hybrid materials for *FLMP* structuring), A. Gaidukevičiūtė (fabrication of microoptical components on optical fibers, general and detailed discussions on *FLMP* applications in solidifying the liquid pre-polymer), I. Sakellari (multi-scan writing technique for improving *FLMP* fabrication spatial resolution), Prof. C. Fotakis (collaboration between Heraklion and Vilnius).

Catalan Institution for Research and Advanced Studies (ICREA), Barcelona, Spain:
Prof. K. Staliūnas (modeling of *PhCs* and poetry), L. Maigytė (measurement of *PhCs*).

Altechna:
Dr. G. Šlekys, T. Gertus, T. Lipinskas, T. Kudrius, E. Pabrėža (continuous support believing in *FLMP* progress).

16.2 Acknowledgements

Special thanks are expressed to *JoKido* for keeping the spirits high! My parents for possibility to do this work and *Harka* for reminding the joy of life. The ones who ran and weightlifted to broaden the horizons and push the limits further!!

17 APPROBATION

The experimental work was done in the laboratories of *VU LRC* (Vilnius, Lithuania), *LZH* (Hannover, Germany) and *FORTH*, (Heraklion, Crete, Greece). Here presented results are supported by 11 publications in scientific journals [18, 13-15]. 7 out of them are in *ISI* list [4-9, 13]. Additionally, the results were presented in 49 scientific conferences, 19 out of them made by the author M. Malinauskas himself.

PUBLICATIONS:

1) M. Malinauskas, V. Purlys, A. Gaidukevičiūtė, A. Čiburys and R. Gadonas, Flexible Fabrication of Three-Dimensional Structures by Means of Two-Photon Polymerization, Proc. Nanosciences and Nanotechnologies (NN07) 2008.

2) M. Malinauskas, V. Purlys, M. Rutkauskas and Gadonas, Two-Photon Polymerization for Fabrication of Three-Dimensional Micro- and Nanostructures over a Large Area, Proc. SPIE 7204, 72040C (2009).

3) M. Malinauskas, H. Gilbergs, V. Purlys, A. Žukauskas, M. Rutkauskas and R. Gadonas, Femtosecond Laser-Induced Two-Photon Photopolymerization for Structuring of Micro-Optical and Photonic Devices, Proc. SPIE 7366, 736622 (2009).

4) M. Malinauskas, H. Gilbergs, A. Žukauskas, V. Purlys, D. Paipulas and R. Gadonas, A Femtosecond Laser-Induced Two-Photon Photopolymerization Technique for Structuring Microlenses, J. Opt. 12(3), 035204 (2010).

5) M. Malinauskas, V. Purlys, M. Rutkauskas, A. Gaidukevičiūtė and R. Gadonas, Femtosecond Visible Light Induced Two-Photon Photopolymerization for *3D* Micro/Nanostructuring in Various Photopolymers and Photoresins, Lithuanian J. Phys. 50(2), in press (2010).

6) A. Žukauskas, M. Malinauskas, L. Kontenis, V. Purlys, D. Paipulas, M. Vengris and R. Gadonas, Doped Polymeric Microstructures for Optically

Active Functional Devices, Lithuanian J. Phys. 50(1), 55-61 (2010).

7) M. Malinauskas, G. Bičkauskaitė, M. Rutkauskas, V. Purlys, D. Paipulas and R. Gadonas, Self-Polymerization of Nano-Fibers and Nano-Membranes Induced by Two-Photon Absorption, Lithuanian J. Phys. 50(1), 135-140 (2010).

8) M. Malinauskas, P. Danilevičius, D. Baltriukienė, M. Rutkauskas, A. Žukauskas, Ž. Kairytė, G. Bičkauskaitė, V. Purlys, D. Paipulas, V. Bukelskienė and R. Gadonas, *3D* Artificial Polymeric Scaffolds for Regenerative Medicine Fabricated by Femtosecond Laser, Lithuanian J. Phys. 50(1), 75-82 (2010).

9) D. Paipulas, V. Kudriašov, K. Kuršelis, M. Malinauskas and V. Sirutkaitis, Manufacturing of Diffractive Elements in Fused Silica by High Repetition Rate Femtosecond *Yb:KGW* Laser Pulses, Lithuanian J. Phys. 50(1), 129-134 (2010).

10) M. Malinauskas, V. Purlys, A. Žukauskas, M. Rutkauskas, P. Danilevičius, D. Paipulas, G. Bičkauskaitė, L. Bukelskis, D. Baltriukienė, R. Širmenis, A. Gaidukevičiūtė, V. Bukelskienė, R. Gadonas, V. Sirvydis and A. Piskarskas, Large Scale Laser Two-Photon Polymerization Structuring For Fabrication Of Artificial Polymeric Scaffolds For Regenerative Medicine, Proc. *ICO*-Photonics, in press (2010).

11) O. Balachninaitė and M. Malinauskas, Naujos Vilniaus universiteto lazerinių tyrimų centro mokslinės kryptys, Fizikų Žinios 36, 5-7 (2009).

12) M. Malinauskas, V. Bukelskienė and R. Širmenis, Biomedžiagos ir audinių inžinerija, Mokslas ir gyvenimas 10, 2-4; 18-19 (2009). http: ausis.gf.vu.lt/mg/nr/2009/11/index.html

13) M. Malinauskas, A. Žukauskas, G. Bičkauskaitė, R. Gadonas and S. Juodkazis, Mechanisms of Three-Dimensional Structuring of Photo-Polymers by Tightly Focused Femtosecond Laser Pulses, Opt. Express 18(10), 10209-10221 (2010).

14) M. Malinauskas, V. Purlys, A. Žukauskas, G. Bičkauskaitė, T. Gertus, P. Danilevičius, D. Paipulas, M. Rutkauskas, H. Gilbergs, D. Baltriukienė, L. Bukelskis, R. Širmenis, V. Bukelskienė, R. Gadonas, V. Sirvydis and A. Piskarskas, Laser Two-Photon Polymerization Micro- and Nanostructuring Over a Large Area on Various Substrates, Proc. SPIE, 7715-49 (2010).

15) M. Malinauskas, H. Gilbergs, A. Žukauskas, K. Belazaras, V. Purlys,

M. Rutkauskas, G. Bičkauskaitė, A. Momot, D. Paipulas, R. Gadonas, S. Juodkazis and A. Piskarskas, Femtosecond laser fabrication of hybrid micro-optical elements and their integration on the fiber tip, Proc. SPIE, 7716-9 (2010).

16) P. Danilevičius, A. Žukauskas, G. Bičkauskaitė, V. Purlys, M. Rutkauskas, T. Gertus, D. Paipulas, J. Matukaitė, D. Baltriukienė and M. Malinauskas, Laser *3D* Micro/Nanofabrication of Polymers for Tissue Engineering Applications, Latvian J. Phys. Tech. Sci., submitted (2010).

17) M. Malinauskas, A. Žukauskas, G. Bičkauskaitė, M. Rutkauskas, K. Belazaras, H. Gilbergs, P. Danilevičius, V. Purlys, D. Paipulas, T. Gertus, R. Gadonas, A. Piskarskas, D. Baltriukienė, V. Bukelskienė and A. Gaidukevičiūtė, Fabrication of Three-Dimensional Nanostructures by Laser Polymerization Technique, Proc. CYSENI (2010).

18) M. Malinauskas, H. Gilbergs, A. Žukauskas, K. Belazaras, V. Purlys, P. Danilevičius, M. Rutkauskas, G. Bičkauskaitė, D. Paipulas, R. Gadonas, A. Gaidukevičiūtė, I. Sakellari, M. Farsari and S. Juodkazis, Femtosecond Laser Polymerization of Hybrid/Integrated Micro-optical Elements and Their Characterization, J. Opt. 10, in press (2010).

19) A. Ovsianikov, M. Malinauskas, S. Schlie, A. Ngezahayo, B.N. Chichkov, Two-photon Polymerization of *Poly(Ethylene Glycol)* Materials for Biomedical Applications, submitted to Adv. Mat. Eng.

20) T. Linkevičius, E. Vindašiūtė, M. Malinauskas, A. Puisys, V. Rutkūnas, R. Juškėnas, Studies of chemical interactions between zirconium oxide and veneering ceramics, submitted to Dental Materials.

21) I. Dumbrytė, I. Andziulienė, M. Malinauskas, L. Linkevičienė, T. Linkevičius, V. Purlys, J. Sinkevičius, R. Gadonas, E. Vindašiūtė, V. Pečiulienė, Evaluation of existing enamel micro-cracks after removal of the metal brackets, submitted to Angle Orthodontics (2010).

22) M. Malinauskas, M. Farsari and S. Juodkazis, Laser and Photonics Reviews, in preparation (2010).

23) D. Paipulas, V. Kudriašov, K. Kurželis, M. Malinauskas and V. Sirutkaitis, Volume Bragg grating formation in fused silica with high repetition rate femtosecond *Yb:KGW* laser pulses, Proc. of LPM (2010).

24) M. Malinauskas, A. Ovsianikov, G. Bičkauskaitė, X. Shizhou, R. Gadonas and B.N. Chichkov, Self-Formation of Nano-Membranes Induced by Two-Photon Absorption, in preparation (2010).

25) D. Paipulas, V. Kudriašov, M. Malinauskas, V. Smilgevičius and V. Sirutkaitis, The Structural Modifications Induced in Lithium Niobate and *KDP* Crystals with High Repetition Rate Femtosecond Laser Pulses, Appl. Phys. A. in preparation (2010).

26) M. Malinauskas, V. Purlys, A. Žukauskas, P. Danilevičius, D. Baltriukienė, K. Belazaras, H. Gilbergs, M. Rutkauskas, G. Bičkauskaitė, Ž. Kairytė, D. Paipulas, T. Gertus, R. Širmenis, V. Bukelskienė, R. Gadonas, V. Sirvydis and A. Piskarskas, Fabrication of functional three-dimensional polymeric micro/nanostructures by laser nonlinear optical nanolithography technique, in preparation (2010).

27) M. Malinauskas, A. Žukauskas, V. Purlys, M. Rutkauskas, G. Bičkauskaitė, D. Paipulas, T. Gertus, A. Kraniauskas, R. Širmenis, D. Baltriukienė, V. Bukelskienė, R. Gadonas, V. Sirvydis and A. Piskarskas, in preparation Eng. Life Sci. (2010).

28) M. Malinauskas, V. Purlys, A. Gaidukevičiūtė, K. Belazaras, A. Žukauskas, G. Bičkauskaitė, R. Gadonas and S. Juodkazis, Sub-Nanosecond Microlaser Induced *3D* Micro/nanostructuring of Photopolymers, in preparation (2010).

29) G. Bičkauskaitė and M. Malinauskas, Funkcinių trimačių darinių formavimas lazerinės daugiafotonės polimerizacijos būdu, Jaunasis tyrėjas, (2010).

CONFERENCES (AS A PRESENTER):

1. 17th Belarus-Lithuanian seminar "Lasers and Optical Technologies", Grodno, Belarus. M. Malinauskas, A. Gaidukevičiūtė and V. Purlys, Laser Microfabrication in Ormocer by Using Two-Photon Polymerization, (2006).

2. Brokerage Event "Embedded Systems Design, Nanoelectronics and Microsystems", Warsaw, Poland, M. Malinauskas, Two-Photon Polymerization with femtosecond Yb:KGW Laser, (2007).

3. NN07-Nanosciences and Nanotechnologies conference, Thessaloniki, Greece, M. Malinauskas, R. Gadonas, V. Purlys, A. Gaidukevičiūtė and A. Čiburys, Flexible Fabrication Of Three-Dimensional Structures By Means Of Two-Photon Polymerization, (2007).

4. NN08-Nanosciences and Nanotechnologies conference, Thessaloniki, Greece. M. Malinauskas, V. Purlys, M. Rutkauskas, A. Gaidukevičiūtė and R. Gadonas, Two-Photon Photopolymerization Enables Commercialization

of 3D Nanostructuring in Various Materials, (2008).

5. Micromachining and Microfabrication Process Technology XIV conference, San Jose, USA. M. Malinauskas, V. Purlys, M. Rutkauskas and R. Gadonas, Two-photon Polymerization for Fabrication of Three-Dimensional Micro- and Nanostructures over a Large Area, (2009).

6. Microtechnologies for the New Millenium, Dresden, Germany, M. Malinauskas, V. Purlys, M. Rutkauskas, V. Chorosajev and R. Gadonas, Femtosecond Laser-Induced Two-Photon Photopolymerization for Structuring of Micro-Optical and Photonic Devices, (2009).

7. 38th Lithuanian National Conference of Physics, Vilnius, Lithuania, M. Malinauskas, V. Purlys, M. Rutkauskas, A. Žukauskas, D. Paipulas and R. Gadonas, Fabrication of Functional Three-Dimensional Nanostructures by Femtosecond Lasers via Two-Photon Polymerization, (2009).

8. 38th Lithuanian National Conference of Physics, Vilnius, Lithuania, M. Malinauskas, D. Baltriukienė, V. Chorosajev, P. Danilevičius, Ž. Kairytė, D. Paipulas, V. Purlys, M. Rutkauskas, V. Bukelskienė, R. Gadonas, A. Piskarskas, V. Sirvydis, Fabrication of Artificial Polymeric Scaffolds for Regenerative Medicine by Femtosecond Lasers, (2009).

9. Northern Optics 2009, Vilnius, Lithuania, M. Malinauskas, A. Ovsia-nikov, X. Shizhou, B.N. Chichkov and R. Gadonas, Formation of Self-Polymerized Nano-Membranes by Femtosecond Laser Pulses, (2009).

10. Lasers and Optical Nonlinearity 2009, Vilnius, Lithuania, R. Gadonas, M. Malinauskas, V. Purlys, A. Žukauskas, M. Rutkauskas, H. Gilbergs, G. Bičkauskaitė, V. Chorosajev, K. Belazaras, D. Paipulas, K. Stankevičiūtė, A. Melninkaitis, V. Bukelskienė and A. Piskarskas, Femtosecond Laser 3D Micro- and Nanostructuring of Photopolymers, (2009).

11. ICO-PHOTONICS, Emerging Trends and Novel Materials in Photonics 2009, Delphi, Greece, M. Malinauskas, V. Purlys, P. Danilevičius, M. Rutkauskas, L. Bukelskis, A. Žukauskas, G. Bičkauskaitė, V. Chorosajev, D. Baltriukienė, D. Paipulas, V. Bukelskienė, R. Gadonas, Large Scale Laser Two-Photon Polymerization Structuring for Fabrication of Artificial Polymeric Scaffolds for Regenerative Medicine, (2009).

12. MediNano-2 Mediterranean Conference on Nano-Photonics, Athens, Greece, M. Malinauskas, A. Ovsianikov, X. Shizhou, B. Chichkov, G. Bičkauskaitė and R. Gadonas, Self-Formation of Nano-Membranes Induced by Two-Photon Absorption, (2009).

13. (Invited) 53rd Scientific Conference for Young Students of Physics and Natural Sciences, Vilnius, Lithuania, M. Malinauskas, Ultrafast laser *3D* nanostructuring of photopolymers, (2010).

14. Photonics Europe, M. Malinauskas, H. Gilbergs, A. Žukauskas, V. Purlys, D. Paipulas and R. Gadonas, Microlenses Fabricated by Two-Photon Polymerization Technique, (2010).

15. Photonics Europe, M. Malinauskas, V. Purlys, A. Žukauskas, G. Bičkauskaitė, T. Gertus, P. Danilevičius, D. Paipulas, M. Rutkauskas, H. Gilbergs, D. Baltriukienė, L. Bukelskis, R. Širmenis, V. Bukelskienė, R. Gadonas, V. Sirvydis and A. Piskarskas, Laser Two-Photon Polymerization Micro- and Nanostructuring Over a Large Area on Various Substrates, (2010).

16. Photonics Europe, M. Malinauskas, A. Ovsianikov, G. Bičkauskaitė, X. Shizhou, R. Gadonas and B. Chichkov, Self-Formation of Nano-Membranes Induced by Two-Photon Absorption, (2010).

17. Developments in Optics and Communications, Riga, Latvia, M. Malinauskas, A. Žukauskas, G. Bičkauskaitė, M. Rutkauskas, D. Paipulas and V. Purlys, Multi-Photon Polymerization Structuring Resolution Enhancement: Optimizing Excitation Conditions and Material Local Response, (2010).

18. Physics and Physical Computation, G. Bičkauskaitė, M. Malinauskas, A. Žukauskas, M. Rutkauskas, V. Purlys and R. Gadonas, Fabrication of Functional Three-Dimensional Microstructures by Laser Multiphoton Fabrication, (2010).

19. CYSENI 2010, M. Malinauskas, A. Žukauskas, G. Bičkauskaitė, M. Rutkauskas, K. Belazaras, H. Gilbergs, P. Danilevičius, V. Purlys, D. Paipulas, T. Gertus, R. Gadonas and A. Piskarskas, D. Baltriukienė, V. Bukelskienė, A. Gaidukevičiūtė, (2010).

CONFERENCES (AS A COAUTHOR): 33 presentatios in international and national scientific conferences were made M. Malinauskas being as a coauthor.

18 ABOUT AUTHOR

Name:.....Mangirdas Malinauskas

Date of Birth:.....1981 12 27

Place of Birth:.....Vilnius, Lithuania

Nationality:.....Lithuanian

Occupation:.....:
Junior Research Assistant in Laser Physics and Optical Technologies

Address:.....:
Laser Nanophotonics Group
Laser Research Center
Department of Quantum Electronics
Physics Faculty, Vilnius University
Saulėtekio avenue 10
LT-10223 Vilnius, Lithuania
Mob. +37060002843
Tel. +37052366014
Fax. +37052366006
E-mail: mangirdas.malinauskas@ff.vu.lt
Website: http://www.lasercenter.vu.lt

Education:.....:
Vilniaus S. Nėries Secondary School: with citation (2000)
Vilnius University, Physics Faculty: B.S. in Physics (2004)
Vilnius University, Physics Faculty: M.S. in Physics (2006)

Academic appointments:.....:
2004 09 – 2005 03 VU Laser Research Center, Laboratory assistant
2005 04 – 2005 08 Laser Zentrum Hannover, Laboratory assistant
2005 10 – 2006 06 VU Laser Research Center, Laboratory assistant
2006 07 – 2006 11 Altechna Co. Ltd., Lithuania, Physicist investigator
2006 10 – 2007 10 VU Laser Research Center, Young research fellow
2007 11 – 2008 01 Laser Zentrum Hannover, Research assistant
2008 02 – 2008 09 VU Laser Research Center, Young research fellow
2008 10 – 2008 11 Laser Zentrum Hannover, Cooperate researcher
2008 12 – 2009 08 VU Laser Research Center, Young research fellow
2009 09 – 2009 12 FORTH institute, Greece Cooperate researcher
2010 01 – 2010 12 VU Laser Research Center, Young research fellow

Scientific interests:.....:
Multiphoton polymerization, *3D* nanostructuring, development of photopolymers for direct laser writing, functional structures for bio-applications, photonics and microoptics, characterization of microstructures, nonlinear microscopy, laser assisted microfabrication, *UV* lithography, digital image processing, solar cells.

Other:.....:
4th Kyu in Karate Kyokushin;
Drummer of former extreme metal band *GROL*;
Has completed running marathon (42195 m) 3 times.

Bibliography

[1] S. Maruo, O. Nakamura, and S. Kawata. Three-dimensional microfabrication with two-photon-absorbed photopolymerization. *Opt. Lett.*, 2(22):132–134, 1997.

[2] M. Miwa, S. Juodkazis, T. Kawakami, S. Matsuo, and H. Misawa. Femtosecond two-photon stereo-lithography. *Appl. Phys. A*, 73:561–566, August 2001.

[3] C.N. LaFratta, J.T. Fourkas, T. Baldacchini, and R.A. Farrer. Multiphoton fabrication. *Angew. Chem. Int. Ed*, 46:6238–6258, 2007.

[4] M. Farsari and B. Chichkov. Materials processing: Two-photon fabrication. *Nature Photonics*, 3:450 – 452, 2009.

[5] G. von Freymann. Direct laser writing. *Nat. Photonics*, 4:22–23, 1 2010.

[6] S. Juodkazis, V. Mizeikis, K.K. Seet, M. Miwa, and H. Misawa. Two-photon lithography of nanorods in su-8 photoresist. *Nanotechnology*, 16:846–849, November 2005.

[7] F. Qi, Y. Li, D. Tan, H. Yang, and Q. Gong. Polymerized nanotips via two-photon photopolymerization. *Opt.Express*, 15(3):971–976, 2007.

[8] S.H. Park, T.W. Lim, D.-Y. Yang, N.C. Cho, and K.-S. Lee. Fabrication of a bunch of sub-30-nm nanofibers inside microchannels using photopolymerization via a long exposure technique. *Appl. Phys. Lett.*, 89(17):173133, 2006.

[9] D. Tan, Y. Li, F. Qi, H. Yang, Q. Gong, X. Dong, and X. Duan. Reduction in feature size of two-photon polymerization using scr500. *Appl. Phys. Lett.*, 90(7):071106, 2007.

[10] T. Baldacchini, C.N. LaFratta, R.A. Farrer, M.C. Teich, B.E.A. Saleh, M.J. Naughton, and J.T. Fourkas. Acrylic-based resin with favorable properties for three-dimensional two-photon polymerization. *J. Appl. Phys.*, 95(11):6072–6076, June 2004.

[11] T. Kondo, S. Juodkazis, V. Mizeikis, and H. Misawa. Three-dimensional high-aspect-ratio recording in resist. *Journ. Non-Crys. Sol.*, 354(12-13):2010, 2008. Proceedings of the 2005 International Conference on Glass - In conjunction with the Annual Meeting of the International Commission on Glass.

[12] L.H. Nguyen, M. Straub, and M. Gu. Acrylate-based photopolymer for two-photon microfabrication and photonic applications. *Adv. Funct. Mater.*, 15(2):209–216, 2005.

[13] J. Stampfl, S. Baudis, C. Heller, R. Liska, A. Neumeister, R. Kling,

A. Ostendorf, and M. Spitzbart. Photopolymers with tunable mechanical properties processed by laser-based high-resolution stereolithography. *J. Micromech. Microeng.*, 18:1–9, 2008.

[14] J. Serbin, A. Egbert, A. Ostendorf, B.N. Chichkov, R. Houbertz, G. Domann, J. Schulz, C. Cronauer, L. Frohlich, and M. Popall. Femtosecond laser-induced two-photon polymerization of inorganic-organic hybrid materials for applications in photonics. *Opt. Lett.*, 28(5):301–303, 2003.

[15] T. Tanaka. Plasmonic metamaterials produced by two-photon-induced photoreduction technique. *JLMN*, 3(3):152–156, 2008.

[16] J.C. Halimeh, T. Ergin, J. Mueller, N. Stenger, and M. Wegener. Photorealistic images of carpet cloaks. *Opt. Express*, 17(22):19328–19336, 2009.

[17] T. Ergin, N. Stenger, P. Brenner, J.B. Pendry, and M. Wegener. Three-Dimensional Invisibility Cloak at Optical Wavelengths. *Science*, 328(5976):337–339, 2010.

[18] A. Ovsianikov, S. Schlie, A. Ngezahayo, A. Haverich, and B. N. Chichkov. *J. Tiss. Eng. Regen. Med.*, 1(6):443–449, 2007.

[19] C. Heller, M. Schwentenwein, G. Russmueller, F. Varga, J. Stampfl, and R. Liska. Vinyl esters: Low cytotoxicity monomers for the fabrication of biocompatible 3d scaffolds by lithography based additive manufacturing. *J. Polym. Sci. A Polym. Chem.*, 47(24):6941–6954, 2009.

[20] F. Claeyssens, E.A. Hasan, A. Gaidukeviciute, D.S. Achilleos, A. Ranella, C.Reinhardt, A. Ovsianikov, X. Shizhou, C. Fotakis M. Vamvakaki, and B.N. Chichkov andM. Farsari. Three-dimensional biodegradable structures fabricated by two-photon polymerization. *Langmuir*, 25(5):3219–3223, 2009.

[21] D. Psaltis, S.R. Quake, and C. Yang. Developing optofluidic technology through the fusion of microfluidics and optics. *Nature*, 442:381–386, 2006.

[22] D. Janasek, J. Franzke, and A. Manz. Scaling and the design of miniaturized chemical-analysis systems. *Nature*, 442:374–380, 2006.

[23] S. Boutami, B. Ben Bakir, J.-L. Leclercq, X. Letartre, P. Rojo-Romeo, M. Garrigues, P. Viktorovitch, I. Sagnes, L. Legratiet, and M. Strassner. Highly selective and compact tunable moems photonic crystal fabry-perot filter. *Opt. Express*, 14(8):3129–3137, 2006.

[24] S Bargiel, K Rabenorosoa, C ClÃ©vy, C Gorecki, and P Lutz. Towards micro-assembly of hybrid moems components on a reconfigurable silicon free-space micro-optical bench. *Journal of Micromechanics and Microengineering*, 20(4):045012, 2010.

[25] A. Ovsianikov, J. Viertl, B.N. Chichkov, M. Oubaha, B. MacCraith, I. Sakellari, A. Giakoumaki, D. Gray, M. Vamvakaki, M. Farsari, and C. Fotakis. Ultra-low shrinkage hybrid photosensitive material for

two-photon polymerization microfabrication. *ACS Nano*, 2(11):2257–2262, 2008.

[26] M. Farsari, A. Ovsianikov, M. Vamvakaki, I. Sakellari, D. Gray, B.N. Chichkov, and C. Fotakis. Fabrication of three-dimensional photonic crystal structures containing an active nonlinear optical chromophore. *Appl. Phys. A*, 93:11–15, 2008.

[27] H.-B. Sun, S. Matsuo, and H. Misawa. Three-dimensional photonic crystal structures achieved with two-photon-absorption photopolymerization of resin. *Appl. Phys. Lett.*, 74(6):786–788, February 1999.

[28] R.A. Borisov, G.N. Dorojkina, N.I. Koroteev, V.M. Kozenkov, S.A. Magnitskii, D.V. Malakhov, A.V. Tarasishin, and A.M. Zheltikov. Femtosecond two-photon photopolymerization: a method to fabricate optical photonic crystals with controllable parameters. *Laser Physics*, 8(5):1105–1105, 1998.

[29] C. Reinhardt, R. Kiyan, S. Passinger, A. stepanov, A. Ostendorf, and B.N. Chichkov. Rapid laser prototyping of plasmonic components. *Appl. Phys. A.*, 89:321–325, 2007.

[30] A. Seidel, C. Ohrt, S. Passinger, C. Reinhardt, R. Kiyan, and B.N. Chichkov. Nanoimprinting of dielectric loaded surface-plasmon-polariton waveguides using masters fabricated by 2-photon polymerization technique. *J. Opt. Soc. Am. B*, 26(4):810–812, 2009.

[31] M.S. Rill, C. Plet, M. Thiel, I. Staude, G. von Freymann, S. Linden, and M. Wegener. Photonic metamaterials by direct laser writing and silver chemical vapor deposition. *Nat. Mater.*, 7(7):543–546, 2008.

[32] L. Li and J.T. Fourkas. Multiphoton polymerization. *Mater. Today*, 10(6):30–37, 2007.

[33] S. Maruo and J.T. Fourkas. Recent progress in multiphoton microfabrication. *Laser & Photonics Review*, 2(1-2):100–111, 2008.

[34] S.-H. Park, D.Y. Yang, and K.S. Lee. Two-photon stereolithography for realizing ultra precisethree-dimensional nano/microdevices. *Laser & Photon. Rev.*, 3(1-2):1–11, 2009.

[35] S. Juodkazis, V. Mizeikis, and H. Misawa. Three-dimensional microfabrication of materials by femtosecond lasers for photonics applications. *J. Appl. Phys.*, 106(5):051101, 2009.

[36] M. Farsari, M. Vamvakaki, and B.N. Chichkov. Multiphoton polymerization of hybrid materials. *J. Opt.*, 0000(0000):00–00, 2010.

[37] I. Sakellari, A. Gaidukeviciute, A. Giakoumaki, D. Gray, C. Fotakis, M. Farsari, M. Vamvakaki, C. Reinhardt, A. Ovsianikov, and B. Chichkov. Two-photon polymerization of titanium sol-gel containing composites for three-dimensional structure fabrication. *Appl. Phys. A*, 100:359–364, 2010.

[38] S. Juodkazis, V. Mizeikis, and H. Misawa. Three-dimensional structuring of resists and resins by direct laser writing and holographic recording. *Adv. Polym. Sci.*, 213:157–206, 2008.

[39] H.-B. Sun and S. Kawata. Two-photon photopolymerization and 3d lithographic microfabrication. *Adv. Polym. Sci.*, 170:169–273, 2004.

[40] J.-I. Kato, N. Takeyasu, Y. Adachi, H.-B. Sun, and S. Kawata. Multiple-spot parallel processing for laser micronanofabrication. *Appl. Phys. Lett.*, 86(4):044102, 2005.

[41] K.-S. Lee, R.H. Kim, D.-Y. Yang, and S.H. Park. Advances in 3d nano/microfabrication using two-photon initiated polymerization. *Prog. Polym. Sci.*, 33:631–681, 2008.

[42] P.P. Naulleau, C.N. Anderson, J. Chiu, P. Denham, S. George, K.A. Goldberg, M. Goldstein, B. Hoef, R. Hudyma, G. Jones, C. Koh, B. La Fontaine, A. Ma, W. Montgomery, D. Niakoula, J. Park, T. Wallow, and S. Wurm. 22-nm half-pitch extreme ultraviolet node development at the sematech berkeley microfield exposure tool. *Microelectron. Eng.*, 86(4-6):448–455., 2009.

[43] G.R. Sunne. Electron beam lithography for nanofabrication. *PhD thesis, University of Barcelona, Barcelona*, 2008.

[44] E. Di Fabrizio, R. Fillipo, S. Cabrini, R. Kumar, F. Perennes, M. Altissimo, L. Businaro, D. Cojac, L. Vaccari, M. Prasciolu, and P. Candeloro. X-ray lithography for micro- and nano-fabrication at elettra for interdisciplinary applications. *J. Phys.: Condens. Matter*, 16(33):3517–3535, 2004.

[45] H. Schift. Nanoimprint lithography: An old story in modern times? a review. *J. Vac. Sci. Technol. B*, 26(2):458–480, 2008.

[46] M. Walther, A. Ortner, H. Meier, U. Löffelmann, P. J. Smith, and J. G. Korvink. Terahertz metamaterials fabricated by inkjet printing. *Appl. Phys. Lett.*, 95(25):251107, 2009.

[47] T. Boland, X. Tao, B.J. Damon, B. Manley, P. Kesari, S. Jalota, and S. Bhaduri. Drop-on-demand printing of cells and materials for designer tissue constructs. *Mat. Sci. Eng. C*, 27(3):372–376, 2007.

[48] H. Benkreira and M.I. Khan. Air entrainment in dip coating under reduced air pressures. *Chem. Eng. Sci.*, 63(2):448–459, 2008.

[49] K.H. Tan, C.K. Chua, K.F. Leong, C.M. Cheah, P. Cheang, M.S. Abu Bakar, and S. W. Cha. Scaffold development using selective laser sintering of polyetheretherketone-hydroxyapatite biocomposite blends. *Biomaterials*, 247(18):3115–3123, 2003.

[50] V. Mizeikis, K.K. Seet, S. Juodkazis, and H. Misawa. Three-dimensional woodpile photonic crystal templates for the infrared spectral range. *Opt. Lett.*, 29(17):2061–2063, 2004.

[51] M. Deubel, G. Von Freymann, M. Wegener, S. Pereira, K. Busch, and C.M. Soukoulis. Direct laser writing of three-dimensional photonic-crystal templates for telecommunications. *Nature Mater.*, 3:444–447, July 2004.

[52] J. Serbin, A. Ovsianikov, and B.N. Chichkov. Fabrication of woodpile structures by multi-photon polymerization and investigation of their

optical properties. *Opt. Express*, 12:5221–5228, 2004.

[53] R. Guo, S. Xiao, X. Zhai, J. Li, A. Xia, and W. Huang. Micro lens fabrication by means of femtosecond two photon photopolymerization. *Opt. Express*, 14(2):810–816, 2006.

[54] M. Malinauskas, H. Gilbergs, A. Žukauskas, V. Purlys, D. Paipulas, and R. Gadonas. A femtosecond laser-induced two-photon photopolymerization technique for structuring microlenses. *J. Opt.*, 12(3):035204, 2010.

[55] S. Maruo, A. Takaura, and Y. Saito. Optically driven micropump with a twin spiral microrotor. *Opt. Express*, 17(18525-18532), 2009.

[56] D. Wu, Q.D. Chen, L.G. Niu, J.N. Wang, J. Wang, R. Wang, H. Xia, and H.B. Sun. Femtosecond laserrapid prototyping of nanoshells and suspending components towards microfluidic devices. *Lab Chip.*, 9(16):2391–2394, 2009.

[57] R.J. Narayan, C. Jin, A. Doraiswamy, I.N. Mihailescu, M. Jelinek, A. Ovsianikov, B.N. Chichkov, and D.B. Chrisey. Laser processing of advanced bioceramics. *Adv. Eng. Mater.*, 7(12):1083–1098, 2005.

[58] O. Adunka H. Pillsbury A. Doraiswamy A. Ovsianikov, B. Chichkov and R. J. Narayan. Rapid prototyping of ossicular replacement prostheses. *Appl. Surf. Sci.*, 253(15):6603–6607, 2007.

[59] A. Ovsianikov, S. Schlie, A. Ngezahayo, A. Haverich, and B.N. Chichkov. Two-photon polymerization technique for microfabrication of cad-designed 3d scaffolds from commercially available photosensitive materials. *J. Tissue. Eng. Regen. Med.*, 1:443–449, 2007.

[60] Y.M. Ha, J.W. Choi, and S. H. Lee. Mass production of 3-d microstructures using projection microstereolithography. *J. Mec. Sci. Technol.*, 22(3):5154–5261, 2008.

[61] I.B. Park, Y.M. Ha, and S.H. Lee. Cross-section segmentation for improving the shape accuracy of microstructure array in projection microstereolithography. *Int. J. Adv. Manuf. Technol.*, 46:151–161, 2010.

[62] D.Y. Yang, S.H. Park, T.W. Lim, H.-J. Kong, S.W. Yi, H.K. Yang, and K.-S. Lee. Ultraprecise microreproduction of a three-dimensional artistic sculpture by multipath scanning method in two-photon photopolymerization. *Appl. Phys. Lett.*, 90:013113, 2007.

[63] M. Malinauskas, H. Gilbergs, V. Purlys, A. Žukauskas, M. Rutkauskas, and R. Gadonas. Femtosecond laser-induced multi-photon photopolymerization for structuring of micro-optical and photonic devices. *Proc. SPIE*, 7366:736622, 2009.

[64] K.E. Gonsalves, L. Merhari, H. Wu, and Y. Hu. Organic-inorganic nanocomposites: Unique resists for nanolithography. *Adv. Mater.*, 13(10):703–714, 2001.

[65] T. Tanaka, A. Ishikawa, and S. Kawata. Two-photon-induced reduction of metal ions for fabricating three-dimensional electrically con-

ductive metallic microstructure. *Appl. Phys. Lett.*, 88:081107, 2006.
[66] V. Mizeikis, S. Juodkazis, R. Tarozaitė, J. Juodkazytė, K. Juodkazis, and H. Misawa. Fabrication and properties of metalo-dielectric photonic crystal structures for infrared spectral region. *Opt. Express*, 15:8454–8464, 2007.
[67] M.S. Rill, C. Plet, M. Thiel, I. Staude, G. von Freymann, S. Linden, and M. Wegener. Photonic metamaterials by direct laser writing and silver chemical vapour deposition. *Nat. Mater.*, 7:543–546, 2008.
[68] L. Vurth, P. Baldeck, O. Stephan, and G. Vitrant. Two-photon induced fabrication of gold microstructures in polystyrene sulfonate thin films using a ruthenium(ii) dye as photoinitiator. *Appl. Phys. Lett.*, 92(17):171103, 2008.
[69] S.H. Park, T.W. Lim, D.Y. Yang, R.H. Kim, and K.S. Lee. Improvement of spatial resolution in nano-stereolithography using radical quencher. *Macromol. Res.*, 14(5):559–564, 2006.
[70] W. Haske, V.W. Chen, J.M. Hales, W. Dong, S. Barlow, S.R. Marder, and J.W. Perry. 65 nm feature sizes using visible wavelength 3-d multiphoton lithography. *Opt. Express*, 15(6):3426–3436, March 2007.
[71] X.Z. Dong, Z.S. Zhao, and X.M. Duan. Improving spatial resolution and reducing aspect ratio in multiphoton polymerization nanofabrication. *Appl. Phys. Lett.*, 92:091113, 2008.
[72] http://www.nanoscribe.de/.
[73] http://www.lzh.de.
[74] http://www.newport.com.
[75] http://www.teemphotonics.com.
[76] S. Passinger, A. Ovsianikov, R. Kiyan, C. Reinhardt, A. Ostendorf, and B. N. Chichkov. Two-photon polymerization for industrial applications. *Proc. LPM2007*, 2007.
[77] M. Malinauskas, V. Purlys, A. Žukauskas, G. Bičkauskaitė, T. Gertus, P. Danilevičius, D. Paipulas, M. Rutkauskas, H. Gilbergs, D. Baltriukienė, L. Bukelskis, R. Širmenis, V. Bukelskienė, R. Gadonas, V. Sirvydis, and A. Piskarskas. Laser two-photon polymerization micro- and nanostructuring over a large area on various substrates. *Proc. SPIE*, 7715:77151F–1, 2010.
[78] J. Stampfl, R. Inführ, K. Stadlmann, N. Pucher, V. Schmidt, and R. Liska. Materials for the fabrication of optical waveguides with two photon photopolymerization. *Proc. Fifth International WLT-Conference on Lasers in Manufacturing*, 2009.
[79] S. Passinger. Two-photon polymerization and the application for surface plasmon polaritons. *PhD thesis, Leibniz Universitat Hannover*, pages 1–126, 2008.
[80] A. Ovsianikov. Investigation of two-photon polymerization technique for applications in photonics and biomedicine. *PhD thesis, Leibniz Universitat Hannover*, pages 1–116, 2008.

[81] K.-S. Lee, P. Prabhakaran, J. Park, R.H. Kim, N. Cho, D.-Y. Yang, S.H. Park, T.W. Lim, S. Yong, and H.J. Kong. Recent advances in two-photon lithography. *CIF'8 Proc.*, 08, 2008.

[82] H.-B. Sun, K.Takada, M.-S. Kim, K.-S. Lee, and S. Kawata. Scaling laws of voxels in two-photon photopolymerization nanofabrication. *Appl. Phys. Lett.*, 83:1104, 2003.

[83] M. Malinauskas, V. Purlys, M. Rutkauskas, and R. Gadonas. Two-photon polymerization for fabrication of three-dimensional micro- and nanostructures over a large area. *Proc. SPIE*, 7204(72040C):72040C–72040C–11, 2009.

[84] V. Purlys A. Žukauskas M. Rutkauskas M. Malinauskas, H. Gilbergs and R. Gadonas. Femtosecond laser-induced two-photon photopolymerization for structuring of micro-optical and photonic devices. *Proc. of SPIE*, 7366, 2009.

[85] M. Malinauskas, V. Purlys, M. Rutkauskas, A. Gaidukevičiutė, and R. Gadonas. Femtosecond visible light induced two-photon photopolymerization for 3d micro/nanostructuring in photoresists and photopolymers. *Lithuanian J. Phys.*, 50(2):201–208, 2010.

[86] www.sartomer.com.

[87] *http://memscyclopedia.org/su8.html*.

[88] W.H. Teh, U. Durig, G. Salis, R. Harbers, U. Drechsler, R.F. Mahrt, C.G. Smith, and H.-J.Guntherodt. Su-8 for real three-dimensional subdiffraction-limittwo-photon microfabrication. *Appl. Phys. Lett.*, 84(20).

[89] G. Witzgall, R. Vrijen, E. Yablonovitch, V. Doan, and B.J. Schwartz. Single-shot two-photon exposure of commercial photoresist for the production of three-dimensional structures. *Opt. Lett.*, 23:1745–1747, 1998.

[90] I. Sakellari, A. Gaidukeviciute, A. Giakoumaki, D. Gray and. C. Fotakis, M. Vamvakaki, M. Farsari and. C. Reinhardt, A. Ovsianikov, and B.N. Chichkov. Direct laser writing of photonic nanostructures. *Proc. SPIE*, 7392:73920Y, 2009.

[91] R. Houbertz, L.Fröhlich, M. Popall, U. Streppel, P. Dannberg, A. Bräuer, J. Serbin, and B.N. Chichkov. Inorganic-organic hybrid polymers for information technology: from planar technology to 3D nanostructures. *Adv. Eng. Mater.*, 5(8):551–555, 2003.

[92] J. Serbin, A. Egbert, A. Ostendorf, B. N. Chichkov, R. Houbertz, G. Domann, J. Schulz, C. Cronauer, L. Frohlich, and M. Popall. Femtosecond laser-induced two-photon polymerization of inorganic-organic hybrid materials for applications in photonics. *Opt. Lett.*, 28(5):301–303, 2003.

[93] A. Ovsianikov, S. Schlie, A. Ngezahayo, A. Haverich, and B.N. Chichkov. Two-photon polymerization technique for microfabrication of cad-designed 3d scaffolds from commercially available photosensi-

tive materials. *J. Tissue. Eng. Regen. Med.*, 1:443–449, 2007.

[94] A. Ovsianikov, B. N. Chichkov, M. Malinauskas, S. Schlie, A. Ngezahayo, S. Gittard, and R. Narayan. Two-photon polymerization of poly(ethylene glycol) materials for biomedical applications. submitted, 2010.

[95] M. Malinauskas, P. Danilevičius, D. Baltriukienė, M. Rutkauskas, A. Žukauskas, Ž. Kairytė, G. Bičkauskaitė, V. Purlys, D. Paipulas, V. Bukelskienė, and R. Gadonas. 3d artificial polymeric scaffolds for stem cell growth fabricated by femtosecond laser. *Lithuanian J. Phys.*, 50(1):75–82, 2010.

[96] M. Malinauskas, V. Purlys, A. Zukauskas, M. Rutkauskas, P. Danilevicius, D. Paipulas, G. Bickauskaite, L. Bukelskis, D. Baltriukiene, R. Sirmenis, A. Gaidukeviciute, V. Bukelskiene, R. Gadonas, V. Sirvydis, and A. Piskarskas. Large scale laser two- photon polymerization structuring for fabrication of artificial polymeric scaffolds for regenerative medicine. *Proc. of ICO-Photonics: Emerging Trends & Novel Materials in Photonics 2009*, in press, 2010.

[97] A. Žukauskas, M. Malinauskas, L. Kontenis, V. Purlys, D. Paipulas, M. Vengris, and R. Gadonas. Organic dye doped microstructures for optically active functional devices fabricated via two-photon polymerization technique. *Lithuanian J. Phys.*, 50(11):55–61, 2010.

[98] M.J. Ventura, C. Bullen, and M. Gu. Direct laser writing of three-dimensional photonic crystal lattices within a pbs quantum-dot-doped polymer material. *Opt. Express*, 15:1817–1822, 2007.

[99] Y. Xia and G.M. Whitesides. Sof-lithography. *Annu. Rev. Mater. Sci.*, 28(00):153–184, 1998.

[100] Y. Li, H. Cui, F. Qi, H. Yang, and Q. Gong. Uniform suspended nanorods fabricated by bidirectional scanning via two-photon photopolymerization. *Nanotechnol.*, 19:375304, 2008.

[101] H.B. Sun, T. Suwa, K. Takada, R.P. Zaccaria, M.-S. Kim, K.-S. Lee, and S. Kawata. Shape precompensation in two-photon laser nanowriting of photonic lattices. *Appl. Phys. Lett.*, 85(17):3708–3710, 2004.

[102] H. Lorenz, M. Despont, N Fahrni, N. LaBianca, P. Renaud, and P. Vettiger. Su-8: a low-cost negative resist for mems. *J. Micromech. Microeng.*, 7:121–124, 1997.

[103] N. Tétreault, G. von Freymann, M. Deubel, M. Hermatschweiler, F. Pérez-Willard, S. John, M. Wegener, and G.A. Ozin. New route to three-dimensional photonic bandgap materials: Silicon double inversion of polymer templates. *Adv. Mater.*, 18:457–460, 2006.

[104] www.microresist.de.

[105] J. Li, B. Jia, and M. Gu. Engineering stop gaps of inorganic-organic polymeric 3d woodpile photonic crystals with post-thermal treatment. *Opt. Express*, 16:20073–20080, 2008.

[106] A. Ovsianikov, A. Gaidukevičiutė, B.N. Chichkov, M. Oubaha, B.D.

MacCraith, I. Sakellari, A. Giakoumaki, D. Gray, M. Vamvakaki, M. Farsari, and C. Fotakis. Multi-photon polymerization of hybrid sol-gel materials for photonics applications. *Laser Chem.*, 2008:1–7, 2008.

[107] J.L. Li, B. Jia, G. Zhou, and M. Gu. Fabrication of three-dimensional woodpile photonic crystals in a PbSe quantum dot composite material. *Opt. Express*, 14(22):10740–10745, 2006.

[108] M. Malinauskas, P. Danilevicius, A. Zukauskas, D. Paipulas, G. Bickauskaite, V. Purlys, R. Gadonas, and A. Piskarskas. In vitro and in vivo biocompatibility of laser 3d microstructurable polymers. *Eng. Life Sci.*, 0000(000):0–00, 2010.

[109] T. Matsuda, M. Mizutani, and S.C. Arnold. Molecular design of photocurable liquid biodegradable copolymers. 1. synthesis and photocuring characteristics. *Macromolecules*, 33:795–800, 2000.

[110] P. Sanguansri and M.A. Augustin. Nanoscale materials development e a food industry perspective. *Trends Food Sci. Technol.*, 17:547–556, 2006.

[111] M. Loden and C. Wessman. The antidandruff efficacy of a shampoo containing piroctone olamine and salicylic acid in comparison to that of a zinc pyrithione shampoo. *Int. J. Cosmetic. Sci.*, 22(4):285–289, 2000.

[112] N. Subrahmanyam. Addition of antioxidants and polyethylene glycol 4000 enhances the healing property of honey in burns. *Ann. Burns Fire Disasters*, 9(2), 1996.

[113] S. Gabler, J. Stampf, T. Koch, S. Seidler, G. Schuller, H. Redl, V. Juras, S. Trattnig, and R. Weidisch. Determination of the viscoelastic properties of hydrogels based on polyethylene glycol diacrylate(peg-da) and human articular cartilage. *Int. J. Materials Engineering Innovation*, 1(1):3–20, 2009.

[114] M.S. Hahn, J.S. Miller, and J.L. West. Three-dimensional biochemical and biomechanical patterning ofhydrogels for guiding cell behavior. *Adv. Mater.*, 18(20):2679–2684, 2006.

[115] R. Marchal, E. Nicolau, J.-P. Ballaguet, and F. Bertoncini. Biodegradability of polyethylene glycol 400 by complex microfloras. *Intern. Biodeter. Biodegr.*, 62:384–390, 2008.

[116] A. Ovsianikov, M. Gruene, M. Pflaum, L. Koch, F. Maiorana, M. Wilhelmi, A. Haverich, and B. Chichkov. Laser printing of cells into 3d scaffolds. *Biofabrication*, 2(1):014104, 2010.

[117] M. Malinauskas, A. Žukauskas, G. Bičkauskaitė, M. Rutkauskas, K. Belazaras, H. Gilbergs, P. Danilevičius, V. Purlys, D. Paipulas, T. Gertus, R. Gadonas, A. Piskarskas, D. Baltriukienė, V. Bukelskienė, and A. Gaidukeviči_utė. Fabrication of three-dimensional nanostructures by laser polymerization technique. *Proc. CYSENI*, 2010:354–366, 2010.

[118] T. Kondo, S. Juodkazis, and H. Misawa. Reduction of capillary force for high-aspect ratio nanofabrication. *Appl. Phys. A*, 81(8):1583–1586, 2005.

[119] S. Maruo, T. Hasegawa, and N. Yoshimura. Single-anchor support and supercritical *co_2* drying enable high-precision microfabrication of three-dimensional structures. *Opt. Express*, 17(23):20945–20951, 2009.

[120] M. Malinauskas, R. Gadonas, V. Purlys, A. Gaidukeviciute, and A. Ciburys. Flexible fabrication of three-dimensional structures by means of two-photon polymerization. *Proc. NN07-Nanosciences and Nanottechnologies conference*, 07, 2007.

[121] H.B. Sun and S. Kawata. Multi-photon photopolymerization and 3d lithographic microfabrication. *Adv. Polym. Sci.*, 170:169–273, 2004.

[122] T. Tanaka, H.B. Sun, and S. Kawata. Rapid sub-diffraction-limit laser micro/nanoprocessing in a threshold material system. *Appl. Phys. Lett.*, 80(2):312–314, 2002.

[123] G.M.Whitesides, E. Ostuni, S. Takayama, X. Jiang, and D.E. Ingber. Soft lithography in biology and biochemistry. *Annu. Rev. Biomed. Eng.*, 3:335–373, 2001.

[124] A. Seidel, C. Ohrt, S. Passinger, C. Reinhardt, R. Kiyan, and B.N. Chichkov. Nanoimprinting of dielectric loaded surface-plasmon-polariton waveguides using masters fabricated by 2-photon polymerization technique. *J. Opt. Soc. Am. B*, 26(4):810–812, 2009.

[125] Y.-K. Kim, J.-H. Park, G.-C. Shin, J.S. Ha, S.J.Park, S.M. Yi, and G.T. Kim. Nanofabrication via direct transfer of boe treated pdms stamppatterns onto sio2 surfaces. *J. Phys.*, 61:560–564, 2007.

[126] C.N. LaFratta. Multiphoton absorption polymerization issues and solutions. *PhD thesis, University of Maryland*, 2006.

[127] C.A. Coenjarts and C.K. Ober. Two-photon three-dimensional microfabrication of poly(dimethylsiloxane) elastomers. *Chem. Mater.*, 16:5556–5558, 2004.

[128] A.L. Thangawng, R.S. Ruoff, M.A. Swartz, and M.R. Glucksberg. An ultra-thin pdms membrane as a bio/micro-nano interface: fabrication and characterization. *Biomed. Microdevices*, 9:587–595, 2007.

[129] V.J. Cadarsoa, A. Llobera, G. Villanueva, J.A. Plazaa, J. Brugger, and C. Dominguez. Mechanically tuneable microoptical structure based on pdms. *Procedia Chem.*, 1:560–563, 2009.

[130] G. Kumi, C.O. Yanez, K.D. Belfield, and J.T. Fourkas. High-speed multiphoton absorption polymerization: fabrication of microfluidic channels with arbitrary cross-sections and high aspect ratios. *Lab Chip*, 10:1057–1060, 2010.

[131] M. Malinauskas, A. Žukauskas, G. Bičkauskaitė, R. Gadonas, and S. Juodkazis. Mechanisms of three-dimensional structuring of photopolymers by tightly focussed femtosecond laser pulses. *Opt. Express*,

18(10):10209–10221, 2010.

[132] M. Straub and M. Gu. Near-infrared photonic crystals with higher-order bandgaps generated by two-photon photopolymerization. *Opt. Lett.*, 27(20):1824–1826, 2002.

[133] S.H. Park, S.H. Lee, D.-Y. Yang, H.J. Kong, and K.-S. Lee. Subregional slicing method to increase three-dimensional nanofabrication efficiency in two-photon polymerization. *Appl. Phys. Lett.*, 87:154108, 2005.

[134] A. Pikulin and N. Bityurin. Spatial resolution in polymerization of sample features at nanoscale. *Phys. Rev. B*, 75(19):195430, 2009.

[135] N. Uppal and P.S. Shiakolas. Modeling of temperature-dependent diffusion and polymerization kinetics and their effects on two-photon polymerization dynamics. *J. Micro/Nanolith. MEMS MOEMS*, 7(4):043002, 2008.

[136] K.K. Seet, S. Juodkazis, V. Jarutis, and H. Misawa. Feature-size reduction of photopolymerized structures by femtosecond optical curing of su-8. *Appl. Phys. Lett.*, 89(024106), 2006.

[137] H. Xia, W.-Y. Zhang, F.-F. Wang, D. Wu, X.-W., L.L. Chen, Q.-D. Chen, Y.-G. Ma, and H.-B. Sun. Three-dimensional micronanofabrication via two-photon-excited photoisomerization. *Appl. Phys. Lett.*, 95(8):083118, 2009.

[138] F. Qi, Y. Li, D. Tan, H. Yang, and Q. Gong. Polymerized nanotips via two-photon photopolymerization. *Opt.Express*, 15(3):971–976, 2007.

[139] G. Witzgall, R. Vrijen, E. Yablonovitch, V. Doan, and B.J. Schwartz. Single-shot two-photon exposure of commercial photoresist for the production of three-dimensional structures. *Opt. Lett.*, 23(22):1745–1747, November 1998.

[140] S. Juodkazis, V. Mizeikis, K. K. Seet, M. Miwa, and H. Misawa. Two-photon lithography of nanorods in SU-8 photoresist. *Nanotechnol.*, 16:846 – 849, 2005.

[141] K. Venkatakrishnan, S. Jariwala, and B. Tan. Maskless fabrication of nano-fluidic channels by two-photon absorption (tpa) polymerization of su-8 on glass substrate. *Opt. Express*, 17(4):2756–2762, February 2009.

[142] F. Heinroth, S. Munzer, A. Feldhoff, S. Passinger, W. Cheng, C. Reinhardt, B.N. Chichkov, and P. Behrens. Three-dimensional titania pore structures produced by using a femtosecond laser pulse technique and a dip coating procedure. *J. Mater. Sci.*, 44:6490–6497, March 2009.

[143] M. Miwa, S. Juodkazis, T. Kawakami, S. Matsuo, and H. Misawa. Femtosecond two-photon stereo-lithography. *Appl. Phys. A*, 73(5):561–566, 2001.

[144] M. Farsari, G. Filippidis, and C. Fotakis. Fabrication of three-dimensional structures by three-photon polymerization. *Opt. Lett.*, 30(23):3180–3182, December 2005.

[145] L.E. Abolghasemi, S.Eaton, A.Hosseini, and P.R. Herman. Three-dimensional laser nano-structuring: Contrast in three-photon and two-photon polymerization of su-8. *Proc. CLEO*, CThN6:1–2, May 2007.

[146] I. Wang, M. Bouriau, L. Baldeck, C. Martineau, and C. Andraud. Three-dimensional microfabrication by two-photon-initiated polymerization with a low-cost microlaser. *Opt. Lett.*, 27(15):1348–1350, August 2002.

[147] M. Malinauskas, V. Purlys, A. Gaidukevičiutė, K. Belazaras, A. Žukauskas, G. Bičkauskaitė, and R. Gadonas. Sub-nanosecond microlaser induced two-photon 3d microstructuring of polymers. unpublished results, 2010.

[148] R.W. Boyd. *Nonlinear Optics*. Academic Press, London, 2nd ed. edition, 2003.

[149] S. Maruo and K. Ikuta. Three-dimensional microfabrication by use of single-photon-absorbed polymerization. *Appl. Phys. Lett.*, 76(19):2656–2658, 2000.

[150] S. Juodkazis, V. Mizeikis, S. Matsuo, K. Ueno, and H. Misawa. Three-dimensional micro- and nano-structuring of materials by tightly focused laser radiation. *Bull. Chem. Soc. Jpn.*, 81:411–448, 2008.

[151] M. Sheik-Bahae, A.A. Said, T.H. Wei, D.J. Hagan, and E.W. van Stryland. Sensitive measurement of optical nonlinearities using a single beam. *IEEE J. Quantum Electr.*, 26(4):760–769, 1990.

[152] K. Kamada. Characterization of two-photon absorption and its resonance enhancement by z-scan method. *Proc. SPIE*, 5516:97–105, 2004.

[153] K. Kamada, K. Matsunaga, A. Yoshino, and K. Ohta. Two-photon-absorption-induced accumulated thermal effect on femtosecond z-scan experiments studied with time-resolved thermal-lens spectrometry and its simulation. *J. Opt. Soc. Am. B*, 20:529–537, 2003.

[154] R. DeSalvo, A.A. Said, D.J. Hagan, E.W. VanStryland, and M. Sheik-Bahae. Infrared to ultraviolet measurements of two-photon absorption and n(2) in wide bandgap solids. *IEEE J. Quantum Electr.*, 32(8):1324–1333, 1996.

[155] M. Rumi, J. Ehrlich, A. Heikal, J. Perry, S. Barlow, Z. Hu, D. McCord-Maughon, T.C. Parker, H. Rockel, S.Thayumanavan, S.R. Marder, D. Beljonne, and J.-L. Bredas. Structure-property relationships for two-photon absorbing chromophores: Bis-donor diphenylpolyene and bis(styryl)benzene derivatives. *J. Am. Chem. Soc.*, 122(39):9500–9510, 2000.

[156] N. Murazawa, S. Juodkazis, H. Misawa, and K. Kamada. Two-photon excitation of dye-doped liquid crystal by a cw-laser irradiation. *Mol. Cryst. Liq. Cryst.*, 489:310 – 319, 2008.

[157] H.J. Eichler, F. Massmann, E. Biselli, K. Richter, M. Glotz, L. Konet-

zke, and X. Yang. Laser-induced freecarrier and temperature gratings in silicon. *Phys. Rev. B*, 36:3247–3253, 1987.

[158] E. Gamaly, A. Rode, B. Luther-Davies, and V. Tikhonchuk. Ablation of solids by femtosecond lasers: Ablation mechanism and ablation thresholds for metals and dielectrics. *Phys. Plasmas*, 9:949–957, 2002.

[159] B.C. Stuart, M.D. Feit, S. Herman, A.M. Rubenchik, B.W. Shore, and M.D. Perry. Nanosecond-to-femtosecond laser-induced breakdown in dielectrics. *Phys. Rev. B*, 53(4):1749–1761, 1996.

[160] Y.P. Raizer. Laser-induced discharge phenomena. *Consultant Bureau, New York*, 1977.

[161] A. Vogel, J. Noack, G. Huttman, and G. Paltauf. Mechanisms of femtosecond laser nanosurgery of cells and tissues. *Appl. Phys. B*, 81:1015–1047, 2005.

[162] S. Juodkazis, V. Mizeikis, K.K. Seet, H. Misawa, and U.G.K. Wegst. Mechanical properties and tuning of three-dimensional polymeric photonic crystals. *Appl. Phys. Lett.*, 91:241904, 2007.

[163] Q. Sun, S. Juodkazis, N. Murazawa, V. Mizeikis, and H. Misawa. Free-standing and movable photonic microstructures fabricated by photopolymerization with femtosecond laser pulses. *J. Micromech. Microeng.*, 20:035004, 2010.

[164] K. K. Seet, S. Juodkazis, V. Jarutis, and H. Misawa. Feature-size reduction of photopolymerized structures by femtosecond optical curing of SU-8. *Appl. Phys. Lett.*, 89:024106, 2006.

[165] S. Juodkazis, A. V. Rode, E. G. Gamaly, S. Matsuo, and H. Misawa. Recording and reading of three-dimensional optical memory in glasses. *Appl. Phys. B*, 77:361–368, 2003.

[166] S. Juodkazis, V. Mizeikis, Y. Nishijima, W. Ebina, H. Misawa, M. Kondo, and V.Švrček. Three-dimensional femtosecond laser fabrication. *ECS Transactions*, 16(41):57–63, 2009.

[167] J. Morikawa, A. Orie, T. Hashimoto, and S. Juodkazis. Thermal diffusivity in femtosecond-laser-structured micro-volumes of polymers. *Appl. Phys. A.*, 98(3):551–556, 2010.

[168] K. Ueno, S. Juodkazis, T. Shibuya, V. Mizeikis, Y. Yokota, and H. Misawa. Nano-particle-enhanced photo-polymerization. *J. Phys. Chem. C*, 113:11720–11724, 2009.

[169] H. B. Sun and S. Kawata. Two-photon photopolymerization and 3d lithographic microfabrication. *Adv. Polym. Sci.*, 170, 2004.

[170] H.-B. Sun K. Takada and S. Kawata. The study on spatial resolution in two-photon induced polymerization. *Proc. of SPIE*, 6110, 2006.

[171] K. K. Seet M. Miwa S. Juodkazis, V. Mizeikis and H. Misawa. Two-photon lithography of nanorods in su-8 photoresist. *Nanotechnology*, 16, 2005.

[172] D. Y. Yang N. C. Cho S. H. Park, T. W. Lim and K. S. Lee. Fabrication of a bunch of sub-30-nm nanofibers inside microchannels using

photopolymerization via a long exposure technique. *Appl. Phys. Lett.*, 89, 2006.

[173] F. Qi H. Yang Q. Gong X. Dong D. Tan, Y. Li and X. Duan. Reduction in feature size of two-photon polymerization using scr500. *Appl. Phys. Lett.*, 90, 2007.

[174] K. Takada H.-B. Sun and S. Kawata. Elastic force analysis of functional polymer submicron oscillators. *Appl. Phys. Lett.*, 79, 2001.

[175] J. P. Fouassier and J. F.Rabek. *Lasers in Polymer Science and Technology*, volume 1. CRC Press, Inc, Boca Raton, Fl, 1990.

[176] T. W. Lim D.-Y. Yang and K.-S. Lee S.-H. Park, K. H. Kim. Investigation of three-dimensional pattern collapse owing to surface tension using an imperfection finite element model. *Microelectron. Eng.*, 85, 2008.

[177] M. Malinauskas, H. Gilbergs, A. Žukauskas, K. Belazaras, V. Purlys, M. Rutkauskas, G. Bičkauskaitė, A. Momot, D. Paipulas, R. Gadonas, S. Juodkazis, and A. Piskarskas. Femtosecond laser fabrication of hybrid micro-optical elements and their integration on the fiber tip. *Proc. SPIE*, 7716:77160A, 1977.

[178] M. Malinauskas, A. Žukauskas, V. Purlys, K. Belazaras, A. Momot, D. Paipulas, R.Gadonas, A. Piskarskas, H. Gilbergs, A. Gaidukeviči_utė, I. Sakellari, M. Farsari, and S. Juodkazis. Femtosecond laser polymerization of hybrid/integrated micro-optical elements and their characterization. *J. Opt.*, page 2010, 1977.

[179] V. Mizeikis, S. Juodkazis, A. Marcinkevièius, S. Matsuo, and H. Misawa. Tailoring and characterization of photonic crystals. *J. Photochem. Photobio. C*, 2(1):35–69, 2001.

[180] K. Kaneko, H.-B. Sun X.-M. Duan, and S. Kawata. Submicron diamond-lattice photonic crystals produced by multi-photon laser nanofabrication. *Appl. Phys. Lett.*, 83:2091–2093, 2003.

[181] Q.-D. Chen, D. Wu, L.-G. Niu, J. Wang, X.-F. Lin, H. Xia, and H.-B. Sun. Phase lenses and mirrors created by laser micronanofabrication via multi-photon photopolymerization. *Appl. Phys. Lett.*, 91(17):171105, 2007.

[182] Y. Li, Y. Yu, L. Guo, S. Wu, C. Chen, L. Niu, A. Li, and H. Yang. High efficiency multilevel phase-type fresnel zone plates produced by multi-photon polymerization of SU-8. *J. Opt.*, 12(3):035203, 2010.

[183] H. Nishiyama, J. Nishii, M. Mizoshiri, and Y. Hirata. Microlens arrays of high-refractive-index glass fabricated by femtosecond laser lithography. *Appl. Surf. Sci.*, 255(24):9750–9753, 2009.

[184] K. Yamasaki, S. Juodkazis, S. Matsuo, and H. Misawa. Three-dimensional micro-channels in polymers: one-step fabrication. *Appl. Phys. A*, 77(3-4):371–373, 2003.

[185] A. Ovsianikov, X. Shizhou, M. Farsari, M. Vamvakaki, C. Fotakis, and B.N. Chichkov. Shrinkage of microstructures produced by two-

photon polymerization of Zr-based hybrid photosensitive materials. *Opt. Express*, 17(4):2143–2148, 2009.

[186] R. Houbertz. Laser interaction in sol-gel based materials–3-d lithography for photonic applications. *Appl. Surf. Sci.*, 247(1-4):504–512, 2005.

[187] A. Marcinkevičius, V. Mizeikis, S. Juodkazis, S. Matsuo, and H. Misawa. Effect of refractive index-mismatch on laser microfabrication in silica glass. *Appl. Phys. A.*, 76:257–260, 2003.

[188] S.M. Mansfield and G.S. Kino. Solid immersion microscope. *Appl. Phys. Lett.*, 57(24):2615–2617, 1990.

[189] M. Yoshita, M. Baba, and H. Akiyama. Improved high collection efficiency in fluorescence microscopy with a weierstrass-sphere solid immersion lens. *Jpn. J. Appl. Phys.*, 41:858–860, 2002.

[190] A. Cannistra and T.J. Suleski. Characterization of hybrid molding and lithography for su-8 micro-optical components. *J. Micro/Nanolith. MEMS MOEMS*, 9(1):013025, 2010.

[191] S. Sinzinger and M. Testorf. Transition between diffractive and refractive micro-optical components. *Appl. Opt.*, 34(26):5970–5976, 1995.

[192] F. Schiappelli, R. Kumar, M. Prasciolu, D. Cojoc, S. Cabrini, M. De Vittorio, G. Visimberga, A. Gerardino, C. Degiorgio, and E. Di Fabrizio. Efficient fiber-to-waveguide coupling by a lens on the end of the optical fiber fabricated by focused ion beam milling. *Microelectron. Eng.*, 73-74:397–404, 2004.

[193] C. Paquet and E. Kumacheva. Nanostructured polymers for photonics. *Mater. Today*, 11(4):48–56, 2008.

[194] A. Ovsianikov, S. Passinger, R. Houbertz, and B.N. Chichkov. Three dimensional material processing with femtosecond lasers. *Laser Ablation and its Applications*, pages 121–157, 2007.

[195] J. Serbin and M. Gu. Superprism phenomena in waveguide-coupled woodpile structures fabricated by two-photon polymerization. *Opt. Express*, 14(8):3563–3568, 2006.

[196] L. Li, E. Gershgoren, G. Kumi, W.-Y. Chen, P.-T. Ho, W.N. Herman, and J.T. Fourkas. High-performance microring resonators fabricated with multiphoton absorption polymerization. *Adv. Mater.*, 20:3668–3671, 2008.

[197] S. Wu, J. Serbin, and M. Gu. Multi-photon polymerisation for three-dimensional micro-fabrication. *J. Photochem. Photobiol. A*, 181(1):1–11, 2006.

[198] S. Yokoyama, T. Nakahama, H. Miki, and S. Mashiko. Two-photon-induced polymerization in a laser gain medium for optical microstructure. *Appl. Phys. Lett.*, 82(19):3221–3223, 2003.

[199] H.-B. Sun, T. Tanaka, K. Takada, and S. Kawata. Two-photon photopolymerization and diagnosis of three-dimensional microstructures containing fluorescent dyes. *Appl. Phys. Lett.*, 79(10):1411–1413,

2001.

[200] S. Constantino, K.G. Heinze, O.E. Martinez, P. Koninck, and P.W. Wiseman. Two-photon fluorescent microlithography for live-cell imaging. *Microsc. Res. Tech.*, 68:272–276, 2005.

[201] A. Ovsianikov T. Fabian H.A. Kolb-H. Haferkamp B.N. Chichkov S. Schlie, A. Ngezahayo. Three-dimensional cell growth on structures fabricated from ormocer by two-photon polymerization technique. *J. Biomater. Appl.*, 22(3):275–287, 2007.

[202] T. Woggon, T. Kleiner, M. Punke, and U. Lemmer. Nanostructuring of organic-inorganic hybrid materials for distributed feedback laser resonators by multi-photon polymerization. *Opt. Express*, 17(4):2500–2507, 2009.

[203] M.B. Christiansen, M. Scholer, and A. Kristensen. Integration of active and passive polymer optics. *Opt. Express*, 7:3931–3939, 2007.

[204] T. Baldacchini, M. Zimmerley, E.O. Potma, and R. Zadoyan. Chemical mapping of three-dimensional microstructures fabricated by two-photon polymerization using cars microscopy. *Proc. SPIE*, 7201:7201–0Q, 2009.

[205] M. Gersborg-Hansen and A. Kristensen. Tunability of optofluidic distributed feedback dye laser. *Opt. Express*, 15(1):137–142, 2006.

[206] L. G. Griffith and G. Naughton. *Sci.*, 295(5557):1009–1014, 2002.

[207] M. Malinauskas, P. Danilevičius, D. Baltriukienė, M. Rutkauskas, A. Žukauskas, Ž. Kairytė, G. Bičkauskaitė, V. Purlys, D. Paipulas, V. Bukelskienė, and R. Gadonas. *Lith. J. Phys.*, 50(1):75–82, 2010.

[208] D. W. Hutmacher. *Biomater.*, 21(24):2529–2543, 2000.

[209] M. P. Lutolf and J. A. Hubbell. *Nat. Biotechnol.*, 23(1):47–55, 2005.

[210] Y. Li and S. T. Yang. *Biotechnol. Bioprocess Eng.*, 6(5):311–325, 2001.

[211] J. H. Brauker, V. E. Carr-Brendel, L. A. Martinson, J. Crudele, W. D. Johnston, and R. C. Johnson. *J. Biomed. Mater. Res.*, 29(12):1517–1524, 1995.

[212] S. Nehrer, H. A. Breinan, A. Ramappa, G. Young, S. Shortkroff, L. K. Louie, C. B. Sledge, I. V. Yannas, and M. Spector. *Biomater.*, 18(11):769–776, 1997.

[213] K. Whang, C. H. Thomas, K. E. Healy, and G. Nuber. *Polym. J.*, 36:837–842, 1995.

[214] M. C. Wake, C. W. Patrick, Jr., and A. G. Mikos. *Cell Transplant*, 3(4):339–343, 1994.

[215] I. V. Yannas, E. Lee, D. P. Orgill, E. M. Skrabut, and G. F. Murphy. *Proc. Nat. Acad. Sci. U.S.A.*, 86(3):933–937, 1989.

[216] C. W. Patrick, P. B. Chauvin, J. Hobley, and G. P. Reece. *Tissue Eng.*, 5(2):139–151, 1999.

[217] B. D. Boyan, T. W. Hummert, D. D. Dean, and Z. Schwartz. *Biomater.*, 17(2):137–146, 1996.

[218] P. X. Ma. *Mater. Today*, 7(5):30–40, 2004.
[219] P. Tayalia, C. R. Mendonca, T. Baldacchini, D. J. Mooney, and E. Mazur. *Adv. Mater.*, 20(23):4494–4498, 2008.
[220] J. C. Chachques, J. C. Trainini, N. Lago, M. Cortes-Morichetti, O. Schussler, and A. Carpentier. *Ann. Thorac. Surg.*, 85(3):901–908, 2008.
[221] J. Weng and M. Wang. *J. Mater. Sci. Lett.*, 20(15):1401–1403, 2001.
[222] S. J. Hollister, R. D. Maddox, and J. M. Taboas. *Biomater.*, 235(20):4095–4103, 2002.
[223] V. Bukelskienė, D. Baltriukienė, D. Bironaitė, A. Imbrasaitė, R. Širmenis, M. Balčiūnas, E. Žurauskas, and A. Kalvelytė. *Semin Cardiol*, 11(3):99–105, 2005.
[224] R. Širmenis, V. Bukelskienė, V. Domkus, and V. Sirvydis. *Acta Med Lituanica*, 6:178–181, 1999.
[225] H.B. Sun, T. Suwa, K. Takada, R.P. Zaccaria, M.-S. Kim, K.-S. Lee, and S. Kawata. Shape precompensation in two-photon laser nanowriting of photonic lattices. *Appl. Phys. Lett.*, 85(17):3708–3710, 2004.
[226] L. Li, R.R. Gattass, E. Gershgoren, H. Hwang, and J.T. Fourkas. Achieving lambda/20 Resolution by One-Color Initiation and Deactivation of Polymerization. *Science*, 324(5929):910–913, 2009.
[227] N. Anscombe. Direct laser writing. *Nat. Photonics*, 4:22–23, 2010.